*Manuscript (with LINE NUMBERS)

Investigating the Goban Spur rifted continental margin, offshore Ireland, through integration of new seismic reflection and potential field data

Pei Yang[a], J. Kim Welford[a], Alexander L. Peace[a,b], and Richard Hobbs[c]

[a] Department of Earth Sciences, Memorial University, St. John's, NL, Canada

[b] School of Geography and Earth Sciences, McMaster University, Hamilton, ON, Canada

[c] Department of Earth Sciences, Durham University, Durham, UK

Abstract

The Goban Spur, offshore Ireland, is a magma-poor rifted continental margin conjugate to the well-studied Newfoundland margin, offshore Canada. Published studies demonstrated that a 70-km-wide zone of exhumed serpentinized mantle lies between oceanic crust and stretched continental crust at the seaward limit of Goban Spur. However, the along-strike extent of this serpentinized zone has, until now, been unknown due to insufficient data coverage. The crustal architecture of the margin is complicated due to its multi-staged tectonic history. Here, six newly acquired multi-channel seismic reflection lines are processed and interpreted, along with vintage seismic profiles, to characterize its structure and evolution. These seismic profiles reveal significant along-strike structural variations along the Goban Spur margin, suggestive of different extension rates, rifting styles and stages. In the northwest, the transitional zone between oceanic crust and stretched continental crust consists of a narrow zone of shallow peridotite ridges and a wider zone of the deeper exhumed serpentinized mantle, much like the conjugate Iberian and Newfoundland margins. Toward the southeast, the zone of peridotite ridges pinches out. Magmatic contributions are interpreted to increase from NW to SE, based on contrasting basement characteristics observed on the seismic profiles. In total, five distinct crustal zones related to different rifting stages are identified and their regional extents are evaluated, providing a more detailed characterization of this margin.

1. Introduction

Studies of magma-poor rifted continental margins around the southern North Atlantic Ocean have been plentiful, particularly for the Newfoundland-Iberia and Flemish Cap-Galicia Bank conjugate margin pairs (Reston, 2007; Sibuet et al., 2007; Peron-Pinvidic et al., 2013; Sauter et al., 2018). In recent years, attention has increasingly focused on the Newfoundland-Irish and Flemish Cap-Goban Spur conjugate rifted continental margins (Fig. 1a) (Welford et al., 2010a; Gerlings et al., 2012). Rifting along these margins occurred to the north of the Biscay Triple Junction (BTJ), which formed due to divergent movement between Iberia, North America, and Europe during the breakup of Pangaea (Sibuet and Collette, 1991). Rifting proceeded until the initiation of seafloor spreading between them, beginning in the Cretaceous at magnetic Chron 34 (Fig. 1a) (Sibuet and Collette, 1991). By studying the continent-ocean transitional zones (COTZ) across these margin pairs, the geodynamic processes that contributed to rifting can be deduced.

While early studies of the Goban Spur margin originally interpreted a sharp continent-ocean boundary (COB) (e.g., Masson et al., 1985; Keen and de Voogd, 1988; Horsefield et al., 1994; Peddy et al., 1989), a 70-km-wide transitional zone of exhumed serpentinized subcontinental mantle has since been interpreted for the COTZ of the Goban Spur margin based on seismic refraction modelling (Bullock and Minshull, 2005). Similar transitional zones have also been observed along the Newfoundland and Flemish Cap, Iberia and Galicia Bank margins (Boillot et al., 1987; Whitmarsh et al., 1998; Dean et al., 2000; Welford et al., 2010a; Gerlings et al., 2011; Dean et al., 2015).

Due to limited data coverage, the rift-related domains along the Goban Spur margin have remained poorly defined and their architecture has been primarily delineated on the basis of a small number of co-located 2-D seismic profiles (Keen and de Voogd, 1988; Peddy et al., 1989; Horsefield et al., 1994; Bullock and Minshull, 2005). Consequently, knowledge of the rifting evolution of the Goban Spur margin has been limited by the 2-D nature of previous studies and the sparsity of available geophysical data.

In order to improve understanding of the offshore Irish Atlantic rifted continental margins, deep long-offset multichannel seismic reflection data were acquired in 2013 by Eni Ireland for the Department of Communications, Climate Action & Environment of Ireland. In this study, six newly acquired seismic reflection profiles along the Goban Spur margin are processed and interpreted, providing improved regional coverage (Fig. 1b). Using the structural unit subdivision scheme for magma-poor margins proposed by Peron-Pinvidic et al. (2013), distinct crustal domains are identified and regionally extrapolated across the Goban Spur margin. This is achieved using a combination of seismic interpretation, gravity inversion results, magnetic and gravity anomaly observations, and constraints from drilling data. The improved data coverage allows for better characterization of the variations in rifting mode, rift-related magmatism, and insights into the tectonic evolutionary history of the Goban Spur margin.

2. Geological setting

The Goban Spur is a magma-poor rifted continental margin, situated offshore Ireland, south of the Porcupine Seabight Basin and Porcupine Bank, and west of the Fastnet Basin, the Comubian Platform, and the Western Approaches Basin (Fig. 1) (Horsefield et al., 1994; Bullock and Minshull, 2005). The Armorican margin is situated to the southeast of the Goban Spur margin forming the northern limit of the Bay of Biscay, which experienced rifting from the Jurassic to the Cretaceous (de Graciansky & Poag, 1985). At the southwest edge of the Goban Spur continental shelf, the bathymetry gradually increases from ~1000 m to 2500 m, before dropping off abruptly at the Pendragon Escarpment (Fig. 1b). Farther seaward, the Goban Spur transitions to the Porcupine Abyssal Plain (Fig. 1b) (de Graciansky & Poag, 1985).

Generally, the structural features of the Goban Spur can be attributed to the rifting of the European plate from the North American plate, with crustal thinning occurring at the end of the rifting phase during the early Cretaceous to middle Albian (Masson et al., 1984; de Graciansky et al., 1985). However, the formation of the Goban Spur margin has also been influenced by additional interrelated factors, including the formation of the Bay of Biscay, its interaction with its conjugate margin, and the presence of pre-existing structures (Dingle and Scrutton, 1977; Sibuet et al., 1985). The interaction between the margin-parallel NW- trending faults due to rifting and the pre-existing NE- trending fault system primarily controls the structure of the Goban Spur continental crust, with the northern Goban province likely an extension of the Fastnet Basin rather than the Cormubian Platform (Naylor et al., 2002). At the northern limit of the Goban Spur, the ENE-trending Porcupine Fault separates the Spur from the Porcupine Basin (Dingle and Scrutton, 1979) while the southern margin may be associated with faults developed in the northern Western Approaches Basin (Naylor et al., 2002). Based on seismic evidence, the NW-trending faults become more complicated and less continuous with more varied orientations towards the southeastward limit of the Goban Spur margin (Naylor et al., 2002). This complexity may be due to the influence of variable basement structure, interactions between the NW-trending fault systems and E-trending faults close to the Jean Charcot Escarpment (Sibuet et al., 1985), and transfer faults that segment the Goban Spur margin (Naylor et al., 2002).

During the Deep Sea Drilling Project (DSDP) Leg 80, four sites (548, 549, 550, and 551) were drilled on the Goban Spur (Fig. 1b) (de Graciansky et al., 1985). Site 548 was drilled near the edge of a half-graben with Devonian basement, and site 549 penetrated the Hercynian basement on the crest of the Pendragon Escarpment at 2335.5 m water depth. In addition, the earliest syn-tectonic sediments from the Barremian (possibly late Hauterivian) and oldest post-rift sediments from the early Albian were recovered at site 549, which revealed that the rifting phase lasted about 15 Myrs (de Graciansky et al., 1985; Masson et al., 1985). Site 550, at 4432 m water depth, was located in the abyssal plain southwest of the margin and drilled Albian basement. The site was ~135 km inboard of magnetic anomaly 34, which represents the first undisputed oceanic crust from seafloor spreading (Srivastava et al., 1988; Müller et al., 2016). Additionally, oceanic tholeiites were found at both sites 550 and 551 (de Graciansky et al., 1985).

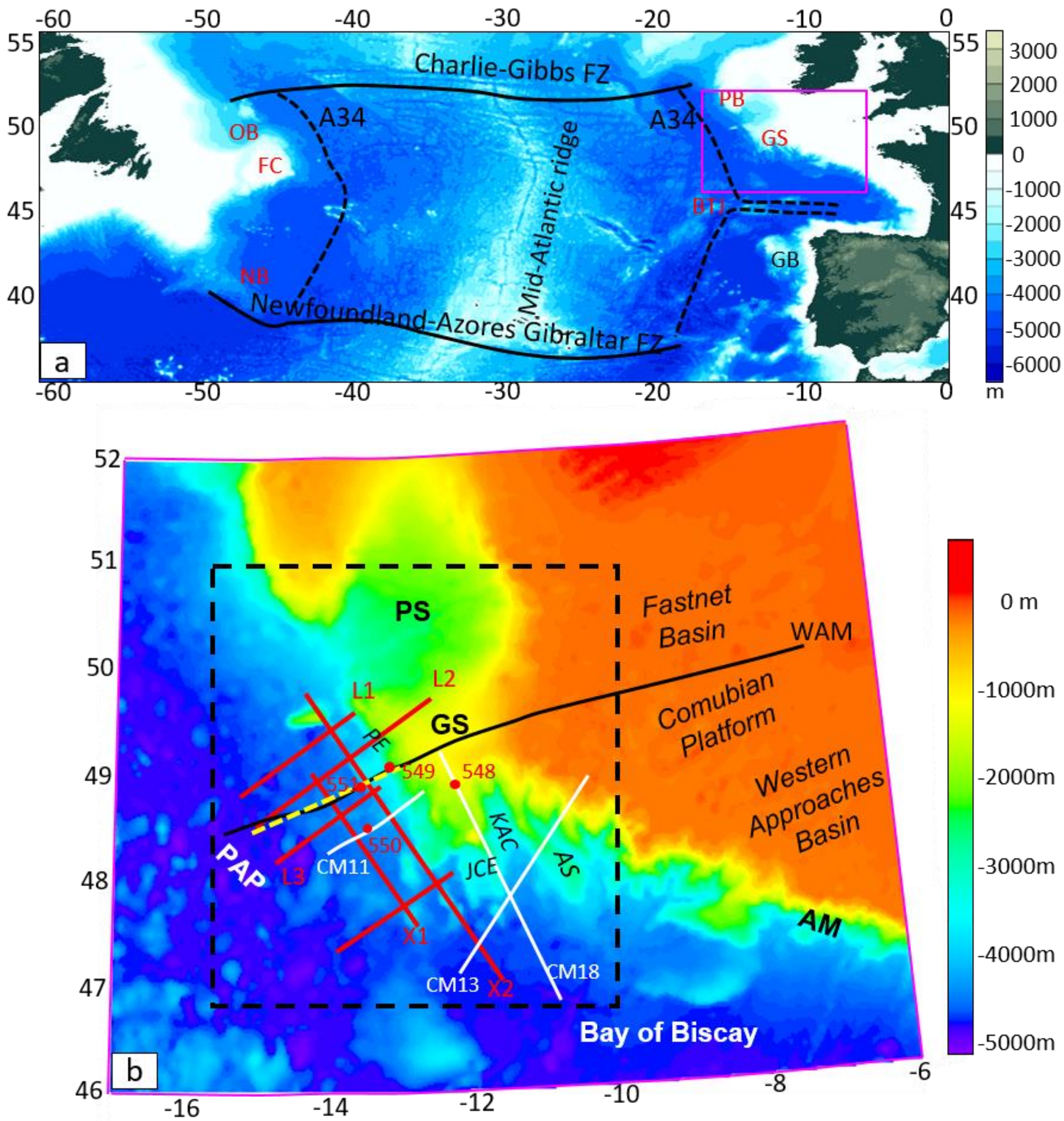

Fig. 1. (a) Bathymetric map of the North Atlantic where the dashed black line shows magnetic anomaly 34 (isochron A34; Müller et al., 2016), and the pink box shows the location of part (b). (b) Bathymetric map of the Goban Spur continental margin. Bathymetry data are from ETOPO1 Global Relief Model of the National Geophysical Data Center (NGDC) of the National Oceanic and Atmospheric Administration (NOAA). Red lines indicate the newly acquired seismic reflection lines (L1, L2, L3, L4, X1, and X2). The black solid line shows the Western Approaches Margin (WAM) line (Peddy et al., 1989). The white lines are the CM multichannel seismic profiles acquired in the 1970s (Masson et al., 1985). The yellow dashed line indicates the refraction line from Bullock and Minshull (2005). The red solid circles represent the DSDP Leg 80 drill sites (548, 549, 550, and 551). Crustal domains will be primarily delineated within the dashed black box. Abbreviations: AM: Armorican Margin; AS:Austell Spur; BTJ: Biscay Triple Junction; FC: Flemish Cap; FZ: Fracture zone; GB: Galicia Bank; GS: Goban Spur; JCE: Jean Charcot Escarpment; KAC: King Arthur Canyon; NB: Newfoundland Basin; PAP: Porcupine Abyssal Plain; PE: Pendragon Escarpment; PS: Porcupine Seabight Basin; PB: Porcupine Bank.

Due to the interpreted differential extension between the upper crust and the lower lithosphere at the Goban Spur, Masson et al. (1985) suggested that a uniform-stretching model was not applicable to the margin. Keen et al. (1989) favoured pure shear rifting and asymmetric lithosphere rupture based on seismic reflection data acquired across the NE Flemish Cap-Goban Spur conjugate margins. Since full lithospheric thinning is estimated to have been considerably greater than the observed thinning of the upper crust in the transitional zone across Goban Spur, Healy and Kusznir (2007) have argued for depth-dependent stretching, precluding a pure shear mechanism for the major deformation processes. Gerlings et al. (2012) argued for asymmetric deformation occurring during each stage of the tectonic evolution of the NE Flemish Cap-Goban Spur conjugate margins. Based on similarities in the inferred tectonic processes at the Goban Spur margin and those across the Iberia-Newfoundland margins (Sibuet and Tucholke, 2012), depth-dependent stretching of lithosphere, with crustal rupture preceding lithospheric mantle breakup, has been argued for the Goban Spur margin, just as it has for the Iberia-Newfoundland margins (Huismans and Beaumont, 2011). The geological and tectonic characteristics of the Goban Spur are complex and both time and depth dependent, introducing challenges for geophysical characterization.

3. Geophysical background

A number of single-channel and multi-channel seismic reflection profiles were acquired during the 1970s, including the CM profiles (white lines in Fig. 1b) (Montadert et al., 1979; Roberts et al., 1981; Masson et al., 1985). Although these vintage seismic profiles did not extend into the undisputed oceanic crust defined seaward of magnetic anomaly Chron 34 (Fig. 1b), they provided a good understanding of fault characteristics in the continental portion of the Goban Spur (Masson et al., 1985; Naylor et al., 2002). In 1985, the WAM line (black line in Fig. 1b) was acquired across the continental and oceanic crust of the Goban Spur, from which faults, half grabens, crustal types, volcanic features, and a relatively clear continent-ocean boundary were inferred (Peddy et al., 1989; Louvel et al., 1997). To complement the WAM line and quantitatively characterize the structure of the margin, including the presence and extent of igneous rocks, co-located seismic refraction experiments were acquired in 1987 (Horsefield et al., 1994) and 2000 (Bullock and Minshull, 2005), respectively. Based on the velocity model from the most recent seismic refraction profile (yellow dashed line in Fig. 1b), continental, transitional, and oceanic domains were defined for the Goban Spur margin, with velocities ranging from 5.2 to 5.8 km s^{-1} and from 6.6 to 6.9 km s^{-1} in upper and lower continental crust, respectively (Bullock and Minshull, 2005; Minshull et al., 2014). In the transitional and oceanic zones, P-wave velocity in the crust displays a relatively high gradient (4.5 - 6.8 km s^{-1} within 4 km beneath basement). In addition, P-wave velocities are high (> 7.1 km s^{-1}) at depths of 5-7 km beneath the basement of the 70-km-wide transitional region and Poisson's ratio at top basement of this region is higher than 0.34, indicating serpentinized exhumed mantle (Bullock and Minshull, 2005). Furthermore, the serpentinized exhumed mantle in the transitional zone is relatively highly magnetized, which can be attributed to the formation of magnetite during serpentinization (Bullock and Minshull, 2005; Minshull et al., 2014).

Free-air gravity data from the Goban Spur margin are shown in Figure 2a. The transition from negative to positive gravity anomalies lies parallel to the strike of the margin and coincides with inferred crustal thinning (Bullock and Minshull, 2005). To complement qualitative descriptions of the observed gravity data, gravity forward modelling and inversion have been applied to the margin (Bullock and Minshull, 2005; Welford et al., 2010b). Figure 2b shows crustal thicknesses derived from gravity inversion (Welford et al., 2010b), which reveal that, oceanward, the crust of the Goban Spur margin thins from ~29 km to ~5 km over a distance of ~250 km. Along the northern portion of the margin, the gradient in crustal thickness is larger, consistent with a relatively sharp necking zone. Along the southern portion of the margin, the crustal thickness varies slowly over a wider region, indicating a smoother necking profile. This also suggests that the distribution of continental, oceanic and transitional zones will likely vary from north to south.

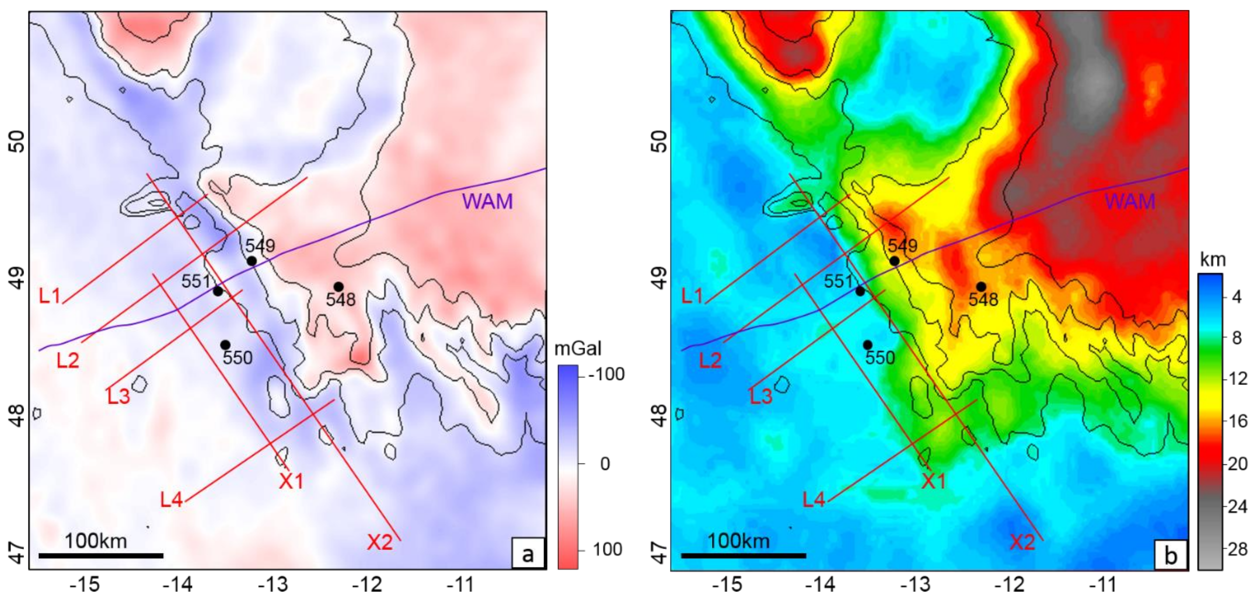

Fig. 2. (a) The free air gravity anomaly with overlying bathymetric contours (Bonvalot et al., 2012). (b) Crustal thickness derived from gravity inversion (adapted from Welford et al., 2010b) with overlying bathymetric contours. Present-day bathymetric contours (black lines) are displayed with a contour interval of 1000 m. The six red lines indicate the new seismic lines in this study; the purple line represents the WAM line. The black circles represent the DSDP Leg 80 drill sites.

Fig. 3 shows the magnetic anomaly data reduced to pole for the Goban Spur margin (Earth Magnetic Anomaly Grid at 2-arc-minute resolution from NOAA - http://www.ngdc.noaa.gov/geomag/emag2/). A linear band of high magnetization lies outboard and parallel to the black dashed line of magnetic Chron 34 (Müller et al., 2016). There also exists a relatively linear magnetic anomaly with a southeastern trend, approximately parallel to the black dashed line between seismic profiles L3 and L4 (purple dashed line in

Fig. 3). Generally, the further landward from magnetic Chron 34, the weaker the magnetic anomaly becomes, which might be associated with minor magmatic addition during rifting, in contrast to increasing magmatism during the initiation of seafloor spreading (Bullock and Minshull, 2005). The magnetic characteristics in the region between the continental slope and magnetic Chron 34 vary dramatically from north to south. Along the northern portion of the Goban Spur margin, a region of negative magnetic anomalies is very prominent (outlined by green dots in Fig. 3), where DSDP Sites 550 and 551 encounter basaltic rocks (de Graciansky et al., 1985). Magnetic modelling along the WAM line also demonstrates that a basalt sill located at the foot of the continental slope produces a prominent magnetic anomaly, with the causative body extending into the basement (Louvel et al., 1997; Bullock and Minshull, 2005).

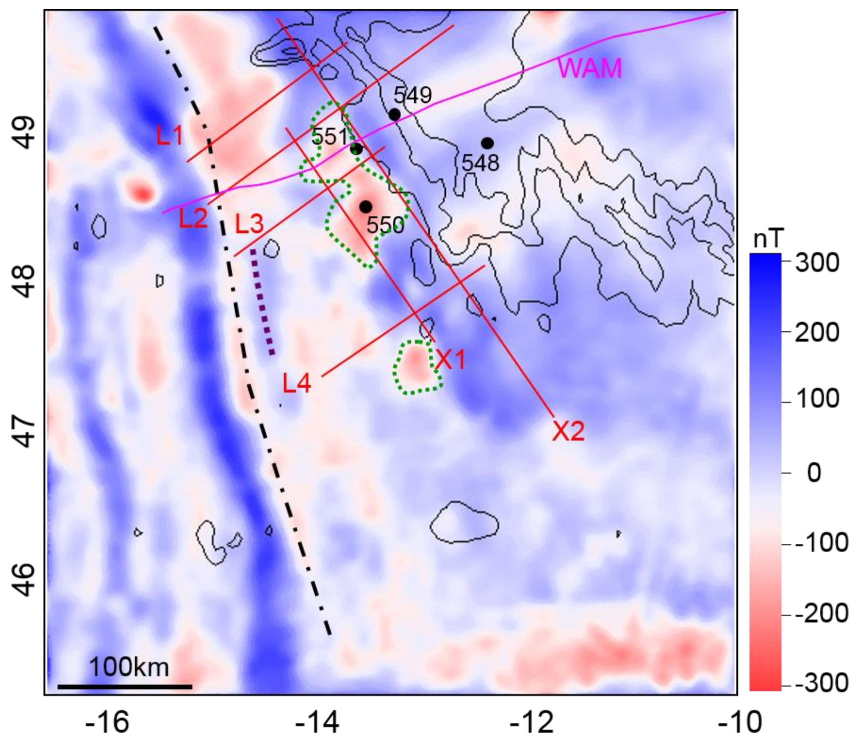

Fig. 3. Magnetic anomaly map across the Goban Spur margin. The dotted-dashed black line shows the location of magnetic Chron 34 from Müller et al. (2016). Bathymetric contours (black lines) are displayed with a contour interval of 1000 m. The two regions outlined by green dots denote highly magnetized regions. The dashed purple line indicates a relatively linear magnetic anomaly. The six red lines indicate the new seismic profiles; the pink line is the WAM line. The black circles represent the DSDP Leg 80 drill sites.

4. Seismic acquisition and methodology

In this study, six new multichannel seismic (MCS) reflection lines (L1, L2, L3, L4, X1, and X2) are processed and interpreted (Fig. 1b). Seismic profiles L1, L2, L3, and L4 are oriented southwest-northeast, and profiles X1 and X2 cross these four lines, with a northwest-southeast orientation (Fig. 1b). During acquisition, the survey vessel BGP Explorer towed an array of 48 air guns that were fired with a total volume of 85 L and a shotpoint interval of 25 m for water depths less than 3000 m and 37.5 m for water depths over 3000 m. The seismic data were acquired with a sampling interval of 2 ms and a trace length of 12 s. Data were recorded using a 10 km-long hydrophone streamer with a 12.5 m receiver group spacing, generating 804 traces per shot.

The seismic data processing workflow involves geometry definition with a common-midpoint (CMP) interval of 6.25 m, amplitude compensation, bandpass filtering, predictive deconvolution, multiple attenuation, velocity analysis, pre-stack Kirchoff time migration, and coherency filtering. Next, the migrated stacked sections are converted from the time domain to the depth domain. Finally, the newly acquired seismic reflection lines across the Goban Spur rifted margin are interpreted in the depth domain by incorporating insights from seismic refraction data, the complementary WAM line, gravity and magnetic data, crustal thickness estimates from seismic refraction surveys and gravity inversion, and borehole data from DSDP Leg 80.

Since L1, L2, the WAM line, and the Bullock and Minshull (2005) refraction line extend into the oceanic domain and cross magnetic anomaly 34 (Figs. 1b and 3), the data coverage is sufficient for investigating the range of tectonic processes from rifting and extension, to the subsequent breakup, and the eventual creation of new oceanic crust. In order to directly compare lines L1 to L4 with the WAM line, the WAM line is reinterpreted in the depth domain. The primary classification standard used for the crustal domains is briefly reviewed in the next section, before discussing the interpreted sections in detail.

5. Interpretations

5.1 Interpretation criterion

Although the crustal architecture of rifted margins can vary significantly, they still share some first-order structural components (Osmundsen and Ebbing, 2008; Minshull, 2009; Sutra et al., 2013; Tugend et al., 2014a). Peron-Pinvidic et al (2013) recommend five structural units to describe the transition from unstretched continental crust to oceanic crust; these include: 1) proximal, 2) necking, 3) hyperextended, 4) exhumed, and 5) outer domains. These structural units show contrasting characteristics in terms of basin types, faulted features, and crustal thickness variations, but also correspond to four evolutionary phases of rifted margins: 1) the stretching phase, 2) the thinning phase, 3) the hyperextension and exhumation phase, and 4) the initiation of seafloor spreading and magmatism phase. Using the structural unit division of rifted margins proposed by Peron-Pinvidic et al. (2013) in this study, the corresponding interpretations laterally divide each seismic line into different crustal domains.

The proximal domain undergoes stretching with low extensional values and is commonly characterized by grabens or half-grabens containing syn-rift sediments (Mohn et al., 2012; Peron-Pinvidic et al., 2013). Tilted blocks bounded by listric faults are often observed at the top basement of proximal basins (Whitmarsh et al., 2001). These faults generally terminate in the middle crust without affecting the Moho (Peron-

Pinvidic et al., 2013). Although crustal thickness is generally greater than 30 km in the proximal setting (Peron-Pinvidic et al., 2013), in this study, it appears to be approximately 21 km at the Goban Spur margin based on seismic refraction modelling (Scrutton et al., 1979; Bullock and Minshull, 2005). The new seismic profiles in the study do not extend to the proximal region so the seaward limit of the proximal zone is primarily delineated according to crustal thickness greater than ~21 km as derived from gravity inversion (Welford et al., 2010b).

The delineation of hyperextended and necking zones on the new seismic profiles is based on basement morphology, imaged crustal faulting, evidence of tilted fault blocks, and crustal thicknesses derived from gravity inversion. The lithospheric thickness dramatically decreases in the necking zone, which gives the crust a wedged structure (Mohn et al., 2012). Within the wedged region, the Moho drastically shallows due to crustal thinning from ~30 km to less than 10 km (Peron-Pinvidic and Manatschal, 2009). The crustal thickness from gravity inversion (Fig. 2b) and the fault patterns and basement topography on seismic profiles are used to delineate proximal and necking zones for each seismic line in this study.

Hyper-thinning of the crust is often observed in both hyperextended and exhumed zones (Peron-Pinvidic et al., 2013). Generally, there is a prominent change in seismic facies at the boundary between the stretched continental crust and exhumed serpentinized mantle (Nirrengarten et al., 2018). The hyper-thinned crust is characterized by hyperextended sag basins and half-grabens and the corresponding crustal thickness is generally less than 10 to 15 km (Tugend et al., 2014b). The hyperextension stage is important in the evolution of magma-poor margins, and it often, but not always, leads to mantle exhumation (Peron-Pinvidic et al., 2013). Therefore, we try to interpret both the hyperextended and exhumed domains separately to distinguish the hyperextension stage and the exhumation stage. Currently, understanding of the nature of the basement in the hyperextended and exhumed domains still lacks consensus. In this study, these two domains are delineated based on the interpretation of the Bullock and Minshull (2005) velocity model, in which the continental crust, the oceanic crust, and the serpentinized mantle domain are identified. Following the subdivision of the exhumed mantle zone proposed for the Galicia Bank margin (Dean et al., 2000; 2015) and the southeastern margin of Flemish Cap (Welford et al., 2010a), we also subdivide the exhumation zone between the oceanic and the hyperextended domains into a region of shallower peridotite ridges and a region of deeper exhumed serpentinized mantle with more subdued topography. By specifically following the subdivision from Welford et al. (2010a), labelled subdomains T1 and T2 are used to differentiate between the transitional crust characterized by smooth basement relief (subdomain T1) and peridotite ridges (subdomain T2) in the exhumed mantle domain, respectively (Fig. 4). This does not mean that the shallower peridotite ridges (subdomain T2) are identified on all of the seismic profiles in the study area. The identification of the shallow peridotite ridge zone is based primarily on basement morphology and weak reflectivity patterns within syn-rift sedimentary layers.

In this paper, the outer domain is not interpreted on the seismic profiles because it is indistinct and poorly imaged, and thus may be included into the exhumed domain (Moulin et al., 2005). Crustal thickness in the oceanic domain ranges from 4 km to 7 km in proximity to the Goban Spur margin (Scrutton, 1979). The interpretation of oceanic crust is also constrained by magnetic Chron 34 and the interpretation of the Bullock and Minshull (2005) refraction line.

In addition, as sediments deposited on continental margins record rifting and final lithospheric rupture, pre-, syn-, and post-rift sequences are used to describe the stratigraphic successions at the Goban Spur margin. Pre-rift sequences are commonly onlapped by syn-rift infills in the wedge-shaped half-graben basins bounded by faults, recognized by angular unconformities on seismic data (Franke, 2013).

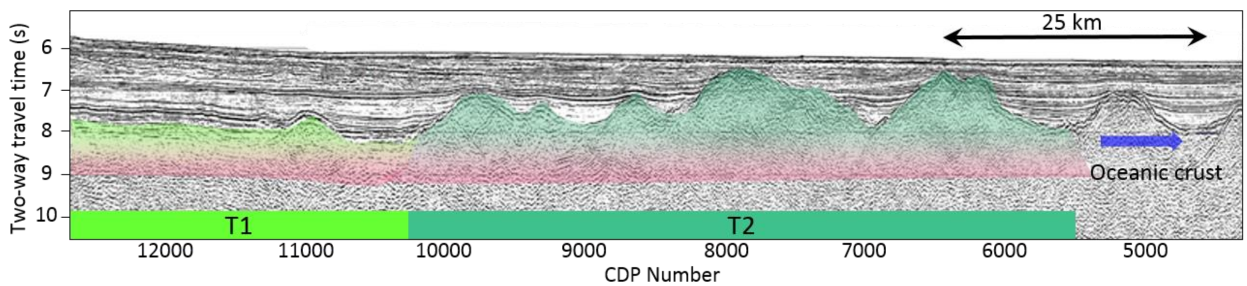

Fig. 4. Portion of the interpreted seismic profile Erable 56 along the Flemish Cap margin (Welford et al., 2010a). Labelled subdomains T1 and T2 represent the exhumed serpentinized mantle with relatively deep basement and shallow ridges, respectively.

5.2 WAM line interpretation

The WAM line, which crosses magnetic Chron 34, is presented first as it is the only line with approximately coincident constraints from seismic refraction modelling (Fig. 5a). The Bullock and Minshull (2005) velocity model interpretation, when projected to the WAM line, helps constrain the landward limit of the oceanic domain, which defines the boundary between the oceanic domain and the exhumed mantle domain (Fig. 5d). Along with the velocity model, the slow-spreading oceanic domain spans ~45 km with an average crustal density of 2.74 kg m^{-3} (Bullock and Minshull, 2005; Minshull et al., 2014). Correspondingly, the newly interpreted oceanic domain along the WAM line spans ~70 km and its landward limit lies to the northeast of magnetic Chron 34 (Fig. 5c). The basement relief of the oceanic domain between model distances of 44 km and 70 km is more subdued than that of the normal oceanic zone seaward of magnetic Chron 34. Although the zone between the thinned continental crust and the oceanic crust is interpreted as exhumed serpentinized mantle based on the velocity-depth structure (Fig. 5d) (Minshull et al., 2014), a further subdivision into three parts is warranted based on the basement morphology and seismic character; these three parts are the hyperextended zone (shaded brown), and the exhumed mantle zone, further subdivided into a section with deeper basement displaying smooth basement morphology (subdomain T1, shaded light green), and a section of serpentinized peridotite ridges with relatively shallower basement with rougher relief (subdomain T2, shaded dark green) (Fig. 5c).

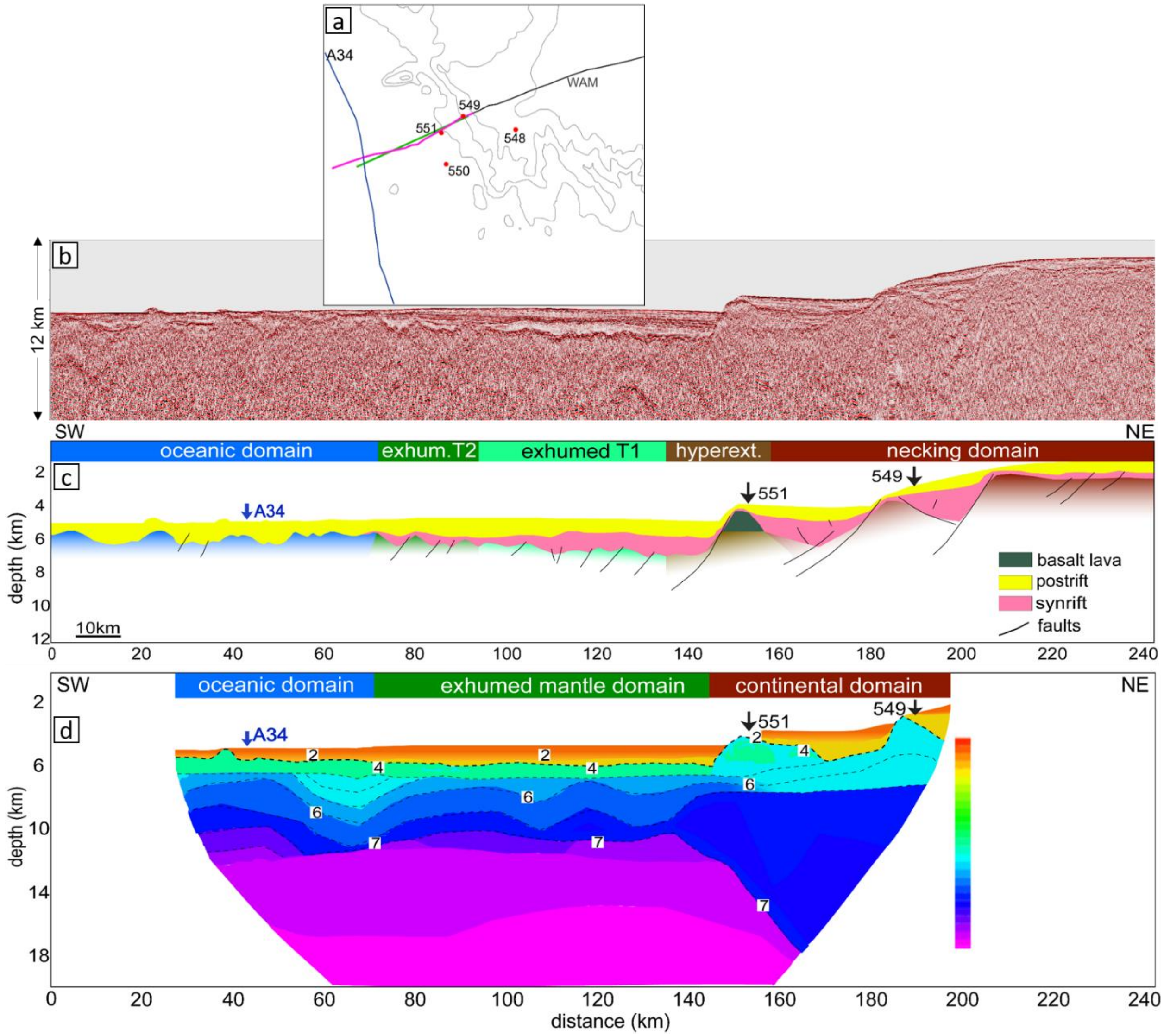

Fig. 5. (a) Location of the WAM line and refraction line across the Goban Spur, as indicated by the pink and green lines, respectively. Bathymetric contours (black lines) are displayed with an interval of 1000 m. The solid blue line shows the trend of magnetic Chron 34 (Müller et al., 2016). (b) Portion of uninterpreted WAM line. (c) Interpretation of a segment of the WAM line. (d) Velocity structure derived from seismic refraction modelling (adapted from Minshull et al., 2014). Sites 549 and 551 are projected onto the WAM line from ~2.8 km and ~1.5 km away, respectively.

Transitional subdomain T2 lies adjacent to the oceanic domain and spans ~20 km. The geometry of the peridotite ridges also appears similar to the ridges imaged on the Iberia/Galicia margin (Pickup et al., 1996) and the conjugate Newfoundland/Flemish Cap margin (Fig. 4) (Welford et al., 2010a). Several Ocean Drilling Program (ODP) drill sites on both the Iberia margin and Newfoundland margin have revealed that the equivalently interpreted ridges are composed of exhumed serpentinized mantle material (Sawyer et al., 1994; Whitmarsh et al., 1998; Tucholke et al. 2004), which has been complemented by seismic refraction and reflection data (Pickup et al., 1996; Dean et al., 2000; Shillington et al. 2006; Van Avendonk et al., 2006). At the Goban Spur margin, both Poisson's ratio values (0.34-0.36) and velocities (> 7 km s^{-1} at depths of 5-7 km beneath top basement) obtained from seismic refraction modelling support the presence of serpentinized exhumed mantle in the subdomains T1 and T2 (Bullock and Minshull, 2005; Minshull et al., 2014). However, the velocities ranging from 7.2 km s^{-1} to 7.6 km s^{-1} within ~ 1.5 km of the top basement in the subdomain T1 at the Goban Spur margin are different from those at the Iberia margin (7.3-7.9 km s^{-1} within 2-6 km below basement) (Dean et al., 2000). At a model distance of ~95 km, the depth to basement deepens landward by ~400 m and becomes relatively smoother (Fig. 5c). Reflection amplitudes within the syn-tectonic sedimentary successions typically appear very weak above the top basement of subdomain T1 (Fig. 5b). This characteristic is used to distinguish the transitional subdomain T1 from the hyperextended domain where the reflective events of the syn-rift formations are relatively continuous and clear. The initial oceanic basement is much shallower than the exhumed basement (Fig. 5c). Landward adjacent to the hyperextended zone is the necking zone with multiple tilted faults (Fig. 5c), corresponding to the continental slope of the Goban Spur margin. In the necking domain, the Moho depth derived from gravity inversion decreases from ~20 km to ~10 km over a distance of ~85 km (Welford et al., 2010b). A basaltic body is shown at the toe of the necking zone along the WAM line. This body was sampled by DSDP drilling site 551 and was used to infer the location of initial oceanic crust formation (Horsefield et al., 1994). However, Bullock and Minshull (2005) argued that the emplacement of the basaltic body occurred during lithosphere thinning before the mantle material began to be exhumed at the Goban Spur. Stratigraphically, the post-rift section directly overlies all of the crustal domains along the WAM line, while the syn-rift sediments gradually pinchout towards the oceanic domain, displaying highly variable sedimentary thicknesses from NE to SW (Fig. 5c).

5.3 Crustal domain interpretation

Since seismic profiles L1, L2, L3, and L4 are subparallel to each other (Fig. 1b) and the distance between L1, L2 and L3 is relatively small, with ~ 36 km, and ~42 km between L1 and L2, and L2 and L3, they share numerous features. As the WAM line lies within the region intersected by lines L1, L2, and L3, its interpretation is extrapolated to these other profiles. To ease identification of the boundary delineation between transitional subdomains T1 and T2, the WAM line and the four new seismic lines (L1-L4) are truncated to the same length to highlight the seismic reflection character within the transitional zones in Figure 6. L1 and L2 cross magnetic Chron 34 and extend ~21 km and ~9 km seaward of magnetic Chron 34, respectively. Meanwhile, the seaward ends of seismic profiles L3 and L4 are ~6 km and ~54 km landward of magnetic Chron 34.

As introduced above, the boundary between the oceanic crust and the exhumed domain on the WAM line is based on crustal velocity constraints. By comparing the characteristics of basement topography and reflectivity of syn-rift sedimentary layers against the WAM line interpretation, the subdivisions of the exhumed domain along seismic lines L1 and L2 are inferred (Figs. 6 to 8). West of the interpreted peridotite ridges (shaded dark green) lies oceanic crust along both lines L1 and L2 (Figs. 6b, 6c, 7, and 8). The serpentinized peridotite ridges (subdomain T2) span ~16 km along L1 (Figs. 6b and 7), and ~22 km along L2 (Figs. 6c and 8). In the exhumed mantle domain on seismic lines L1 and L2, sub-horizontal intra-basement reflectors are observed ~ 2.5 km (~ 1 s TWT) below the top basement (red lines in Figs. 7 and 8), where the interpreted normal faults usually root in. These discontinuous intra-basement reflections are also visible in the zone of exhumed mantle at the Iberia-Newfoundland margins and the Armorican margin, and interpreted as the decoupling interfaces (Gillard et al., 2019). Compared with the WAM line, line L1, and line L2, the basement morphology outboard of the interpreted subdomain T2 on seismic profile L3 is more complicated due to the presence of a seamount and more uncertain due to the lack of nearby velocity constraints or intersecting magnetic anomaly trends (Fig. 3). Nonetheless, the interpretation for subdomain T2 from the northern lines is projected to L3 and is restricted to ~28 km based on basement morphology similarities and for regional continuity (Figs. 6e and 9). Normal faults observed in the exhumed mantle zone of profile L3 root in the sub-horizontal and landward-dipping intra-basement reflectors as well (Fig. 9). On lines L1 to L3, the basement relief of transitional subdomain T1 (shaded light green) is generally smoother and deeper than of transitional subdomain T2 (Figs. 6 to 9). The width of the interpreted transitional subdomain T1 consistently ranges from between ~36 km and ~46 km along each of these northern seismic lines (L1, L2, and L3). Weaker reflectivity within the overlying syn-tectonic sedimentary formations for the T1 subdomain are striking and similar for the lines from L1 to L3 (Figs. 6 to 9). Also, chaotic strong reflectors sporadically embedded in the syn-tectonic formations are visible on lines L2 and L3, likely associated with magmatic sills (indicated by the black arrows in Fig. 6).

The exhumed domain interpretation of seismic profile L4 is described last because it is the least constrained and the least like the lines to the north in terms of basement morphology and seismic character (Fig. 6). Profile L4, 113 km to the south of L3, lies significantly landward of magnetic anomaly 34 (Fig. 1b) and lacks velocity constraints. Basement reflectivity along the southwestern half of profile L4 is less continuous and highly faulted, and the depth of the top basement along the segment is ~5.6 km, shallower than the top-basement depth (~6.5 km) of the oceanward northern profiles (L1-L3), possibly due to proximity to the complex stress field near the BTJ. The basement morphology is relatively smooth and without ridges (Fig. 6). In addition, the magnetic anomaly trend is relatively homogeneous along the southwestern half of profile L4 and extends a further ~18 km outboard of the southwestern endpoint of profile L4 (Fig. 3). Moreover, sporadic intra-basement reflectors are also visible in this region (Fig. 10). Therefore, we interpret the southwestern half of L4 as corresponding to subdomain T1 for regional consistency (Figs. 6f and 10).

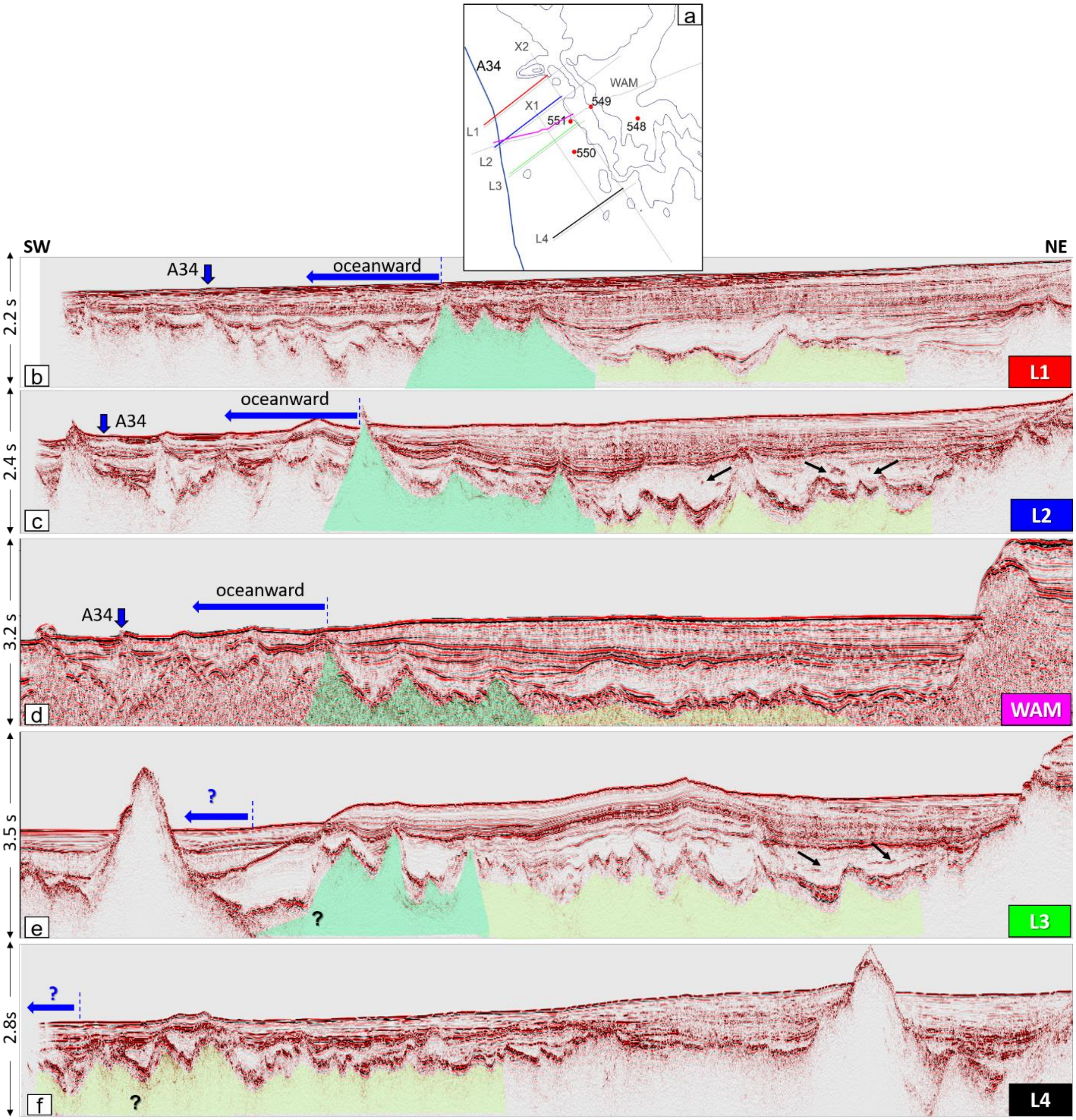

Fig. 6. (a) The location of the parallel seismic lines in the time domain, as indicated by different colors. (b)-(f) show the interpreted seismic lines L1, L2, the WAM line, L3, and L4 from northwest to southeast. The transparent dark green areas indicate the interpreted serpentinized peridotite ridges with rougher shallow basement (subdomain T2). The light green regions correspond to the interpreted exhumed mantle displaying subdued topography at top-basement (subdomain T1).

In Figures 7 and 8, the interpreted hyperextended zone spans ~37 km and ~28 km along profiles L1 and L2, respectively, where sag basins and tilted fault blocks are well developed and crustal thickness ranges from

~5.5 km to ~ 10 km (Fig. 2b). Landward, major west-dipping faults are observed with half-graben basins along both seismic profiles (Figs. 7 and 8). On profile L3, the hyperextended zone is ~9 km wide. Similar to seismic profiles L1 and L2, west-dipping faults in the necking zone are also observed along seismic profile L3 (Fig. 9).

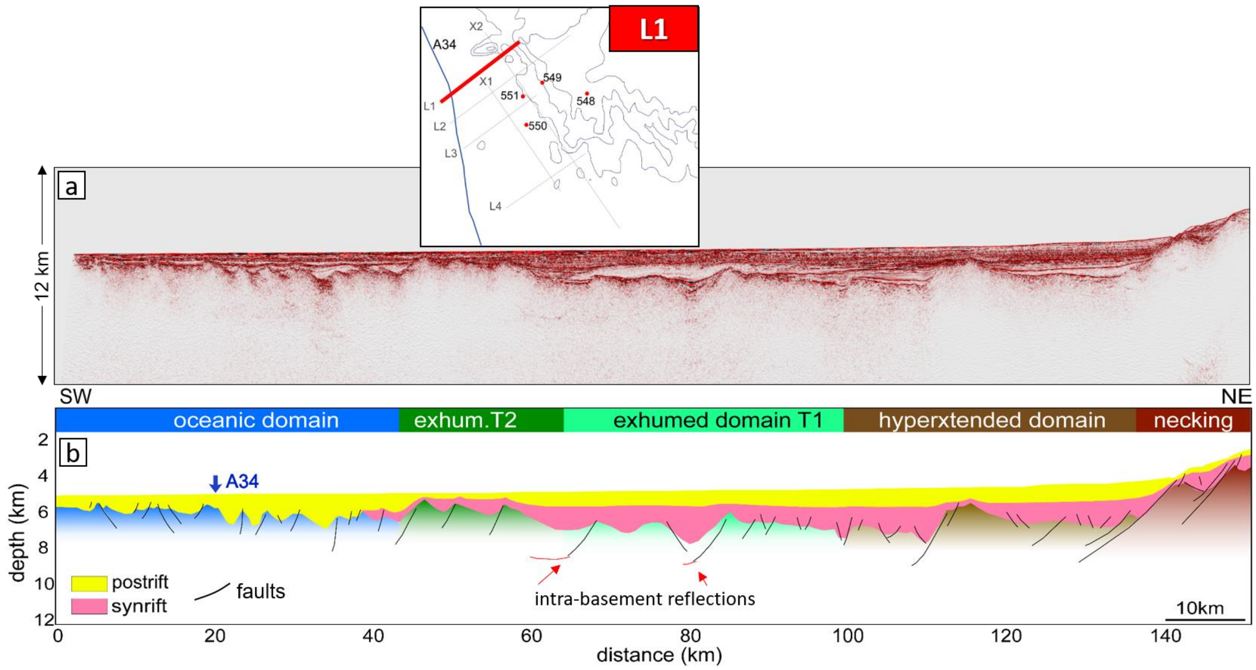

Fig. 7. (a) The uninterpreted depth-converted seismic profile L1. (b) The interpreted seismic profile L1 in the depth domain. The red arrows indicates intra-basement reflections.

Interpretation of the hyperextended and necking domains along profile L4 is again impeded by lack of constraints. Nonetheless, in this study, the two seismic crosslines X1 and X2 are crucial for validating crustal domain subdivisions and ensuring regional consistency in the interpretations. Thus, the interpretation of L4 is aided by extending crustal distribution interpretations from the northern lines (L1 to L3) across and along seismic profile X1 (Fig. 11). To the southeast, the crustal thickness ranges from ~6 km to ~9.3 km along profile X1 (Fig. 2b). At the northwest end of profile X1, weak reflectivity is observed for the syn-rift sedimentary layers over a distance of ~55 km. Immediately to the southeast (55-110 km), the syn-rift sedimentary layers become thinner, and the basement reflectors are more chaotic and highly faulted, likely associated with magmatic activity. Also, this region is consistent with the high-amplitude magnetic anomalies (Fig. 3) and the interpreted sill distribution from Naylor et al. (2002). Further to the southeast, reflectivity becomes more laterally consistent with evidence of crustal faulting with horsts and grabens (Fig. 11). Thus, we interpret the southeasternmost half of profile X1 as corresponding to the hyperextended domain. Consequently, the intersection of profiles L4 and X1 is interpreted as a region of hyperextended crust.

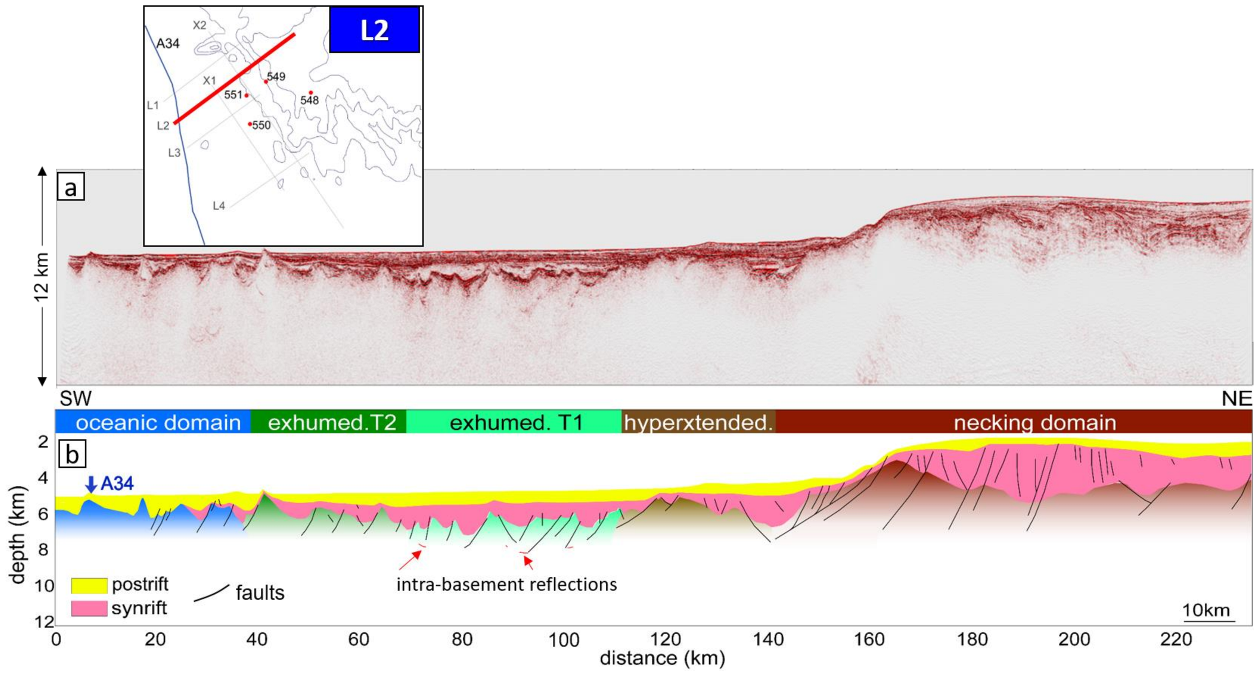

Fig. 8. (a) The uninterpreted depth-converted seismic profile L2. (b) The interpreted seismic profile L2 in the depth domain.

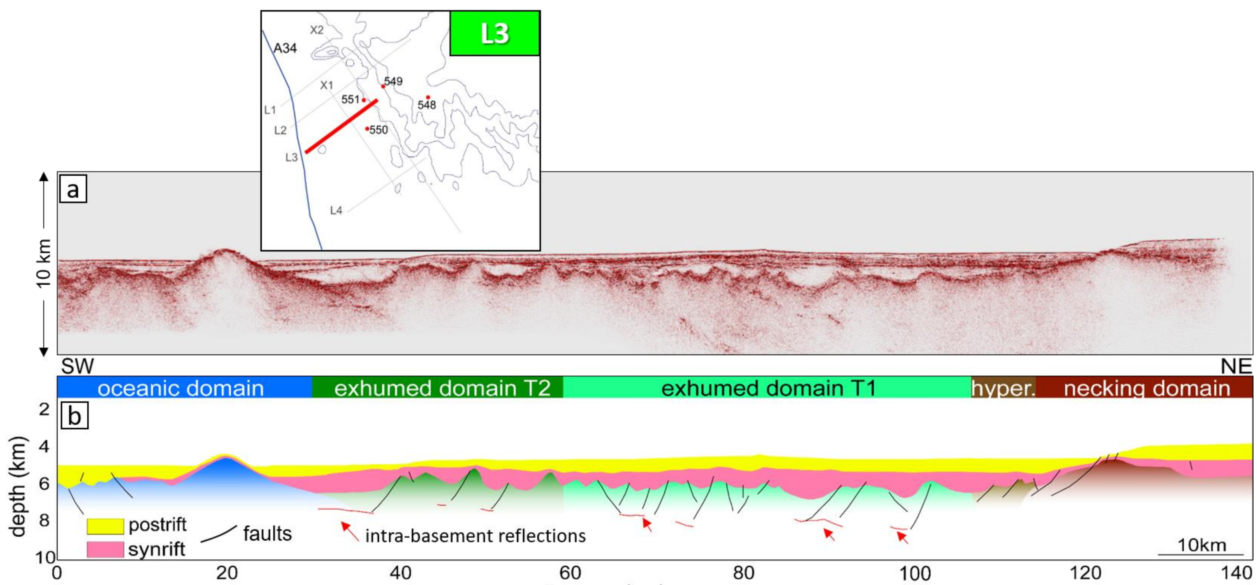

Fig. 9. (a) The uninterpreted depth-converted seismic profile L3. (b) The interpreted seismic profile L3 in the depth domain.

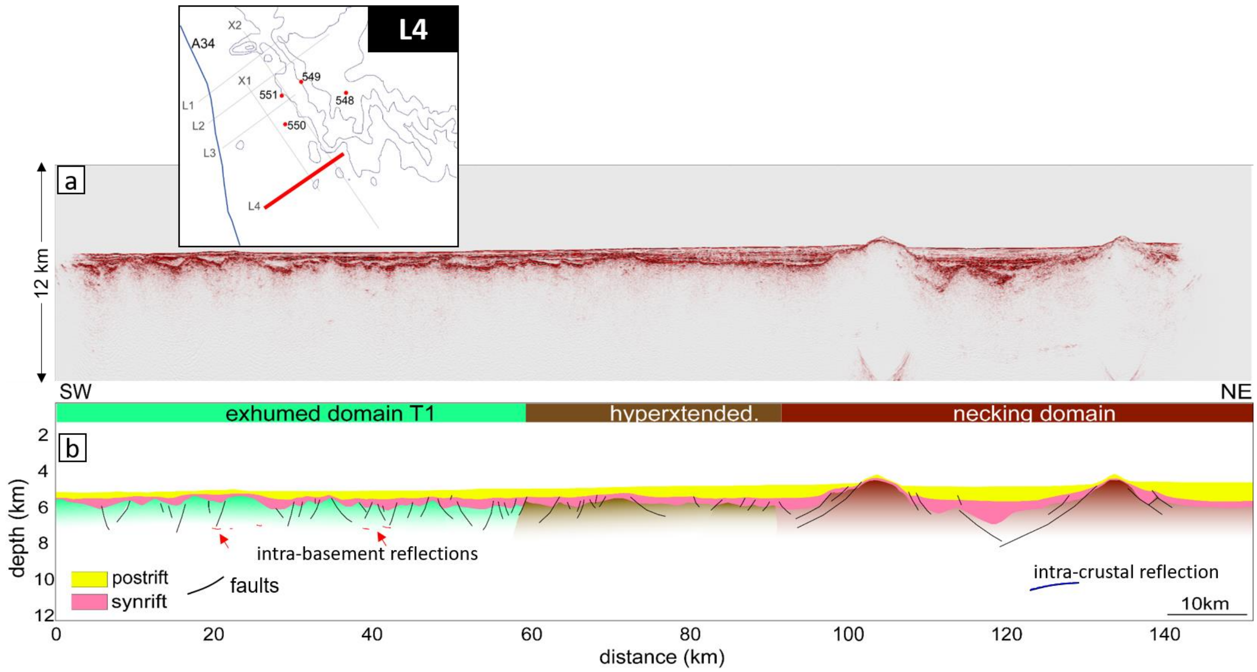

Fig. 10. (a) The uninterpreted depth-converted seismic profile L4. (b) The interpreted seismic profile L4 in the depth domain.

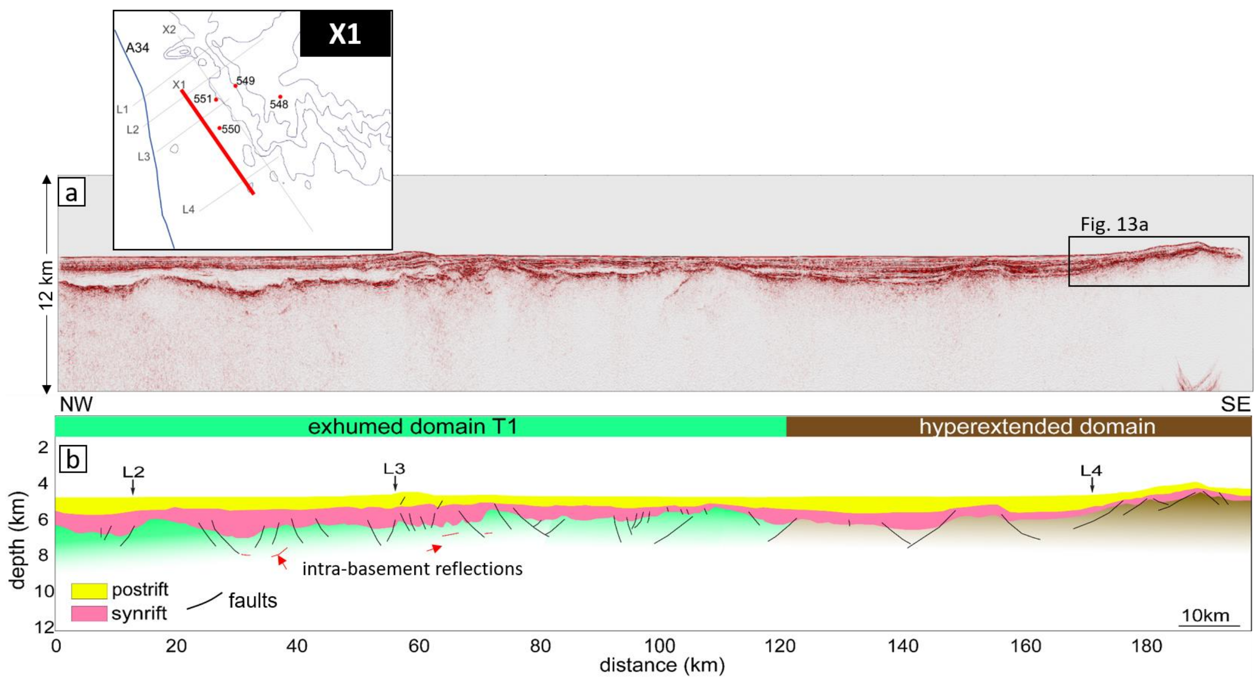

Fig. 11. (a) The uninterpreted depth-converted seismic profile X1. (b) The interpreted seismic profile X1 in the depth domain.

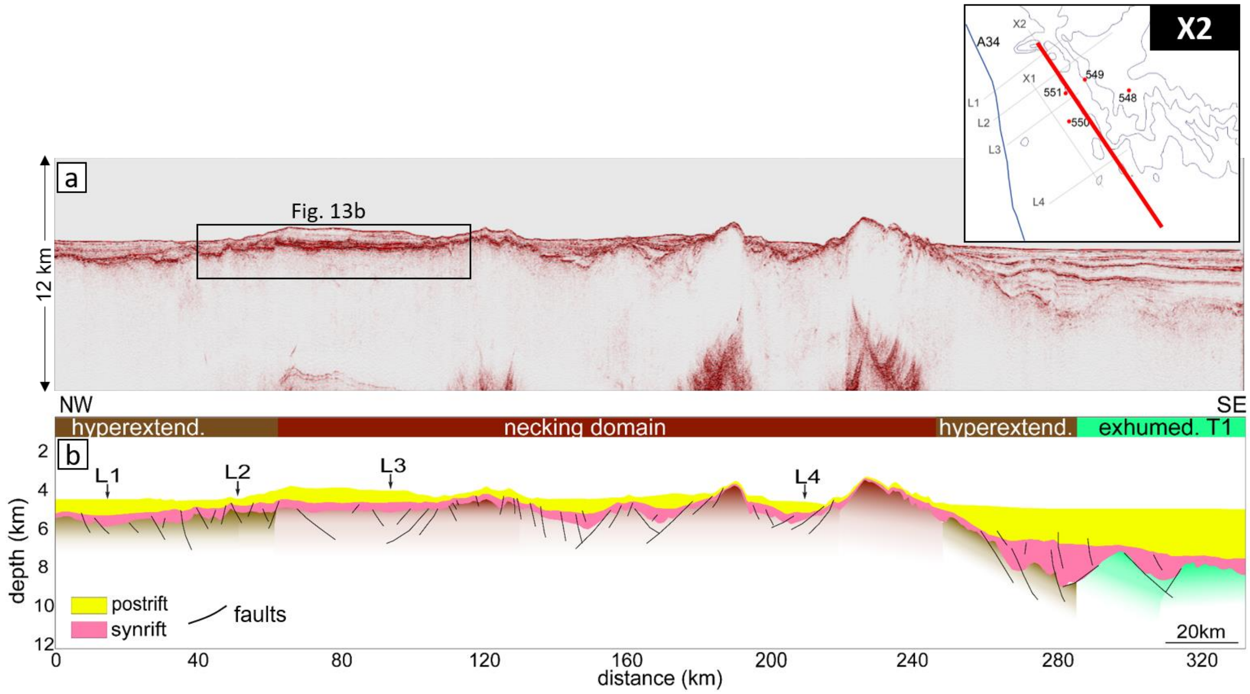

Fig. 12. (a) The uninterpreted depth-converted seismic profile X2. (b) The interpreted seismic profile X2 in the depth domain.

Along L4, the boundary between the exhumed and hyperextended zones is placed at a line distance of ~58 km, at the seaward limit of imaged rotated fault blocks, while the border between the hyperextended and necking zones is placed at ~90 km based on the crustal thicknesses from gravity inversions. The crustal thickness ranges from ~6.9 km to ~9 km in the hyperextended zone, while it has a range of ~ 9.4-12 km in the necking zone (Figs. 2b). In addition, weak amplitudes at a depth of ~10 km in the necking zone along profile L4 indicate intra-crustal reflectivity since Moho depth is about ~15 km based on gravity inversion results (Welford et al., 2010b).

Compared with seismic profile X1, profile X2 is much longer and was acquired closer to the continental shelf (Fig. 1b). Profile X2 intersects seismic profiles L1, L2, L3, L4, and the WAM line (Fig. 1b), and is interpreted in Figure 12 based on the intersecting interpretations (Figs. 5-11). Thus, along profile X2, from northwest to southeast, the hyperextended zone spans ~62 km and the necking zone spans at least 150 km to L4. To the southeast of L4, the crustal domains are interpreted on the basis of the interpreted reflectivity, basement morphology, and a northward extrapolation of the exhumed mantle zone from the Armorican margin interpreted by Tugend et al. (2014b). In addition, the prominent continuous high-amplitude reflectors at the top basement within the thinned continental crust along profiles X2 and X1 display similar features (Fig. 13), roughly corresponding to high magnetic anomalies (green dots in Fig. 3).

Overall, from the new seismic profiles (Figs. 5-13), it is evident that the relief of the top basement varies significantly, which is accompanied by dramatic changes in seismic facies from north to south along the margin. Faults are observed in all crustal-type domains. Furthermore, thicknesses of syn- and post-rift sedimentary layers are highly variable both along and across the strike of the margin.

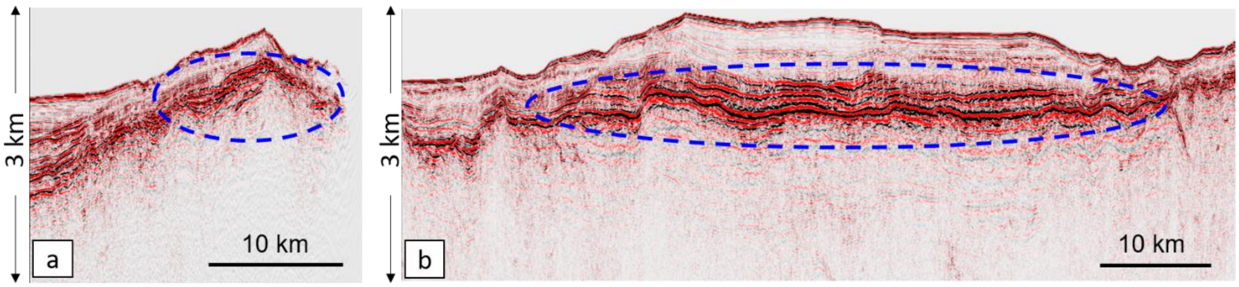

Fig. 13. (a) The expanded seismic section of the black box shown in Fig. 11 and (b) the expanded seismic section of the black box shown in Fig. 12. The blue circles show anomalously strong-amplitude reflectors at the top basement.

6. Discussion

6.1 Crustal architecture

The presented interpretations for the new seismic profiles (Figs. 5 to 13) have allowed us to map the crustal architecture across the Goban Spur margin (Fig. 14). The newly constrained crustal domains are complemented by interpreted domains from the surrounding regions derived from gravity inversion (Welford et al., 2010b; Tugend et al., 2014b; Sandoval et al., 2019). The landward extent of the new seismic lines into the stretched continental crust is limited so the interpretation from Naylor et al. (2002) is used to depict structures in the continental domain (Fig. 14). CM multichannel seismic profiles (white lines shown in Fig. 1b) are also used to help validate our interpretation (Masson et al., 1985), although the data quality is much poorer. Constraints in the south are fewer than to the north, so many uncertainties remain for understanding the southern part of the margin. It is also noted that the boundaries between the crustal domains are much more diffuse than depicted, as reactivation of structures during subsequent rifting stages has likely happened over the tectonic evolution of the margin (Peron-Pinvidic and Manatschal, 2009). Nonetheless, the crustal architecture map in Figure 14 still significantly increases our regional knowledge of the Goban Spur margin structure.

6.1.1 Proximal domain

The proximal domain across the Goban Spur margin experienced limited extension, characterized by normal faults (Fig. 14) (Naylor et al., 2002), which is similar to many other rifted continental margins, such as Iberia-Newfoundland, and the mid-Norway-East Greenland rifted margins (Peron-Pinvidic et al., 2013). The seaward limit of the proximal zone is in agreement with the WAM line interpretation (Peddy et al., 1989), the only seismic line extending into the proximal domain in this study. The formation of the proximal zone corresponds to the initial lithosphere stretching during the late Paleozoic and early Mesozoic, accompanied by regional faulting, forming half-grabens and horsts (de Graciansky and Poag, 1985).

6.1.2 Necking domain

The necking zone is divided into three subdomains according to their crustal thicknesses (Welford et al., 2010b; Fig. 2b), as defined and color-coded by Sandoval et al. (2019). The crustal thicknesses for necking domains 1, 2, and 3 range from ~21 km to ~16 km, from ~16 km to ~12 km, and from ~12 km to ~9 km, respectively. Along strike of the Goban Spur margin, the width of the necking domain increases from northwest to southeast. This may reflect differential extension rates during lithosphere thinning. It has been postulated that the limit of the seaward-thinning continental crust corresponds to a coupling point, separating decoupled deformation (continentward) from coupled deformation (oceanward) from the lithospheric rheology perspective, according to Perez-Gussinye et al. (2003). The differential stretching in the necking zone may result from rheologically-governed detachment structures overlying the lower crust facilitating greater extension of the upper and middle crust, as has been proposed for the Porcupine Seabight Basin (Naylor et al., 2002). Two major orientations of faulting control the structural patterns within the necking zone: NW-SE trending normal faults are approximately parallel to the strike of Goban Spur; and the NE-SW faults are approximately perpendicular to the margin strike (Dingle and Scrutton, 1979), aligned with the new seismic data in this study.

6.1.3 Hyperextended domain

The hyperextended domain consists of a narrow belt with variable widths along strike of the Pendragon Escarpment (Fig. 1b). Toward the Armorican margin in the south, the hyperextended domain becomes wider, although this geometry is only constrained by gravity inversion results (Tugend et al., 2014b). The boundary between the hyperextended and exhumed mantle regions roughly corresponds with the area where the magnetic anomaly features change along the strike of the margin (Fig. 3). The regions of both the necking and hyperextended zones become wider approximately half-way along the margin, which may be attributed to an interpreted transfer fault close to Sites 548 and 550 that obliquely changes the deformation from ENE-WSW to NE-SW (Bellahsen et al., 2013).

6.1.4 Exhumed mantle domain

In the exhumed domain, the crust experiences such intense hyper-extension and embrittlement that the extensional faults that provide the conduits for serpentinizing the mantle become detachment faults along which the serpentinized mantle was ultimately exhumed (Reston, 2007; Mohn et al., 2012). At some magma-poor margins, the extensional detachment faults are visible in the exhumed domain, characterized by high-amplitude reflectors, for instance, the S-reflector at the Galicia margin (Reston, 2009). In contrast, at the Goban Spur, some discontinuous intra-basement reflectors in the exhumed zone along the SW-NE oriented seismic profiles and the SE-NW oriented seismic line X1 have low amplitudes (Figs. 7-11). These sub-horizontal, SW- and NE-dipping intra-basement reflectors may be indicative of the extensional detachment fault system across the Goban Spur, probably acting as a rheological interface that plays a critical part in localized deformation during exhumation and serpentinization according to Gillard et al. (2019). As introduced previously, we divide the exhumed mantle domain into two subdomains to better characterize the margin.

1) Subdomain T1

Landward, the subdomain T1 in the broader exhumed zone, with relatively deep and smooth basement relief, is adjacent to the hyperextended domain. The interpreted subdomain T1, consistent with the 70-km-wide exhumed mantle zone constrained from seismic refraction modelling (Bullock and Minshull, 2005), gradually becomes wider along the margin from NW to SE. The geometry of the T1 subdomain between lines L3 and L4 is mainly defined based on changes in reflectivity patterns along line X1 (Fig. 11), magnetic anomaly trends (Fig. 3), and crustal thickness variations (Fig. 2b). Despite the uncertainty involved in defining the boundary between the exhumed domain and the oceanic domain due to a sparsity of constraints, we argue that the subdomain T1 extends beyond the oceanward limit of line L4 based on the continuity of magnetic anomaly trends (Fig. 3). The width of the transitional subdomain T1 along the Goban Spur margin ranges from ~50 km to ~90 km, wider than that along the Armorican margin (Tugend et al., 2014b), which may reflect enhanced tectonic deformation complexity due to its proximity to the Biscay Triple Junction (Nirrengarten et al., 2018). In addition, Bullock and Minshull (2005) suggest that the low relief basement in the subdomain T1 probably indicates an ultra-slow spreading rate (approximate 10 mm yr-1).

2) Subdomain T2

Subdomain T2, characterized by peridotite ridges with shallow and rough basement relief (Fig. 6), lies between the oceanic crust and the transitional subdomain T1. The identification of the transitional subdomain T2 across the Goban Spur margin is primarily based on the reflectivity characteristics on the seismic profiles, and how they compare with seismic reflection data on the southern Flemish Cap margin, as shown in Figure 4. The relief and elevation of the basement respectively become rougher and higher from the subdomain T1 to the subdomain T2 (Fig. 6), which may suggest a rheological change in the exhumed mantle lithosphere (Sibuet and Tucholke, 2012). To the southeast, this region is not imaged along seismic profile L4 and is interpreted to pinch out. Since variable basement roughness can represent variations in spreading rates during the lithosphere exhumation stage (Bullock and Minshull, 2005; Sauter et al., 2018), variable extension rates along the margin strike could be responsible for the interpreted pinchout of the subdomain T2 and the widening of the subdomain T1. Overall, the width of the whole exhumed mantle domain varies along the margin, suggesting a non-uniform exhumation stage.

6.1.5 Oceanic domain

Seaward of the interpreted peridotite ridges lies the oceanic crust domain, formed by the onset of seafloor spreading. Because of relatively dense constraints (L1, L2, L3, and the WAM line), the interpreted oceanic domain geometry along the northern part of the margin is more robust than it is for the southern part. The border between the exhumed mantle domain and the oceanic domain diverges from magnetic Chron 34 towards the south of the margin. By calculating basement roughness of the initial oceanic zone along both the Flemish Cap and Goban Spur conjugate margins, Sauter et al. (2018) argue that this conjugate pair represents typical slow asymmetric seafloor spreading, consistent with the result from Bullock and Minshull (2005).

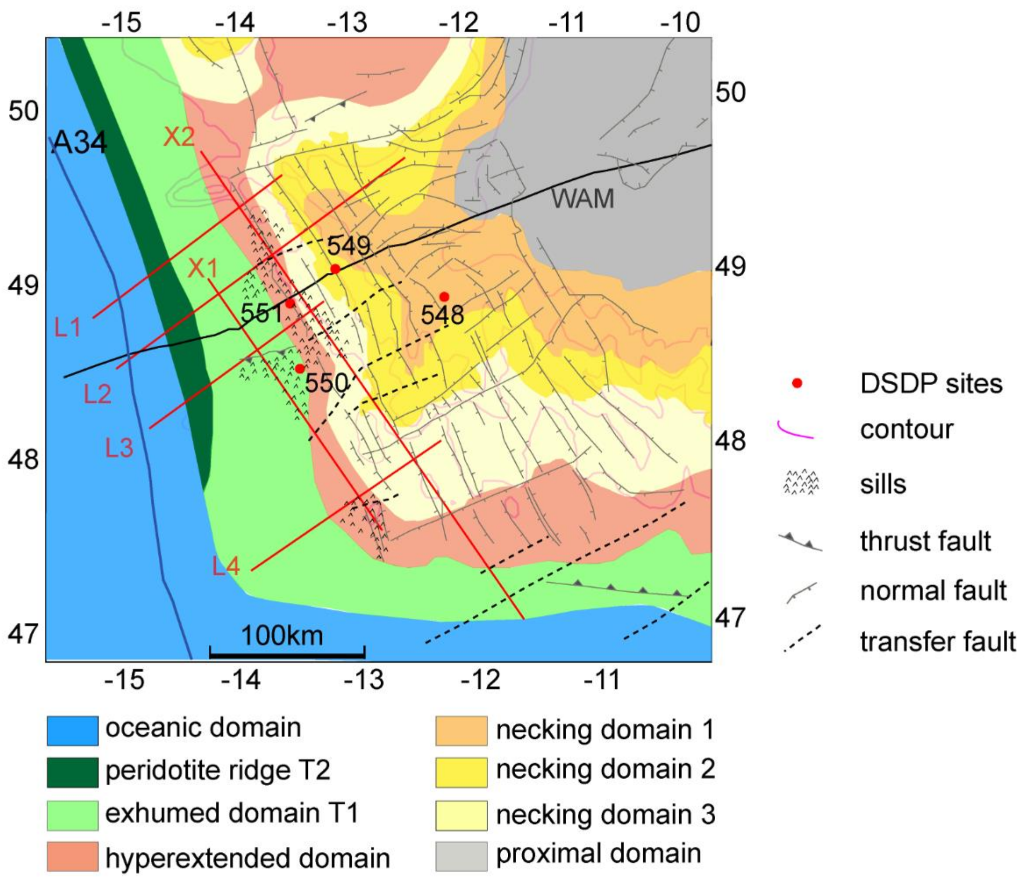

Fig. 14. Map of the Goban Spur margin displaying bathymetry (pink contours) and the interpreted crustal domain distribution. The dark blue line indicates magnetic Chron 34 (Müller et al., 2016). Seismic profiles are plotted in red (L1, L2, L3, L4, X1, and X2), and in black (WAM line). Crustal domains interpreted beyond the new seismic coverage are constrained from gravity inversion results (Welford et al., 2010b; Tugend et al., 2014; Sandoval, 2019). The rift-related structures (thrusts, normal faults, and transfer faults) and sill distribution are from Naylor et al. (2002). Bathymetric contour interval is 1000 m.

6.2 Magmatism on the non-volcanic Goban Spur margin

Based on an interpreted depth-uniform extension of lithosphere across the Goban Spur margin (Peddy et al., 1989), Bullock and Minshull (2005) propose that the basaltic material observed along the WAM line in the necking zone was extruded prior to mantle exhumation due to decompression melting. At Site 550, located in the exhumed mantle domain, basaltic pillow lavas were also recovered. Furthermore, from previous interpretation (Naylor et al., 2002), the interpreted areal coverage of sills along the northern Goban

Spur margin appears much larger than that along the southern margin, and intrusive and extrusive basaltic bodies appear to be distributed across the necking, hyperextended, and mantle exhumation zones (Fig. 14). This suggests that magmatic events were occurring during rifting, thinning, mantle exhumation, and final continental breakup along the Goban Spur margin. The distribution of sills across the Goban Spur margin does not appear to correspond to regions with localized high magnetic anomalies (Fig. 3). Some magnetic anomalies may be associated with serpentinization at the Goban Spur margin (Minshull, 2009). In addition, the igneous bodies appear to be distributed close to the transfer faults that represent tectonic weaknesses in the continental crust (Scrutton et al., 1979) and these faults may provide channels for lava flow migration during margin evolution.

6.3 Reconstruction of the Goban Spur and its conjugates

In Figure 15, the crustal architecture across the Goban Spur margin from this study and the crustal architecture across the "conjugate" northeastern margin of Flemish Cap from Welford et al. (2010c) are mapped using a rigid plate reconstruction, back to the onset of seafloor spreading using GPlates 2.1 at 83 Ma (Müller et al., 2016). In order to compare the two margins consistently, the stretched crust interpreted along the Flemish Cap margin is assumed to correspond to the necking and hyperextended zones along the Goban Spur margin.

At the Goban Spur, the necking zone is of variable width ranging from ~99 km to ~189 km, indicating along-strike variability in lithosphere thinning. In contrast, although the boundary between the necking and hyperextended domains is not clearly defined along the Flemish Cap margin, the width of the necking domain is much narrower (< ~20 km; Welford et al., 2010c), indicating a more abrupt necking of the crust. In addition, the along-strike exhumed serpentinized mantle domain of the Goban Spur margin spans a much wider (~50-65 km) area while it is much narrower (~25 km) at the northeastern Flemish Cap margin (Welford et al., 2010c). In the exhumed domain, only peridotite ridges are observed at the Flemish Cap (Welford et al., 2010c), while both the peridotite ridges and a wide region of exhumed mantle with the deeper basement are observed at the Goban Spur. This may reflect asymmetric rifting with different extension rates for each continental margin.

Overall, the highly variable geometry of each crustal type across the "conjugate" pair is consistent with asymmetric evolutionary mechanisms as hypothesized by Gerlings et al. (2012). However, based on seismic interpretation, Welford et al. (2010c) identified both extensional and strike-slip deformation along the northeastern Flemish Cap margin, consistent with the interpreted rotation and displacement of Flemish Cap with respect to the Orphan Basin during the early Cretaceous period through seismic and potential field data analysis (Sibuet et al., 2007) and more recently deformable plate tectonic reconstructions (Peace et al., 2019). In contrast, the Goban Spur margin experienced mostly margin-perpendicular extension. In addition to the geometric differences in crustal architecture, velocities (> 7 km s^{-1} at depth) in subdomain T2 at the

Goban Spur differ from those (7.4-7.9 km s^{-1}) at depth in the serpentinized mantle domain at the northeastern Flemish Cap margin, which may also reflect different degrees of serpentinization (Bullock and Minshull, 2005; Gerlings et al., 2009). These striking differences call into question the widely-accepted "conjugate" relationship between the northeastern Flemish Cap margin and the Goban Spur margin (de Graciansky and Poag, 1985; Keen et al., 1989; Welford et al., 2010a; Gerlings et al., 2012).

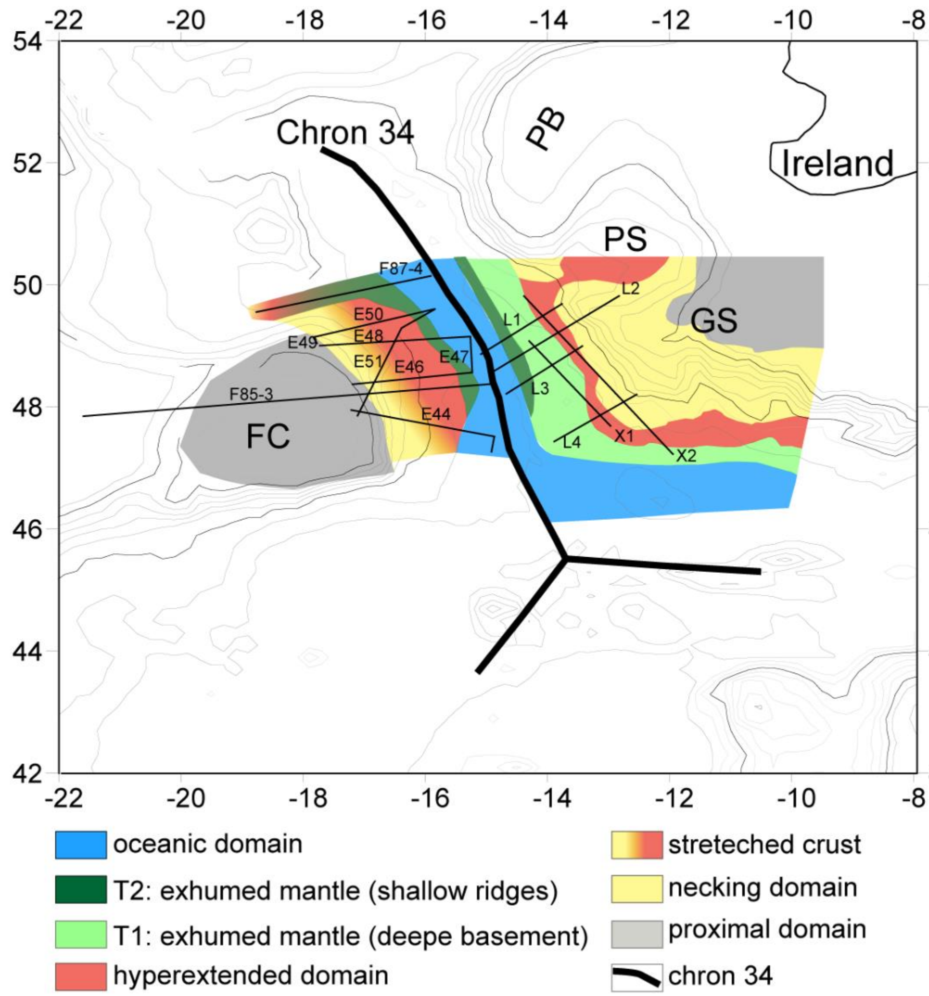

Fig. 15. Crustal architecture across the northeastern Flemish Cap-Goban Spur margins, reconstructed to magnetic Chron 34 at 83 Ma (thick black line from Müller et al., 2016) using a rigid plate reconstruction in GPlates 2.1 (Müller et al., 2016), overlain by the corresponding bathymetric contours (thin grey lines) at 83 Ma. The crustal domains across Flemish Cap are adapted from Welford et al. (2010c). Labelled thin black straight lines show seismic profiles constraining the crustal architecture interpretations. Abbreviations: FC, Flemish Cap; GS, Goban Spur; PS, Porcupine Seabight; PB, Porcupine Bank.

In addition to the observed similarities in the geometrical features of the peridotite ridges in the serpentinized exhumed domain at both the Goban Spur margin and the Galicia Bank margin (Dean et al., 2000; 2015), the former was adjacent to the latter at 200 Ma prior to rifting according to new kinematic evolution models (Nirrengarten et al., 2018; Peace et al., 2019; Sandoval et al., 2019). If so, the prominent asymmetric features recorded at both margins would have resulted from the motion and southward migration of the Flemish Cap (Sibuet et al., 2007; Welford et al., 2010c; Welford et al., 2012; Peace et al., 2019), or, at the least, oblique rifting (Brune et al., 2018). Superimposed on these plate motions, the variable widths of each of the crustal domains across the two margins may also reflect highly variable rifting rates. At the Goban Spur, lower mantle temperatures are supported by geochemical models, suggestive of relatively slower rifting than along other northern Atlantic margins (Minshull et al., 2014). Meanwhile, inferred complexities in the tectonic processes along the northeastern Flemish Cap margin also make it difficult to determine the rifting rate. Overall, these discrepancies and uncertainties are suggestive of a more complex margin evolution than previously thought for the Goban Spur margin and its possible conjugates.

7. Summary

Six new multichannel seismic reflection profiles, integrated with previous seismic reflection and refraction data, magnetic and gravity data, and DSDP drilling sites, on the Goban Spur rifted margin have revealed the following:

(1) Five distinct crustal domains related to different rifting stages are identified and their regional extents are evaluated, significantly increasing knowledge of the crustal architecture of the Goban Spur rifted continental margin.

(2) Along strike, the width of the necking domain on the Goban Spur margin gradually increases from northwest to southeast, suggesting along-strike variations in extension, likely related to the variable pre-existing rheological architecture across the Goban Spur margin.

(3) In the northwest, the exhumed domain consists of a narrow zone of shallower peridotite ridges (transitional subdomain T2) and a wider zone of the deeper exhumed serpentinized mantle (transitional subdomain T1). The different styles of mantle exhumation are inferred to reflect different exhumation rates. Toward the southeast along the Goban Spur margin, the zone of serpentinized peridotite ridges is interpreted to pinch-out.

(4) During the evolution of the Goban Spur continental margin, localized syn-rift magmatism occurred during lithosphere stretching, thinning, subsequent hyperextension and serpentinized mantle exhumation, and final lithosphere rupture, all prior to seafloor spreading initiation.

(5) The striking asymmetries between the Goban Spur margin and its "conjugate" margin, the northeastern Flemish Cap margin, call into question the conjugate relationship between the two margins.

Future work involving the restoration of the margins using deformable plate reconstructions will help resolve this debate. Such research will help unravel the geological significance of the Goban Spur during opening of the southern North Atlantic Ocean, which led to the separation of the Irish, Newfoundland, and Iberian margins.

Acknowledgement

We are grateful to the Department of Communications, Climate Action & Environment of Ireland for providing the multichannel seismic reflection data. WAM data were acquired by the UK NERC BIRPS programme in 1985. Great thanks are also given to Schlumberger for donating Petrel software to Memorial University. AP's postdoctoral fellowship at Memorial was funded by the Hibernia Project Geophysics Support Fund and Innovate NL. We would like to thank the members of the Memorial Applied Geophysics for Rift Tectonics (MAGRiT) group for providing suggestions for this research.

References

Bellahsen, N., Leroy, S., Autin, J., Razin, P., d'Acremont, E., Sloan, H., Pik, R., Ahmed, A., Khanbari, K., 2013. Pre-existing oblique transfer zones and transfer/transform relationships in continental margins: New insights from the southeastern Gulf of Aden, Socotra Island, Yemen. Tectonophysics 607, 32-50.

Brune, S., Simon E. Williams., R. D. Müller., 2018. Oblique rifting: the rule, not the exception. Solid Earth 9, 1187-1206.

Boillot, G., Recq, M., Winterer, E.L., Meyer, A.W., Applegate, J., Baltuck, M., Bergen, J.A., Comas, M.C., et al., 1987. Tectonic denudation of the upper mantle alongpassive margins: a model based on drilling results (ODP leg 103, western Galicia margin, Spain). Tectonophysics 132, 335-342.

Bonvalot, S., Balmino, G., Briais, A., M. Kuhn, Peyrefitte, A., Vales N., Biancale, R., Gabalda, G., Reinquin, F., Sarrailh, M., 2012. World Gravity Map. Commission for the Geological Map of the World. Eds. BGI-CGMW-CNES-IRD, Paris.

Bullock, A.D., Minshull, T.A., 2005. From continental extension to seafloor spreading: crustal structure of the Goban Spur rifted margin, southwest of the UK. Geophysics Journal International 163, 527-546.

de Graciansky, P. C., Poag, C. W., Cunningham, R., Loubere, P., Masson, G.D., et al., 1985. The Goban Spur transect: Geologic evolution of a sediment-starved passive continental margin. Geological Society of America Bulletin 96, 58-76.

de Graciansky, P. C., Poag, C. W., 1985. Geologic history of Goban Spur, northwest Europe continental margin. Deep Sea Drilling Project Initial Reports, 80. US Government Printing Office, Washington DC, pp. 1187-1216.

Dean, S., Minshull, T., Whitmarsh, R., Louden, K., 2000. Deep structure of the ocean-continent transition in the southern Iberia Abyssal Plain frosm seismic refraction profiles: the IAM-9 transect at 40 20'N. Journal Geophysical Research 105, 5859-5886.

Dean, S.L., Sawyer, D.S., Morgan, J.K., 2015. Galicia Bank ocean-continent transition zone: New seismic reflection constraints. Earth and Planetary Science Letters 413:197-207.

Dingle, R. V., Scrutton, R. A., 1977. Continental margin fault pattern mapped south-west of Ireland. Nature 268, 720-722.

Dingle, R. V., Scrutton, R. A., 1979. Sedimentary succession and tectonic history of a marginal plateau (Goban Spur, southwest of Ireland). Marine Geology 33:45-69.

Franke, D., 2013. Rifting, lithosphere breakup and volcanism: Comparison of magma-poor and volcanic rifted margins. Marine and Petroleum Geology 43, 63-87.

Gerlings, J., Louden, K.E., Jackson, H.R., 2011. Crustal structure of the Flemish Cap Continental Margin (eastern Canada): an analysis of a seismic refraction profile. Geophysics Journal International 185, 30-48.

Gerlings, J., Louden, K. E., Minshull, T. A., Nedimovi´c, R.M., 2012. Flemish Cap-Goban Spur conjugate margins: New evidence of asymmetry. Geology 40, 1107-1110.

Gillard, M., Tugend, J., Muntener, O., Manatschal, G., Karner, G.D., Autin, J., Sauter, D., Figueredo, P.H., Ulrich, M., 2019. The role of serpentinization and magmatism in the formation of decoupling interfaces at magma-poor rifted margins. Earth-Science Reviews, 196, 102882.

Healy, D., Kusznir, N.J., 2007. Early kinematic history of the Goban Spur rifted margin derived from a new model of continental breakup and sea-floor spreading initiation, in: Karner, G., Manatschal, G. & Pinheiro, L. (Ed.), Imaging, Mapping and Modelling Continental Lithosphere Extension and Breakup. Geological Society, London, Special Publications, Vol. 282, pp. 199-215.

Horsefield, S.J., Whitmarsh, R.B., White, R.S., and Sibuet, J. C., 1994. Crustal structure of the Goban Spur rifted continental margin, NE Atlantic. Geophysics Journal International 119, 1-19.

Huismans, R., Beaumont, C., 2011. Depth-dependent extension, two-stage breakup, and cratonic underplating at rifted margins. Nature 473, 74-78.

Keen, C.E., de Voogd, B., 1988. The continent-ocean boundary at the rifted margin off eastern Canada: New results from deep seismic reflection studies. Tectonics 7, 107-124.

Keen, C.E., Peddy, C., deVoogd, B., Mathews, D., 1989. Conjugate margins of Canada and Europe: Results from deep reflection profiling. Geology 17, 173-176.

Louvel, V., Dyment, J., Sibuet, J., 1997. Thinning of the Goban Spur continental margin and formation of early oceanic crust: constraints from forward modelling and inversion of marine magnetic anomalies. Geophysics Journal International 128,188-196.

Masson, D., Montadert, L., Scruiton, R., 1985. Regional geology of the Goban Spur continental margin. Initial Reports of the Deep Sea Drilling Project, US Government Printing Office, Washington DC, pp. 1115-1139.

Minshull, T.A., 2009. Geophysical characterisation of the ocean-continenttransition at magma-poor rifted margins. Comptes Rendus Geoscience 341, 382-393.

Minshull, T.A., Bullock, A.D., Dean, S.M., Henstock, T.J., Murton, B.J., Taylor, R.N., White, R.S., 2014. Extenstion and magmatism at the Goban Spur rifted continental margin: geophysical and geochemical approaches. https://www.slideserve.com/huslu/extension-and-magmatism-at-the-goban-spur-rifted-continental-margin.

Mohn, G., Manatschal, G., Beltrando, M., Masini, E., Kusznir, N., 2012. Necking of continental crust in magma-poor rifted margins: evidence from the fossil Alpine Tethys margins. Tectonics 31, 1-28.

Montadert, L., Roberts, D. G., de Charpal. O., and Guennoc, P., 1979b, Rifting and subsidence of the northern continental margin of the Bay of Biscay. Deep Sea Drilling Project Initial Reports. US Government Printing Office, Washington DC, pp. 1025-1060.

Moulin, M., Aslanian, D., Olivet, J.L., Contrucci, I., Matias, L., et al., 2005. Geological constraints on the evolution of the Angolan margin based on reflection and refraction seismic data (ZaiAngo project). Geophysical Journal International 162, 793-810.

Müller, R.D., Seton, M., Zahirovic, S., Williams, S.E., Matthews, K.J., Wright, N.M., Shephard, G.E., Maloney, K.T., Barnett-Moore, N., Hosseinpour, M., Bower, D.J., Cannon, J., 2016. Ocean Basin Evolution and Global-Scale Plate Reorganization Events Since Pangea Breakup. Annual Review of Earth and Planetary Sciences 44, 107.

Naylor, D., Shannon, Murphy, N., 2002. Porcupine-Goban region – a standard structural nomenclature system. Dublin, Ireland: Petroleum Affairs Division.

Nirrengarten, M., Manatschal, G., Tugend, J., Kusznir, N., Sauter, D., 2018. Kinematic evolution of the southern North Atlantic: Implications for the formation of hyperextended rift systems. Tectonics 37, 1-30.

Osmundsen, P.T., Ebbing, J., 2008. Styles of extension offshore mid-Norway and implications for mechanisms of crustal thinning at passive margins. Tectonics 27, TC6016.

Peace, A.L., Welford, J. K., Ball, P.J., Nirrengarten, M., 2019. Deformable plate tectonic models of the southern North Atlantic. Journal of Geodynamics 128, 11-37.

Peddy C., Pinet, B., Masson, D., Scrutton, R., Sibuet, J.C., Warner, M.R., Lefort, J.P., Shroeder, I.J., 1989. Crustal structure of the Goban Spur continental margin Northeast Atlantic, from deep seismic reflection profiling. Journal of the Geological Society 146, 427-437.

Perez-Gussinye, M., Ranero, C.R., Reston, T.J., Sawyer, D., 2003. Mechanisms of extension at nonvolcanic margins: evidence from the Galicia interior basin, west of Iberia. Journal of Geophysical Research-Solid Earth, 108.

Peron-Pinvidic, G., Manatschal, G., 2009. The final rifting evolution at deep magma poor passive margins from Iberia-Newfoundland: a new point of view. International Journal of Earth Sciences 98, 1581-1597.

Peron-Pinvidic, G., Manatschal, G., Osmundsen, P.T., 2013. Structural comparison of archetypal Atlantic rifted margins: A review of observations and concepts. Marine and Petroleum Geology 43, 21-47.

Pickup, S. L. B., Whitmarsh, R. B., Fowler, C.M. R., Reston, T. J., 1996. Insight into the nature of the ocean-continent transition off West Iberia from a deep multichannel seismic reflection profile. Geology 24, 1079-1082.

Reston, T.J., 2007. The formation of non-volcanic rifted margins by the progressive extension of the lithosphere: the example of the west Iberian margin, in: Karner, G., Manatschal, G. & Pinheiro, L. (Ed.), Imaging, Mapping and Modelling Continental Lithosphere Extension and Breakup. Geological Society, London, Special Publications, Vol. 282, pp. 77-110.

Reston, T.J., 2009. The structure, evolution and symmetry of the magma-poor rifted margins of the North and Central Atlantic: a synthesis. Tectonophysics 468, 6-27.

Roberts, D. G., Masson, D. G., Montadert, L., and de Charpal, O., 1981. Continental margin from the Porcupine Seabight to the Armorican marginal basin. Petroleum Geology of the Continental shelf of Northwest Europe: London (Institute of Petroleum), 455-473.

Sandoval, L., Welford, J.K., MacMahon, H., Peace, A.L., 2019. Determining continuous basins across conjugate margins: The East Orphan, Porcupine, and Galicia Interior basins of the southern Atlantic Ocean. Marine and Petroleum Geology, in press.

Sauter, D., Tugend, J., Gillard, M., Nirrengarten, M., Autin, J., Manatschal, G., Cannat, M., Leroy, S., Schaming, M., 2018. Oceanic basement roughness alongside magma-poor rifted margins: insight into initial seafloor spreading. Geophysical Journal International 212, 900-915.

Sawyer, D. S., Whitmarsh, R. B., Klaus, A., 1994. Proceedings of the Ocean Drilling Program, Initial Reports, 149. Ocean Drilling Program, College Station, TX.

Scrutton, R.A., 1979. Structure of the crust and upper mantle at Goban Spur, southwest of the British Isles-some implications for margin studies. Tectonophysics 59, 201-215.

Shillington, D. J., Holbrook, W. S., Van Avendonk, H. J. A., Tucholke, B. E., Hopper, J. R., Larsen, H. C., Nunes, G. T., 2006. Evidence for asymmetric nonvolcanic rifting and slow incipient oceanic accretion from seismic reflection data on the Newfoundland margin. Journal of Geophysical Research 111, B09403.

Sibuet, J. C., Collette, B.J. 1991. Triple junctions of Bay of Biscay and North Atlantic: New constraints on the kinematic evolution. Geology 19, 522-525.

Sibuet, J. C., Mathis, B., Pastouret, L., Auzende, J. M., Foucher, J.P., Hunter, P.M., Guennoc, P., de Graciansky, P. C., Montadert, L., Masson, D.G., 1985. Morphology and basement structure of the Goban Spur continental margin (northeastern Atlantic) and the role of the Pyrenean orogeny. Deep Sea Drilling Project Initial Reports, US Government Printing Office, Washington DC, pp. 1153-1165.

Sibuet, J.C., Srivastava, S., Enachescu, M.E., Karner, G., 2007. Early Cretaceous motion of Flemish Cap with respect to North America: implications on the formation of Orphan Basin and SE Flemish Cap-Galicia Bank conjugate margins, in: Karner, G., Manatschal, G. & Pinheiro, L. (Ed.), Imaging, Mapping and Modelling Continental Lithosphere Extension and Breakup. Geological Society, London, Special Publications, Vol. 282, pp. 63-76.

Sibuet, J.C., Tucholke, B. E., 2012. The geodynamic province of transitional lithosphere adjacent to magma-poor continental margins. in: Mohriak, W.U., Danforth, A., Post, P.J., Brown, D.E., et al. (Ed.), Conjugate Divergent Margins. Geological Society, London, Special Publications, Vol. 369, pp. 429-452.

Srivastava, S., Verhoef, J., Macnab, R., 1988. Results from a detailed aeromagnetic survey across the northeast Newfoundland margin, part ii: Early opening of the North Atlantic between the British Isles and Newfoundland. Marine and Petroleum Geology 5, 324-337.

Sutra, E., Manatschal, G., Mohn, G., Unternehr, P., 2013. Quantification and restoration of extensional deformation along the Western Iberia and Newfoundland rifted margins. Geochemisty, Geophysics, Geosystems 14, 2575-2597.

Tucholke, B. E., Sibuet, J.C., Klaus, A., 2004. Proceedings of the Ocean Drilling Program, Initial Reports, 210. Ocean Drilling Program, College Station, TX.

Tugend, J., Manatschal, G., Kusznir, N. J., Masini, E., 2014a. Characterizing and identifying structural domains at rifted continental margins: Application to the Bay of Biscay margins and its Western Pyrenean fossil remnants, in Gibson, G.M., Roure, F., Manatschal, G. (Ed.), Sedimentary Basins and Crustal Processes at Continental Margins: From Modern Hyper-extended Margins to Deformed Ancient Analogues. Geological Society, London, Special Publications, Vol. 413.

Tugend, J., Manatschal, G., Kusznir, N. J., Masini, E., Mohn, G., Thinon, I., 2014b. Formation and deformation of hyperextended rift systems: Insights from rift domain mapping in the Bay of Biscay-Pyrenees. Tectonics 33, 1239-1276.

Van Avendonk, H. J. A., Holbrook, W. S. Nunes, G.T., Shillington, D.J., Tucholke, B.E., et al., 2006. Seismic velocity structure of the rifted margin of the eastern Grand Banks of Newfoundland, Canada. Journal of Geophysical Research 111, B11404.

Welford, J.K., Smith, J.A., Hall, J., Deemer, S., Srivastava, S.P., Sibuet, J.C., 2010a. Structure and rifting evolution of the northern Newfoundland Basin from Erable multichannel seismic reflection profiles across the southeastern margin of Flemsih Cap. Geophysical Journal International 180, 976-998.

Welford, J.K., Shannon, P.M., O'Relly, B.M., Hall, J., 2010b. Lithospheric density variations and Moho structure of the Irish Atlantic continental margin from constrained 3-D gravity inversion. Geophysical Journal International 183, 79-95.

Welford, J.K., Hall, J., Sibuet, J.C., Srivastava, S.P., 2010c. Structure across the northeastern margin of Flemish Cap, offshore Newfoundland from Erable multichannel seismic reflection profiles: evidence for a transtensional rifting environment. Geophysical Journal International 183, 572-586.

Welford, J.K., Shannon, P.M., O'Relly, B.M., Hall, J., 2012. Comparison of lithosphere structure across the Orphan Basin–Flemish Cap and Irish Atlantic conjugate continental margins from constrained 3D gravity inversions. Journal of the Geological Society, 169, 205-420.

Whitmarsh, R. B., Beslier, M.O., Wallace, P. J., 1998. Proceedings of the Ocean Drilling Program, Initial Reports, 173. Ocean Drilling Program, College Station, TX.

Whitmarsh, R.B., Manatschal, G., Minshull, T.A., 2001. Evolution of magma-poor continental margins from rifting to seafloor spreading. Nature 413, 150-154.

Investigating the Goban Spur rifted continental margin, offshore Ireland, through integration of new seismic reflection and potential field data

Pei Yang[a], J. Kim Welford[a], Alexander L. Peace[b], and Richard Hobbs[c]

[a] Department of Earth Sciences, Memorial University, St. John's, NL, Canada

[b] School of Geography and Earth Sciences, McMaster University, Hamilton, ON, Canada

[c] Department of Earth Sciences, Durham University, Durham, UK

Abstract

The Goban Spur, offshore Ireland, is a magma-poor rifted continental margin conjugate to the well-studied Newfoundland margin, offshore Canada. Published studies demonstrated that a 70-km-wide zone of exhumed serpentinized mantle lies between oceanic crust and stretched continental crust at the seaward limit of Goban Spur. However, the along-strike extent of this serpentinized zone has, until now, been unknown due to insufficient data coverage. The crustal architecture of the margin is complicated due to its multi-staged tectonic history. Here, six newly acquired multi-channel seismic reflection lines are processed and interpreted, along with vintage seismic profiles, to characterize its structure and evolution. These seismic profiles reveal significant along-strike structural variations along the Goban Spur margin, and allow us to delimit five distinct crustal zones related to different rifting stages and their regional extents. The geometries of each crustal domain are variable along the margin strike, probably suggestive of different extension rates during the evolution of the margin or inherited variations in crustal composition and rheology. The transitional zone between oceanic crust and stretched continental crust consists of both shallow peridotite ridges and deeper exhumed serpentinized mantle, much like the conjugate Iberian and Newfoundland margins. Above the top basement in the exhumed domain, the syn-exhumed sediments show strikingly weak reflectivity, rarely seen at other magma-poor margins. Magmatic events occur coincident with each rifting stage, and the volume of magmatic accretions increases from NW to SE, more than previously interpreted. Plate reconstruction of the Goban Spur and its possible conjugate – the Flemish Cap, shows asymmetry in the crustal architectures, likely due to rift evolution involving more 3-D complexity than can be explained by simple 2-D extensional kinematics.

1. Introduction

Studies of magma-poor rifted continental margins around the southern North Atlantic Ocean have been plentiful, particularly for the Newfoundland-Iberia and Flemish Cap-Galicia Bank conjugate margin pairs (e.g., Reston, 2007; Sibuet et al., 2007; Peron-Pinvidic et al., 2013; Sauter et al., 2018). In recent years, attention has increasingly focused on the Newfoundland-Irish and Flemish Cap-Goban Spur conjugate rifted continental margins (Fig. 1a) (Welford et al., 2010a; Gerlings et al., 2012). Rifting along these margins occurred to the north of the Biscay Triple Junction (BTJ), which formed due to divergent movement between Iberia, North America, and Europe during the breakup of Pangaea (Sibuet and Collette, 1991). Rifting proceeded until the initiation of seafloor spreading between them, beginning in the Cretaceous at magnetic Chron 34 (Fig. 1a) (Sibuet and Collette, 1991). By studying the continent-ocean transitional zones (COTZ) across these margin pairs, the geodynamic processes that contributed to rifting can be deduced. While early studies of the Goban Spur originally interpreted a sharp continent-ocean boundary (COB) (e.g., Masson et al., 1985; Keen and de Voogd, 1988; Horsefield et al., 1994; Peddy et al., 1989), a 70-km-wide transitional zone of exhumed serpentinized subcontinental mantle has since been interpreted for the COTZ of the Goban Spur based on seismic refraction modelling (Bullock and Minshull, 2005). Similar transitional zones have also been interpreted along the Newfoundland and Flemish Cap, Iberia and Galicia Bank margins (e.g., Boillot et al., 1987; Whitmarsh et al., 1998; Dean et al., 2000; Welford et al., 2010a; Gerlings et al., 2011; Dean et al., 2015; Davy et al., 2016).

Due to limited data coverage, the rift-related domains along the Goban Spur margin have remained poorly defined and their architecture has been primarily delineated on the basis of a small number of co-located 2-D seismic profiles (Fig. 1b), including CM lines (Montadert et al., 1979), the WAM line (Peddy et al., 1989), and the refraction line (Bullock and Minshull, 2005). Consequently, knowledge of the rifting evolution of the Goban Spur margin has been limited by the 2-D nature of previous studies and the sparsity of available geophysical data.

In order to improve understanding of the offshore Irish Atlantic rifted continental margins, deep long-offset multichannel seismic reflection data were acquired in 2013 by Eni Ireland for the Department of Communications, Climate Action & Environment of Ireland. In this study, six of these newly acquired seismic reflection profiles along the Goban Spur margin are processed and interpreted, providing improved regional coverage (Fig. 1b). By referring to the structural unit subdivision scheme for magma-poor margins proposed in the literature (Peron-Pinvidic et al., 2013; Tugend et al., 2014), distinct crustal domains are identified and regionally extrapolated across the Goban Spur margin. This is achieved using a combination of seismic interpretation, gravity inversion results, magnetic and gravity anomaly observations, and constraints from drilling data. The improved data coverage allows for better characterization of the variations in rifting mode, rift-related magmatism, and insights into the tectonic evolutionary history of the Goban Spur margin.

2. Geological setting

The Goban Spur is a magma-poor rifted continental margin, situated offshore Ireland, south of the Porcupine Seabight Basin and Porcupine Bank, and west of the Fastnet Basin, the Comubian Platform, and the Western Approaches Basin (Fig. 1b) (Horsefield et al., 1994; Bullock and Minshull, 2005). To the southeast is the northern Bay of Biscay margin, which experienced rifting from the Jurassic to the Cretaceous (Montadert et al., 1979). The bathymetry, obtained from ETOPO1 Global Relief Model of the National Geophysical Data Center (NGDC) of the National Oceanic and Atmospheric Administration (NOAA), gradually increases from ~1000 m to 2500 m at the southwest edge of the Goban Spur continental shelf, before dropping off abruptly at the Pendragon Escarpment (Fig. 1b). Farther seaward, the Goban Spur transitions to the Porcupine Abyssal Plain (Fig. 1b) (de Graciansky & Poag, 1985).

Generally, the structural features of the Goban Spur can be attributed to the rifting of the European plate from the North American plate, with crustal thinning occurring at the end of the rifting phase during the early Cretaceous to the early Albian (de Graciansky et al., 1985). However, the formation of the Goban Spur margin has also been influenced by additional interrelated factors, including the formation of the Bay of Biscay (Dingle and Scrutton, 1979), its interaction with the hypothesized conjugate Flemish Cap margin prior to breakup (Cande and Kristoffersen, 1977), and the presence of pre-existing structures (Dingle and Scrutton, 1977; Sibuet et al., 1985). The interaction between the margin-parallel NW- trending faults due to rifting and the pre-existing NE- trending fault system primarily controls the structure of the Goban Spur continental crust, with the northern Goban province likely an extension of the Fastnet Basin rather than the Cormubian Platform (Naylor et al., 2002). At the northern limit of the Goban Spur, the ENE-trending Porcupine Fault separates the Spur from the Porcupine Basin (Dingle and Scrutton, 1979) while the southern margin may be associated with faults developed in the northern Western Approaches Basin (Naylor et al., 2002). Based on seismic evidence, the NW-trending faults become more complicated and less continuous with more varied orientations towards the southeastward limit of the Goban Spur margin (Naylor et al., 2002). This complexity may be due to the influence of variable basement structure, interactions between the NW-trending fault systems and E-trending faults close to the Jean Charcot Escarpment (Sibuet et al., 1985), and transfer faults that segment the Goban Spur margin (Naylor et al., 2002).

During the Deep Sea Drilling Project (DSDP) Leg 80, four sites (548, 549, 550, and 551) were drilled on the Goban Spur (Figs. 1b and 2) (de Graciansky et al., 1985). Site 548 was drilled near the edge of a half-graben with Devonian basement, and site 549 penetrated the Hercynian basement on the crest of the Pendragon Escarpment at 2335.5 m water depth. In addition, the earliest syn-rift sediments from the Barremian (possibly late Hauterivian) and oldest post-rift sediments from the early Albian were recovered at site 549, which revealed that the rifting phase lasted about 15 Myrs (de Graciansky et al., 1985; Masson et al., 1985). Site 550, at 4432 m water depth, was located in the abyssal plain southwest of the margin and drilled Devonian basement composed of basaltic rocks, overlain by late Albian chalks. The site was ~135 km inboard of magnetic anomaly 34, which represents the first undisputed oceanic crust from seafloor spreading (Srivastava et al., 1988; Müller et al., 2016). Site 551 penetrated the basaltic basement imbedded with mudstone, overlain by late Cenomanian chalks (de Graciansky et al., 1985).

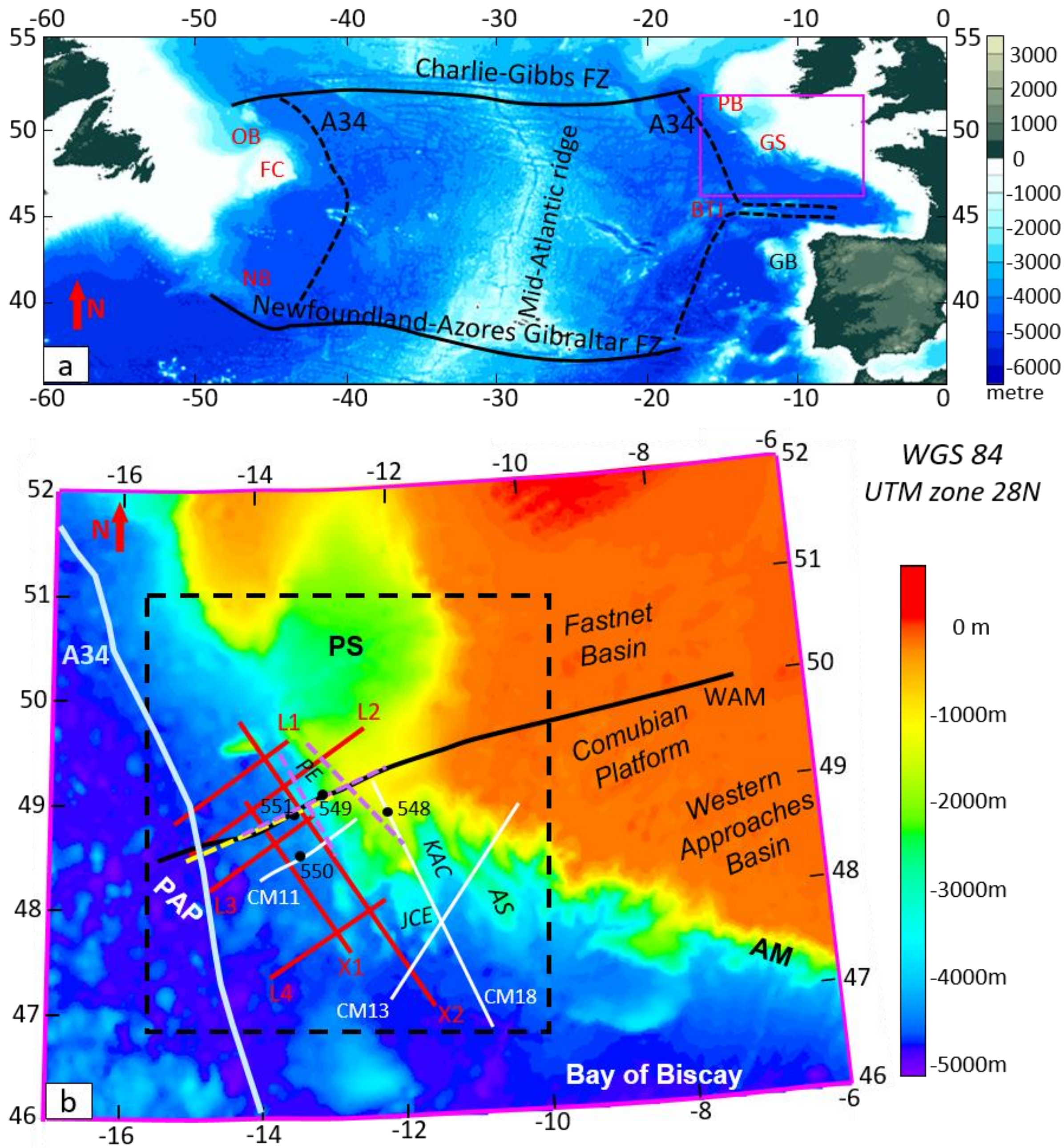

Fig. 1. (a) Bathymetric map of the North Atlantic.The dashed black line shows magnetic anomaly 34 (Müller et al., 2016). The pink box shows the location of part b. (b) Bathymetry of the Goban Spur. Red lines indicate the newly acquired seismic reflection lines. The black and white lines show the Western Approaches Margin (WAM) line (Peddy et al., 1989) and the CM multichannel seismic profiles (Masson et al., 1985), respectively. The purple and yellow dashed lines indicate the refraction profiles from Horsefield et al. (1994) and Bullock and Minshull (2005), respectively. The black solid circles represent the DSDP Leg 80 drill sites. Crustal domains will be delineated within the dashed black box. Abbreviations: AM: Armorican Margin; AS:Austell Spur; BTJ: Biscay Triple Junction; FC: Flemish Cap; FZ: Fracture zone; GB: Galicia Bank; GS: Goban Spur; JCE: Jean Charcot Escarpment; KAC: King Arthur Canyon; NB: Newfoundland Basin; PAP: Porcupine Abyssal Plain; PE: Pendragon Escarpment; PS: Porcupine Seabight Basin; PB: Porcupine Bank.

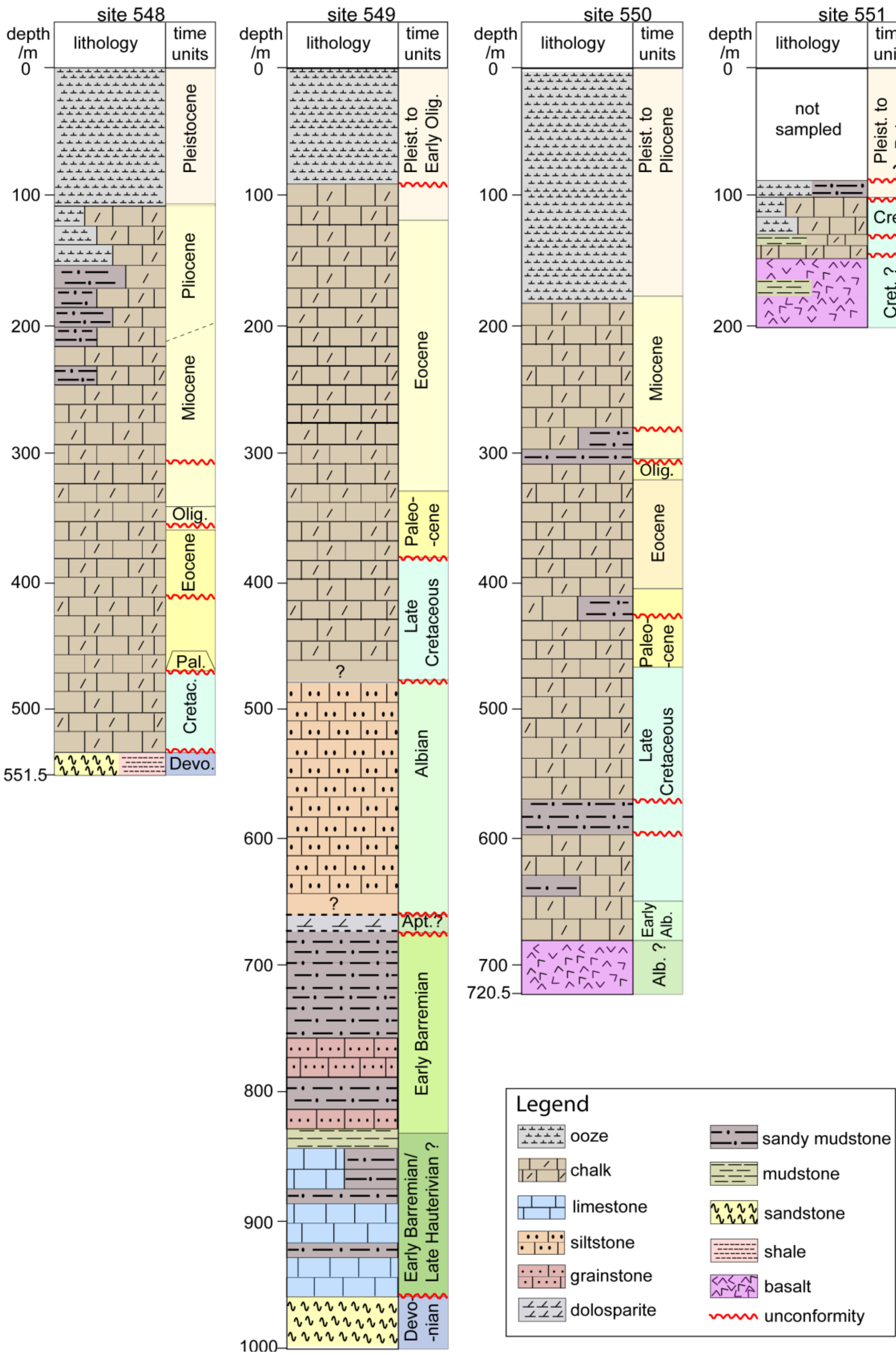

Fig. 2. Lithological columns for drilling sites 548, 549, 550, and 551 at the Goban Spur margin (modified from De Graciansky et al., 1985; De Graciansky and Poag, 1985).

Due to the interpreted differential extension between the upper crust and the lower lithosphere at the Goban Spur, Masson et al. (1985) suggested that a uniform-stretching model was not applicable to the margin. Keen et al. (1989) favoured pure shear rifting and asymmetric lithosphere rupture based on the interpretation of seismic reflection data acquired across the NE Flemish Cap-Goban Spur conjugate margins. Since full lithospheric thinning is estimated to have been considerably greater than the observed thinning of the upper crust in the transitional zone across Goban Spur, Healy and Kusznir (2007) have argued for depth-dependent stretching, precluding a pure shear mechanism for the major deformation processes. Gerlings et al. (2012) argued for asymmetric deformation occurring during each stage of the tectonic evolution of the NE Flemish Cap-Goban Spur conjugate margins. Based on similarities in the inferred tectonic processes at the Goban Spur margin and those across the Iberia-Newfoundland margins (Sibuet and Tucholke, 2012), depth-dependent stretching of lithosphere, with crustal rupture preceding lithospheric mantle breakup, has been argued for the Goban Spur margin, just as it has for the Iberia-Newfoundland margins (Huismans and Beaumont, 2011). The geological and tectonic characteristics of the Goban Spur are complex and both time and depth dependent, introducing challenges for geophysical characterization.

3. Geophysical background

A number of single-channel and multi-channel seismic reflection profiles were acquired during the 1970s, including the CM profiles (white lines in Fig. 1b) (Montadert et al., 1979; Masson et al., 1985; Sibuet et al., 1985). Although these vintage seismic profiles did not extend into the undisputed oceanic crust defined seaward of magnetic anomaly Chron 34, they provided a good understanding of fault characteristics in the continental portion of the Goban Spur (Masson et al., 1985; Naylor et al., 2002). In 1985, the WAM line (black line in Fig. 1b) was acquired across the continental and oceanic crust of the Goban Spur, from which faults, half grabens, crustal types, volcanic features, and a relatively clear continent-ocean boundary were inferred (Peddy et al., 1989; Louvel et al., 1997). To complement the WAM line and quantitatively characterize the structure of the margin, including the presence and extent of igneous rocks, co-located seismic refraction experiments were acquired in 1987 (dashed purple lines in Fig. 1b; Horsefield et al.,

1994) and 2000 (dashed yellow line in Fig. 1b; Bullock and Minshull, 2005), respectively. Based on the velocity model from the most recent seismic refraction profile (yellow dashed line in Fig. 1b), continental, transitional, and oceanic domains were defined for the Goban Spur margin, with velocities ranging from 5.2 to 5.8 km s^{-1} and from 6.6 to 6.9 km s^{-1} in upper and lower continental crust, respectively (Bullock and Minshull, 2005). In the transitional and oceanic zones, P-wave velocity in the crust displays a relatively high gradient (4.5 - 6.8 km s^{-1} within 4 km beneath basement). In addition, P-wave velocities are high (> 7.1 km s^{-1}) at depths of 5-7 km beneath the basement of the 70-km-wide transitional region and Poisson's ratio at top basement of this region is higher than 0.34, indicating serpentinized exhumed mantle (Bullock and Minshull, 2005). Furthermore, a 1-km magnetized layer is modelled in the transitional zone, which can be attributed to the formation of magnetite during serpentinization (Bullock and Minshull, 2005).

Free-air gravity data from the Goban Spur margin are shown in Figure 3a. The transition from negative to positive gravity anomalies lies parallel to the strike of the margin and coincides with inferred crustal thinning (Bullock and Minshull, 2005). To complement qualitative descriptions of the observed gravity data, gravity forward modelling and inversion have been applied to the margin (Bullock and Minshull, 2005; Welford et al., 2010b). Figure 3b shows crustal thickness derived from gravity inversion (Welford et al., 2010b). Welford et al. (2010b) used the GRAV3D algorithm, developed by Li and Oldenburg (1996; 1998), to carry out the gravity inversion. Briefly, a reference density model (relative to a background density of 2850 kg m^{-3}), depth-weighting function and suitable smoothing parameters are all prescribed. Bathymetric data and sediment thickness data, obtained from the NOAA sediment thickness compilation and adjusted in Welford et al. (2010b), are used to constrain the reference density model. The inversion is performed in the least-square sense and the free air gravity data are the observed data. Through multiple iterations, the predicted density model is obtained. Then, Moho structure and crustal thickness are extracted from the recovered density model by assuming that a density anomaly isosurface of 170 kg m^{-3} corresponds to the base of the crust and represents an appropriate Moho proxy. Note that in the reference density model, the region above the bathymetric depths is assumed to have a constant density anomaly of -1820 kg m^{-3}, corresponding to a seawater density of 1030 kg m^{-3}. Below the bathymetry, the sedimentary layer within the reference model is assigned depth-increasing densities with strict bounds that conform to sandstone and shale trends on similar passive margins (Jackson and Talbot; 1986; Sclater and Christie 1980; Albertz et al., 2010). Beneath the sedimentary layer, the inversion algorithm is given greater freedom to assign densities for the crust and mantle in order to reproduce the observations.

The inferred crustal thickness from the gravity inversion reveals that, oceanward, the crust of the Goban Spur margin thins from ~29 km to ~5 km over a distance of ~250 km (Fig. 3b). Along the northern portion of the margin, the gradient in crustal thickness is larger, consistent with a relatively sharp necking zone. Along the southern portion of the margin, the crustal thickness varies slowly over a wider region, indicating a smoother necking profile. This also suggests that the distribution of continental, oceanic and transitional zones will likely vary from north to south.

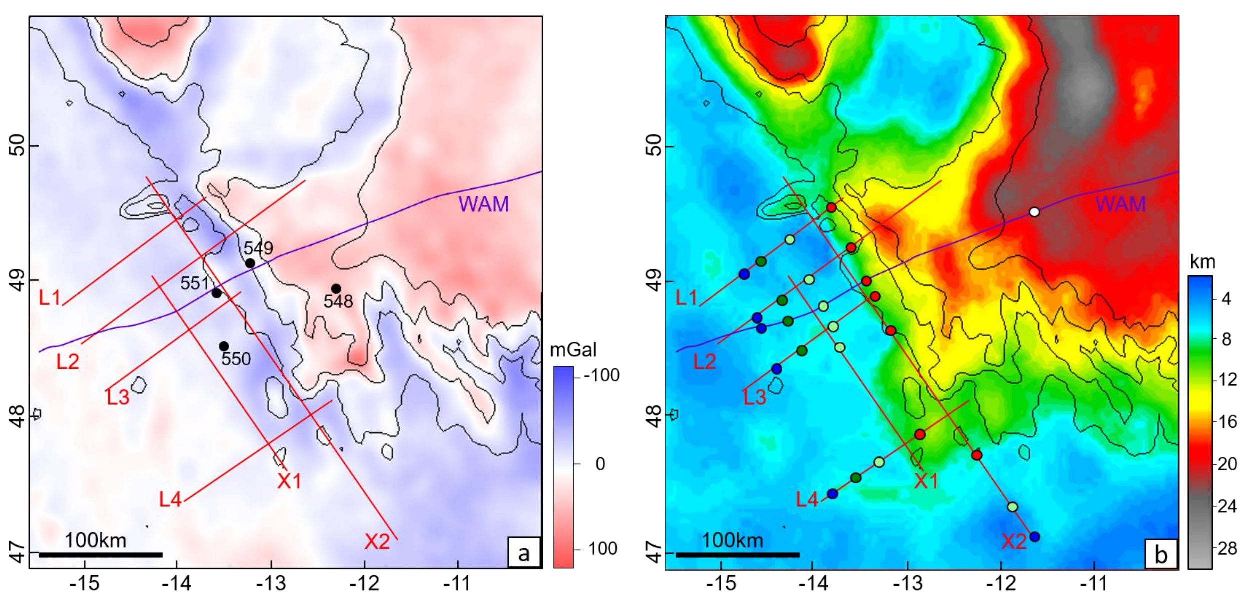

Fig. 3. (a) The free air gravity anomaly with overlying bathymetric contours (Bonvalot et al., 2012). The black circles represent the DSDP Leg 80 drill sites. (b) Crustal thickness derived from gravity inversion (Welford et al., 2010b) with overlying bathymetric contours. Present-day bathymetric contours (black lines) are displayed with a contour interval of 1000 m.The six red lines indicate the new seismic lines in this study; the purple line represents the WAM line. The blue, dark green, light green, red, and white circles respectively mark the landward limits of the oceanic, exhumed subdomain T2, exhumed subdomain T1, hyperextended, necking, and/or proximal domains along each seismic line (Note: these terminologies will be introduced in section 5).

The magnetic anomaly data in Figure 4 are obtained from the Earth Magnetic Anomaly Grid at 2-arc-minute resolution from NOAA - http://www.ngdc.noaa.gov/geomag/emag2/ (EMAG 2). Magnetic Chron 34 (A34) lies along the linear blue band of high magnetization (Müller et al., 2016). There also exists a relatively linear magnetic anomaly with a southeastern trend, approximately parallel to magnetic Chron 34 between seismic profiles L3 and L4 (purple dashed line in Fig. 4b). Generally, the further landward from magnetic Chron 34, the weaker the magnetic anomaly becomes, which might be associated with minor magmatic addition during rifting, in contrast to increasing magmatism during the initiation of seafloor spreading (Bullock and Minshull, 2005). The magnetic characteristics in the region between the continental slope and magnetic Chron 34 vary dramatically from north to south. Along the northern portion of the Goban Spur margin, a region (between X1 and X2) of negative magnetic anomalies is very prominent (Fig. 4b), where DSDP Sites 550 and 551 encounter basaltic rocks (de Graciansky et al., 1985). Magnetic modelling along the WAM line also demonstrates that a basalt sill located at the foot of the continental slope produces a relatively prominent magnetic anomaly, with the causative body extending into the basement (Louvel et al., 1997; Bullock and Minshull, 2005).

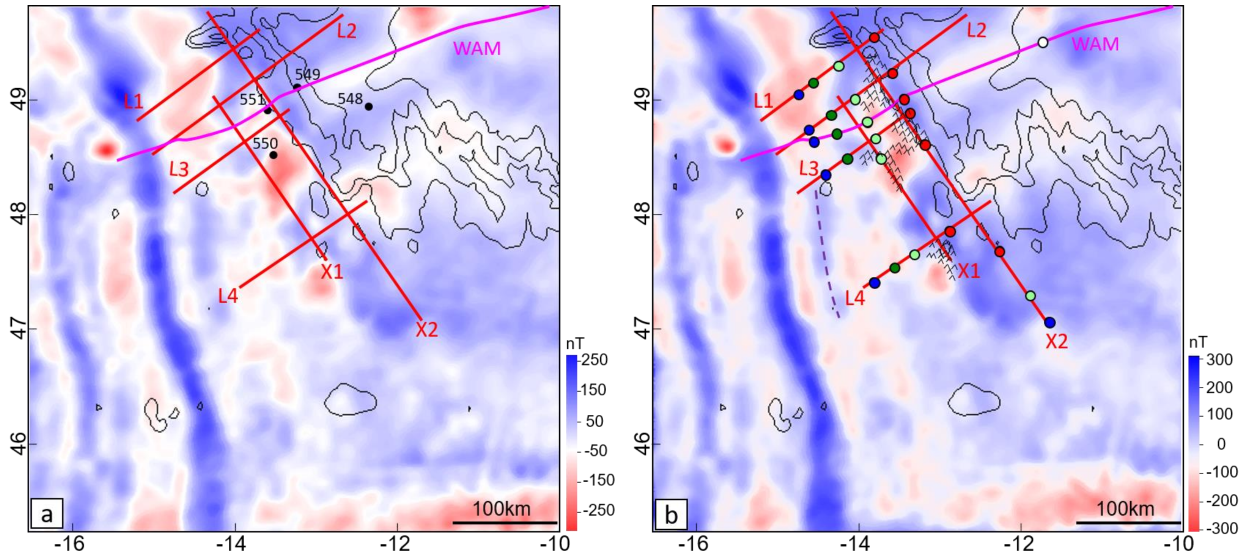

Fig. 4. (a) Magnetic anomaly map across the Goban Spur margin. The black circles represent the DSDP Leg 80 drill sites. (b) Magnetic anomaly data reduced to pole for the Goban Spur margin. Bathymetric contours (black lines) are displayed with a contour interval of 1000 m. The black clusters of open triangles in part b indicate sill distribution from the Petroleum Affairs Division (PAD) of the Department of Communications, Climate Action & Environment, Ireland (http://www.pad.ie). The dashed purple line indicates a relatively linear magnetic anomaly. The six red lines indicate the new seismic profiles; the pink line is the WAM line. The blue, dark green, light green, red, and white circles are defined in Fig. 3b.

4. Seismic acquisition and methodology

In this study, six new multichannel seismic (MCS) reflection lines (L1, L2, L3, L4, X1, and X2) are processed and interpreted (Fig. 1b). Seismic profiles L1, L2, L3, and L4 are oriented southwest-northeast, and profiles X1 and X2 cross these four lines, with a northwest-southeast orientation (Fig. 1b). During acquisition, the survey vessel BGP Explorer towed an array of 48 air guns that were fired with a total volume of 85 L and a shotpoint interval of 25 m for water depths less than 3000 m and 37.5 m for water depths over 3000 m. The seismic data were acquired with a sampling interval of 2 ms and a trace length of 12 s. Data were recorded using a 10 km-long hydrophone streamer with a 12.5 m receiver group spacing, generating 804 traces per shot.

The seismic data processing workflow involves geometry definition with a common-midpoint (CMP) interval of 6.25 m, amplitude compensation, bandpass filtering, predictive deconvolution, multiple attenuation, velocity analysis, pre-stack Kirchoff time migration, and coherency filtering. Next, the time migrated stacked sections are converted from the time domain to the depth domain by using the stacking velocity obtained from velocity analysis. It is worth mentioning that the velocities at and above the basement are primarily picked according to the seismic reflection data, while the velocities beneath the basement are less well constrained and are picked to conform to regional trends derived from seismic refraction data. As for the WAM line, it was not reprocessed in this study, and so the stacking velocities are unavailable. Thus, we interpret the WAM line in the time domain only. Finally, the depth-converted seismic reflection profiles across the Goban Spur rifted margin are interpreted by incorporating insights from seismic refraction data, the complementary WAM line, gravity and magnetic data, crustal thickness estimates from seismic refraction surveys and gravity inversion, and borehole data from DSDP Leg 80.

Since seismic profiles L1, L2, L3, and L4 are subparallel to each other (Fig. 1b) and the distance between L1, L2 and L3 is relatively small, with ~ 36 km, and ~42 km between L1 and L2, and L2 and L3 respectively, they share numerous features (Fig. 1b). Furthermore, since lines L1, L2, the WAM line, and the Bullock and Minshull (2005) refraction line extend into the oceanic domain and cross magnetic anomaly 34 (Fig. 1b), the data coverage is sufficient for investigating the range of tectonic processes from rifting and extension, to the subsequent breakup, and the eventual creation of new oceanic crust. The primary classification standard used for the crustal domains is briefly reviewed in the next section, before discussing the interpreted sections in detail.

5. Interpretation

5.1 Terminology

Although the crustal architecture of rifted margins can vary significantly, they still share some first-order structural components (Osmundsen and Ebbing, 2008; Minshull, 2009; Sutra et al., 2013; Tugend et al., 2014). Peron-Pinvidic et al. (2013) recommend five structural units to describe the transition from unstretched continental crust to oceanic crust; these include: 1) proximal, 2) necking, 3) hyperextended, 4) exhumed, and 5) outer domains. These structural units show contrasting characteristics in terms of basin types, faulted features, and crustal thickness variations, but also correspond to four evolutionary phases of rifted margins: 1) the stretching phase, 2) the thinning phase, 3) the hyperextension and exhumation phase, and 4) the initiation of seafloor spreading and magmatism phase. Using the structural unit division of rifted margins proposed in the literature (Peron-Pinvidic et al., 2013; Tugend et al., 2014), the corresponding interpretations laterally divide each seismic line into different crustal domains in this study.

5.1.1 Proximal domain

The proximal domain undergoes stretching with low extensional values and is commonly characterized by grabens or half-grabens containing syn-rift sediments (Mohn et al., 2012; Peron-Pinvidic et al., 2013). Tilted blocks bounded by listric faults are often observed at the top basement of proximal basins (Whitmarsh et al., 2001). These faults generally terminate in the middle crust without affecting the Moho (Peron-Pinvidic et al., 2013). In addition, the crustal thickness is generally greater than 30 km in the proximal setting (Peron-Pinvidic et al., 2013).

5.1.2 Necking domain

The lithospheric thickness dramatically decreases in the necking zone, which gives the crust a wedged structure (Mohn et al., 2012). Within the wedged region, the Moho drastically shallows due to crustal thinning from ~30 km to less than 10 km (Peron-Pinvidic and Manatschal, 2009).

5.1.3 Hyperextended domain

Hyper-thinning of the crust is often observed in both hyperextended and exhumed zones (Peron-Pinvidic et al., 2013). The hyper-thinned crust is characterized by hyperextended sag basins and half-grabens and the corresponding crustal thickness is generally less than 10 to 15 km (Tugend et al., 2015). The hyperextension stage is important in the evolution of magma-poor margins, and it often, but not always, leads to mantle exhumation (Peron-Pinvidic et al., 2013). Currently, understanding of the nature of the basement in the hyperextended and exhumed domains still lacks consensus. Nonetheless, we still try to interpret both the hyperextended and exhumed domains separately to distinguish the hyperextension stage and the exhumation stage in this study.

5.1.4 Exhumed domain

In the exhumed serpentinized mantle domain, the crust experiences such intense hyper-extension and embrittlement that the extensional faults that provide the conduits for serpentinizing the mantle become detachment faults along which the serpentinized mantle was ultimately exhumed (Reston, 2007; Mohn et al., 2012). P-wave velocity in this domain gradually ranges from ~ 4 km s^{-1} at the seafloor to ~ 8 km s^{-1} at depth (Dean et al., 2000; Bullock and Minshull, 2005; Grevemeyer et al., 2018). The Moho interface is usually unidentifiable in this region (Gillard et al., 2016). At some magma-poor rifted margins, the exhumation zone is subdivided into a region of deeper exhumed serpentinized mantle with more subdued topography and a region of shallower peridotite ridges according to seismic basement relief. By specifically following the subdivision from Welford et al. (2010a), labelled subdomains T1 and T2 are used to differentiate between the transitional crust characterized by smooth basement relief (subdomain T1) and peridotite ridges (subdomain T2) in the exhumed mantle domain, respectively (Fig. 5). This does not mean that the shallower peridotite ridges (subdomain T2) are identified on all of the seismic profiles in the study area. It is worthwhile noting that the outer domain mentioned in Peron-Pinvidic et al. (2013) is not interpreted on the seismic profiles in this study, as it cannot be definitively observed.

5.1.5 Oceanic domain

In the oceanic domain, geophysical patterns can be highly variable, from the linear magnetic anomalies of the Norway Basin, to the disorganized oceanic magnetic anomalies of the Iberian margin (Peron-Pinvidic et al., 2013). Crustal thickness ranges from 6 km to 7 km for normal oceanic crust formed at low to fast spreading rates (White, 2001), while thin oceanic crust (< 5 km) can also be developed in ultra-slow spreading environments (van Avendonk et al., 2017).

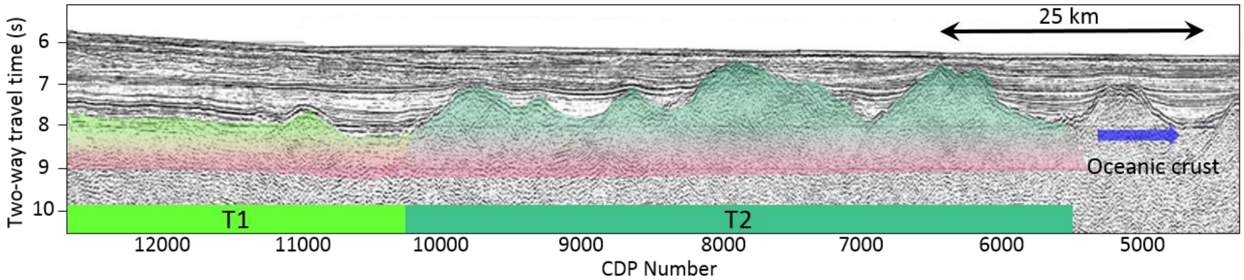

Fig. 5. Portion of the interpreted seismic profile Erable 56 along the Flemish Cap margin showing the exhumed domain and the transition to oceanic crust (Welford et al., 2010a). Labelled subdomain T1 represents the exhumed serpentinized mantle with relatively deep basement. Labelled subdomain T2 represents the shallower exhumed peridotite ridges.

5.2 WAM line interpretation

In this study, although the WAM line is interpreted in the time domain, it is the only line with approximately coincident constraints from seismic refraction modelling (Figs. 1b and 6d) (Bullock and Minshull, 2005). The relatively comprehensive constraints from seismic reflection and refraction data, Moho variations and crustal thickness along the WAM line ensure the robustness of the interpretation of different crustal domains, considered as the baseline. It is worthwhile noting that as sediments deposited on continental margins record rifting and final lithospheric rupture, pre-, syn-, and post-rift sequences are used to describe the stratigraphic successions at rifted continental margins (Franke, 2013). Pre-rift sequences are commonly onlapped by syn-rift infills in the wedge-shaped half-graben basins bounded by faults, recognized by angular unconformities on seismic data (Franke, 2013). Post-rift and syn-rift sediments are also interpreted along the WAM line (Fig. 6c). The post-rift section directly overlies the crustal domains, while the sediments gradually pinchout towards the oceanic domain, displaying highly variable sedimentary thicknesses from NE to SW (Fig. 6c). The Bullock and Minshull (2005) velocity model interpretation (Fig. 6d), when projected to the WAM line, helps constrain the landward limit of the oceanic domain (Figs. 6b and 6c). It is consistent with the crustal domain interpretation of some magma-poor margins (e.g., the Iberia margin and Flemish Cap margin), where the oceanic crust is interpreted to be adjacent to peridotite ridges (Welford et al., 2010a; Davy et al., 2016). From the velocity model (it does not extend to the oceanward limit of the WAM reflection line), the slow-spreading oceanic domain spans ~45 km with an average crustal density of 2740 kg m^{-3} based on gravity forward modelling (Fig. 6d) (Bullock and Minshull, 2005). Correspondingly, the interpreted oceanic domain along the WAM line spans ~70 km and its landward limit lies to the northeast of magnetic Chron 34 (Fig. 6c). The basement relief of the oceanic domain between distances of 44 km and 70 km is more subdued than that of the normal oceanic zone seaward of magnetic Chron 34 (Figs. 6b and 6c).

Although the zone between the thinned continental crust and the oceanic crust is interpreted as exhumed serpentinized mantle along the WAM line based on the velocity-depth structure (Fig. 6d) (Bullock and Minshull, 2005), a further subdivision into three parts is warranted based on the basement morphology and seismic character (Fig. 6c). These three parts are the hyperextended zone (shaded brown), and the exhumed mantle zone, further subdivided into a section with deeper basement displaying smooth basement morphology (subdomain T1, shaded light green in Fig. 6e), and a section of serpentinized peridotite ridges with relatively shallower basement with rougher relief (subdomain T2, shaded dark green in Fig. 6e). It is relatively easy to delimit the boundary (marked by the bold dashed dark green line at the distance of ~95 km in Fig. 6c) between subdomain T1 and T2 due to the apparently different basement morphology, where the top basement deepens landward by ~ 0.5 s and becomes relatively smoother (Fig. 6e). Transitional subdomain T2 spans ~23 km and its basement is deeper than that of the adjacent oceanic domain (Fig. 6c). The geometry of the subdomain T2 also appears similar to the ridges imaged on the Iberia/Galicia margin (Pickup et al., 1996) and the conjugate Newfoundland/Flemish Cap margin (Fig. 5) (Welford et al., 2010a). Several Ocean Drilling Program (ODP) drill sites on both the Iberia margin and the Newfoundland margin have revealed that the equivalently interpreted ridges are composed of exhumed serpentinized mantle material (Sawyer et al., 1994; Whitmarsh et al., 1998; Tucholke et al. 2004), which has been complemented by seismic refraction and reflection data (Pickup et al., 1996; Dean et al., 2000; Shillington et al. 2006; Van Avendonk et al., 2006). At the Goban Spur margin, both Poisson's ratio values (0.34-0.36) and velocities (> 7 km s^{-1} at depths of 5-7 km beneath top basement) obtained from seismic refraction modelling support the presence of serpentinized exhumed mantle in the subdomains T1 and T2 (Bullock and Minshull, 2005). However, the velocities ranging from 7.2 km s^{-1} to 7.6 km s^{-1} within ~ 1.5 km of the top basement in the subdomain T1 at the Goban Spur margin are different from those at the Iberia margin (7.3-7.9 km s^{-1} within 2-6 km below basement) (Dean et al., 2000).

The border (marked by the bold dashed light green line in Figs. 6b and 6f) between the subdomain T1 and the hyperextended domain is determined based on the contrasting seismic patterns at the top basement. The reflection patterns at the top basement are convex upwards in the subdomain T1 and become concave downwards in the hyperextended zone (Fig. 6f). In addition, within the sedimentary formations above the top basement (indicated by the blue arrow in Fig. 6f), the reflective events are relatively weak and continuous above the hyperextended crust, while reflection amplitudes typically appear much weaker (or transparent) and discontinuous above the subdomain T1 (Fig. 6f). The change of seismic facies often occurs during the transition from stretched crust to exhumed mantle at magma-poor rifted margins (Nirrengarten et al., 2018; Gillard et al., 2019). In this study, we refer to these sedimentary formations in the exhumed domain as syn-exhumation sediments. Furthermore, the reflector below the top basement indicated by the black arrow in Figure 6f likely indicates the contact between the hyperextended crust and exhumed serpentinized mantle, similar to the S-reflector at the West Iberia margin (Reston et al., 1996).

The boundary (marked by the bold dashed brown line in Fig. 6b) between the hyperextended zone and the necking zone is primarily defined by the Moho depth derived from gravity inversion (Fig. 6a) (Welford et al., 2010b). The Moho depth shallows from ~23 km to ~15 km over a distance of ~ 145 km in the necking domain, while it ranges from ~ 15 km to ~ 12 km in the hyperextended zone with crustal thickness less than ~ 10 km (Figs. 3b and 6a). Additionally, the wedged structure bounded by tilted faults is a typical feature in the necking zone (~ 180 - 200 km in Fig. 6c), while the “sag” type basin is easily observed in the hyperextended region (~ 155 - 175 km in Fig. 6c), which is consistent with the classification criteria of crustal domains proposed by Tugend et al. (2014; 2015). A basaltic body at the toe of the hyperextended zone was sampled by DSDP drilling site 551 (Fig. 6c) and was used to infer the location of initial oceanic crust formation (Horsefield et al., 1994). However, Bullock and Minshull (2005) argued that the emplacement of the basaltic body occurred during lithosphere thinning before the mantle material began to be exhumed. Dean et al. (2009) used the basaltic lava at sites 550 and 551 to calculate a rift duration of 8-13 Myr at the Goban Spur margin, close to 14-22 Myr assumed by Bullock and Minshull (2005).

The boundary (marked by the bold dashed red line in Fig. 6b) between the necking zone and the proximal zone is mainly dependent on the Moho depth and crustal thickness calculated from gravity inversion (Fig. 6a) (Welford et al., 2010b). The oceanward shallowing Moho and rapid decreasing crustal thickness are evident in the necking zone (Figs. 6a and 3b), while the crustal thickness is roughly 21 km, and the Moho depth varies from ~ 25 km to ~ 22 km in the proximal zone where the Moho depth is ~ 26 km in the velocity model from Horsefield et al. (1994).

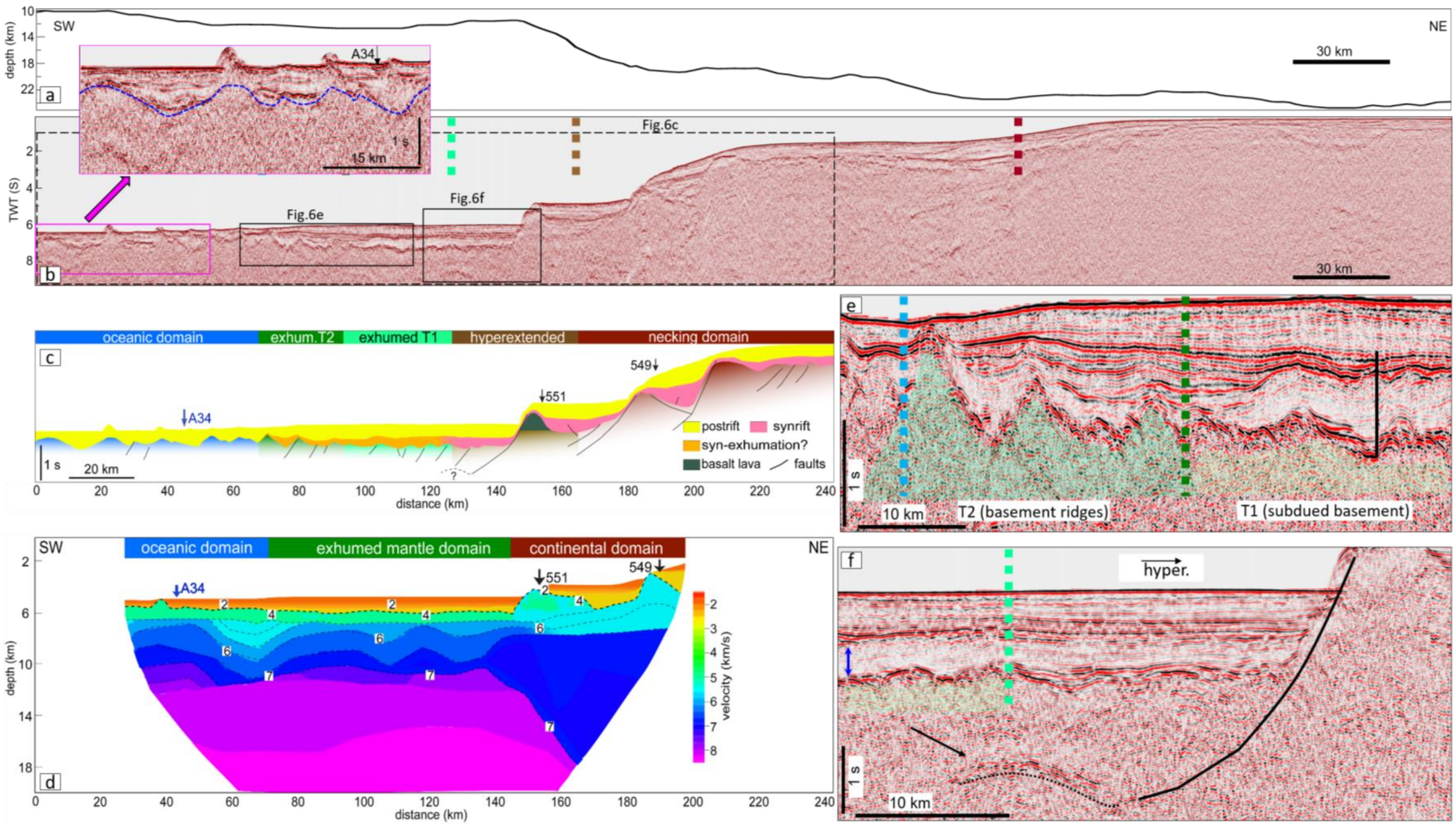

Fig. 6. (a) Moho depth along the WAM line (from Welford et al., 2010b). (b) A section of the WAM line. The bold dashed coloured lines indicate boundaries between crustal domains. (c) Interpretation of the segment of the WAM line, outlined by the thin dashed black line in part b. Sites 549 and 551 are projected onto the WAM line from ~2.8 km and ~1.5 km away, respectively. (d) Velocity structure derived from seismic refraction modelling (adapted from Bullock and Minshull, 2005). (e) The enlarged portion of the seismic profile in part b. It illustrates the shallower peridotite ridges and the deeper exhumed zone with subdued basement. (f) The expanded portion of the seismic profile in part b. It shows the variation in basement morphology in the exhumed domain and the hyperextended domainrs.

5.3 Crustal domain interpretation

As the WAM line lies within the region intersected by lines L1, L2, and L3, its interpretation is extrapolated to these other profiles. To ease identification of the boundary delineations between transitional subdomains T1 and T2, the WAM line and the four new seismic lines (L1-L4) are truncated to the same length to highlight the seismic reflection character within the transitional zones in Figure 7. L1 and L2 cross magnetic Chron 34 and extend ~21 km and ~9 km seaward of magnetic Chron 34, respectively. Meanwhile, the seaward ends of seismic profiles L3 and L4 are ~6 km and ~54 km landward of magnetic Chron 34.

As introduced above, the boundary between the oceanic crust and the exhumed domain on the WAM line is based on crustal velocity constraints. By comparing the characteristics of basement topography and reflectivity of syn-rift sedimentary layers against the WAM line interpretation, the subdivisions of the exhumed domain along lines L1 and L2 are inferred (Figs. 7, 9 and10). West of the interpreted peridotite ridges (shaded dark green Figs. 7b and 7c) lies the oceanic crust. The serpentinized peridotite ridges exhibit relatively sharp peaks on profiles L1 and L2, spanning ~16 km along L1 (Figs. 7b and 9), and ~25 km along L2 (Figs. 7c and 10). Landward, the peridotite ridges become shorter along both the WAM line and line L2 (Figs. 7c and 7d).

In the exhumed domain on lines L1 and L2, sub-horizontal intra-basement reflectors are observed ~ 2.5 km below the top basement (red lines in Figs. 9b and 10b, indicated by black arrows in expanded solid black boxes in Figs. 9a and 10a, respectively), where the interpreted normal faults appear to root. These discontinuous intra-basement reflections are also visible in the exhumed mantle zone at Iberia-Newfoundland margins and the Armorican margin, and are interpreted as decoupling interfaces (Gillard et al., 2019). These intra-basement reflectors are used to identify the exhumed domain in this study.

Compared with the WAM line, on line L1, and line L2, the basement morphology outboard of the interpreted subdomain T2 on seismic profile L3 is more complicated due to the presence of a seamount and is more uncertain due to the lack of nearby velocity constraints. Nonetheless, since the sub-horizontal and landward-dipping intra-basement reflectors are also observed on the profile L3 (indicated by the black arrow in Figs. 8a and 11b), we define the boundary between the oceanic domain and the subdomain T2 at the oceanward end of the intra-basement reflector, where the normal faults terminate (Fig. 8a). Since the basement reflection patterns of the intervening T1-T2 transition segment (58-68 km in Fig. 11) of line L3 fail to be completely consistent with the typical subdomain T1 or T2 described on the WAM line, the border between the two subdomains cannot be accurately defined, but is inferred to lie within the segment (Figs. 7e and 11).

The exhumed domain interpretation of seismic profile L4 is described last because it is the least constrained as it is located 113 km to the south of L3, lying significantly landward of magnetic anomaly 34 (Fig. 1b). Basement reflectivity along the southwestern half of profile L4 is less continuous and highly faulted, and the depth of the top basement along the segment is ~5.6 km, shallower than the top-basement depth (~6.5 km) of the oceanward northern profiles (L1-L3), possibly due to proximity to the complex stress field near the BTJ. Nonetheless, basement structures and geometry of syn-exhumation formations on both L3 and L4 are similar (Fig. 8), which helps to constrain the extent of subdomain T2 along L4 (Figs. 7, 8, and 12).

On lines L1 to L4, the basement relief of transitional subdomain T1 (shaded light green) is generally smoother and deeper than that of transitional subdomain T2 (Fig. 7). The width of the interpreted transitional subdomain T1 consistently ranges from between ~20 km and ~33 km along each of these seismic lines (Fig. 7). In the transitional subdomain T1, the reflectivity in the syn-exhumation formations is strikingly weak, especially for lines from L1 to L3 (Fig. 7).

The boundaries between the exhumed and hyperextended domains are delineated by contrasting basement structure and reflection patterns. The oceanward-dipping listric faults and continuously reflective sedimentary successions in the hyperextended sag basins are clear along lines L1, L3, and L4 (Figs. 7b, 7e, and 7f). In addition, the concave downward continuous top-basement reflections transition into rugged disorganized reflections at the border of the two zones along lines L3 and L4 (Figs. 7e and 7f). As for the border between the two domains along line L2, reflectors (indicated by the dash black line in the expanded yellow box in Fig. 10a) probably also represent the contact between the hyperextended crust and exhumed serpentinized mantle, similar to the deep reflector along the WAM line (Fig. 6f). Thus, the seaward limit of the reflector is interpreted as the landward edge of the exhumed mantle domain along L2 (Figs. 7c and 10).

In this study, the two seismic crosslines, X1 and X2, are crucial for validating crustal domain subdivisions and ensuring regional consistency in the interpretations. By comparing the reflection patterns along L2 and L3, the region spanning ~ 60 km to the northwest along X1 is certainly defined as the exhumed mantle domain since all three lines show striking transparent syn-exhumation layers (Figs. 7 and 13). In terms of the border between the exhumed and hyperextended domains along X1, it is roughly defined at ~ 70 km by taking two aspects into account. The first is the negative flower structure observed across distances of 80 ~ 90 km (expanded box in Fig. 13a). The second is the oceanward-dipping reflectors (indicated by the black arrows in the expanded box in Fig. 13a) that may be similar to those observed along line L2 (expanded in the yellow box in Fig. 10a), representing the oceanward limit of the hyperextended zone. Since the reflection patterns appear to be consistent and Moho depth shows limited variation (12.5 ~ 14.5 km) to the southeast of X1, the remaining part of the line is interpreted as the hyperextended domain (Fig. 13).

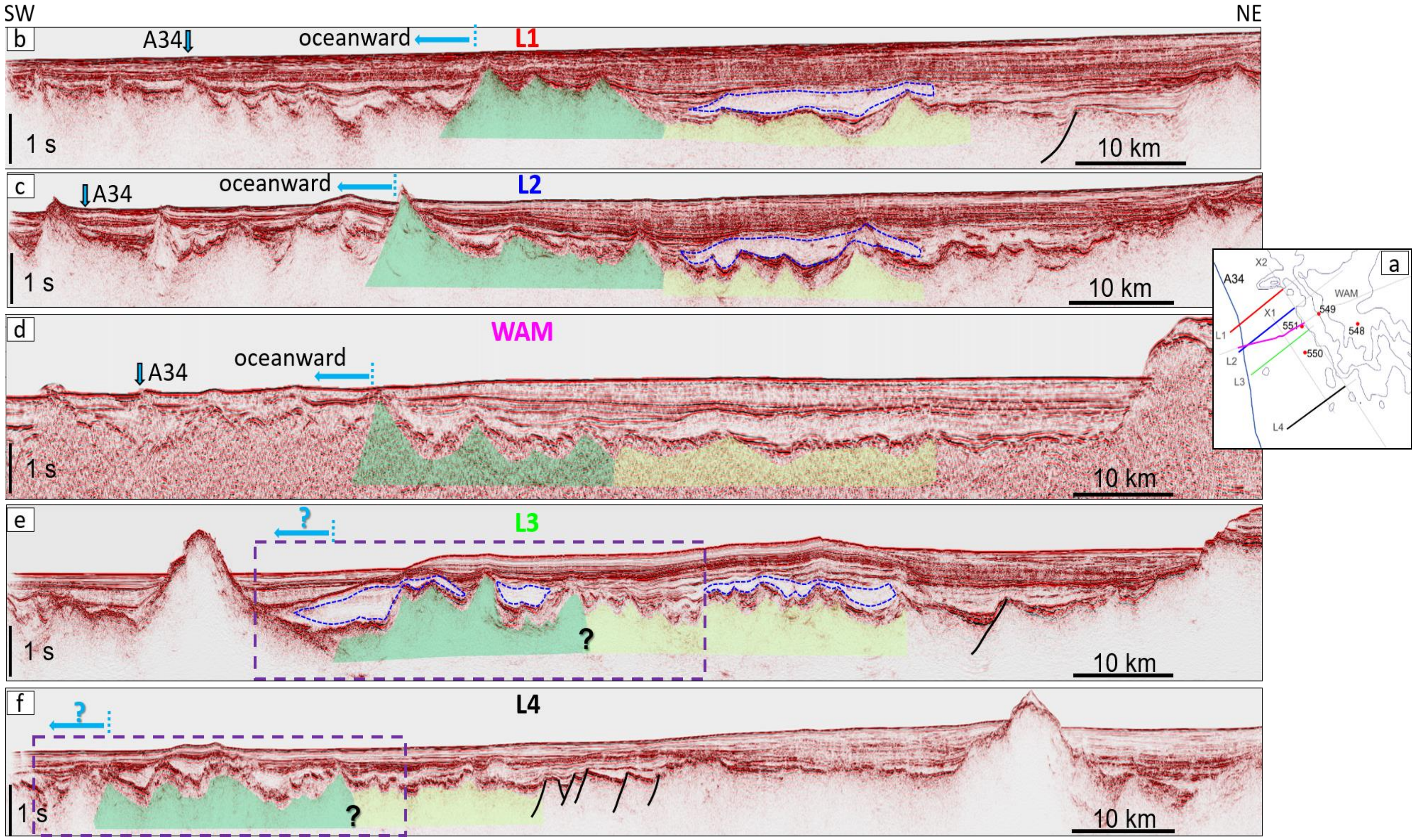

Fig. 7. (a) The location of the parallel seismic lines as indicated by different line colors. (b)-(f) show the interpreted seismic lines L1, L2, the WAM line, L3, and L4 in the time domain,, with label colors matching the line colors in part a.. The transparent dark green areas indicate the interpreted serpentinized peridotite ridges with rougher shallow basement (subdomain T2). The light green regions correspond to the interpreted exhumed mantle displaying subdued topography at top-basement (subdomain T1). Faults (black solid lines) are also interpreted on sections L1, L3, and L4. The blue dashed regions roughly indicate geometries of the transparent/weakly reflective syn-exhumation sedimentary layers.

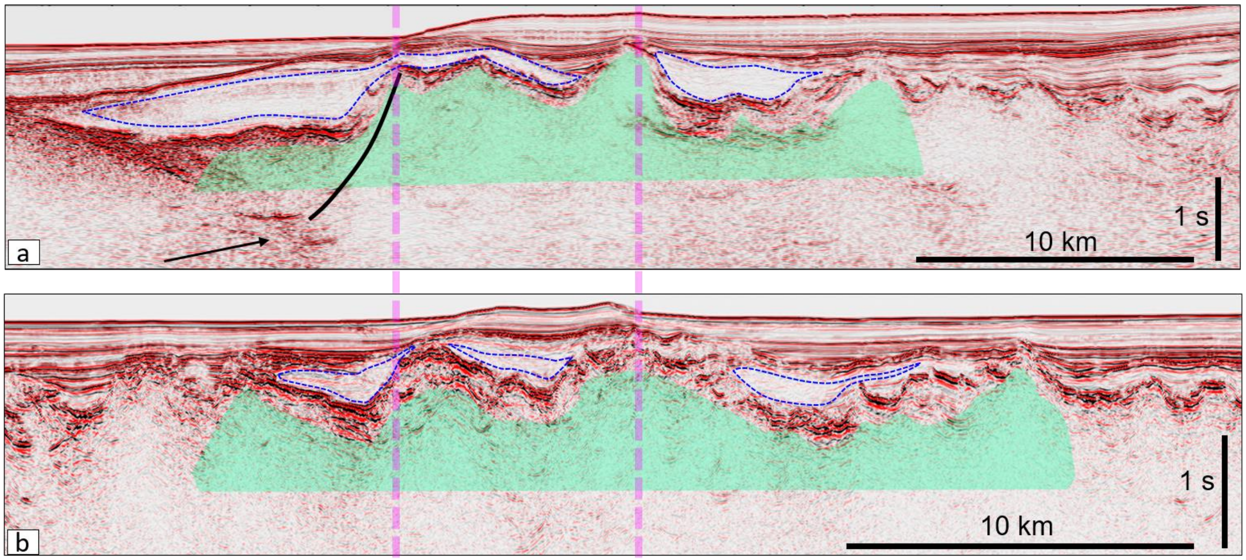

Fig. 8. The upper and lower panels show the enlarged sections outlined in the dashed purple boxes in Figure 7e and 7f, respectively. The blue dashed regions roughly indicate geometries of the transparent/weakly reflective syn-exhumation sedimentary packages.

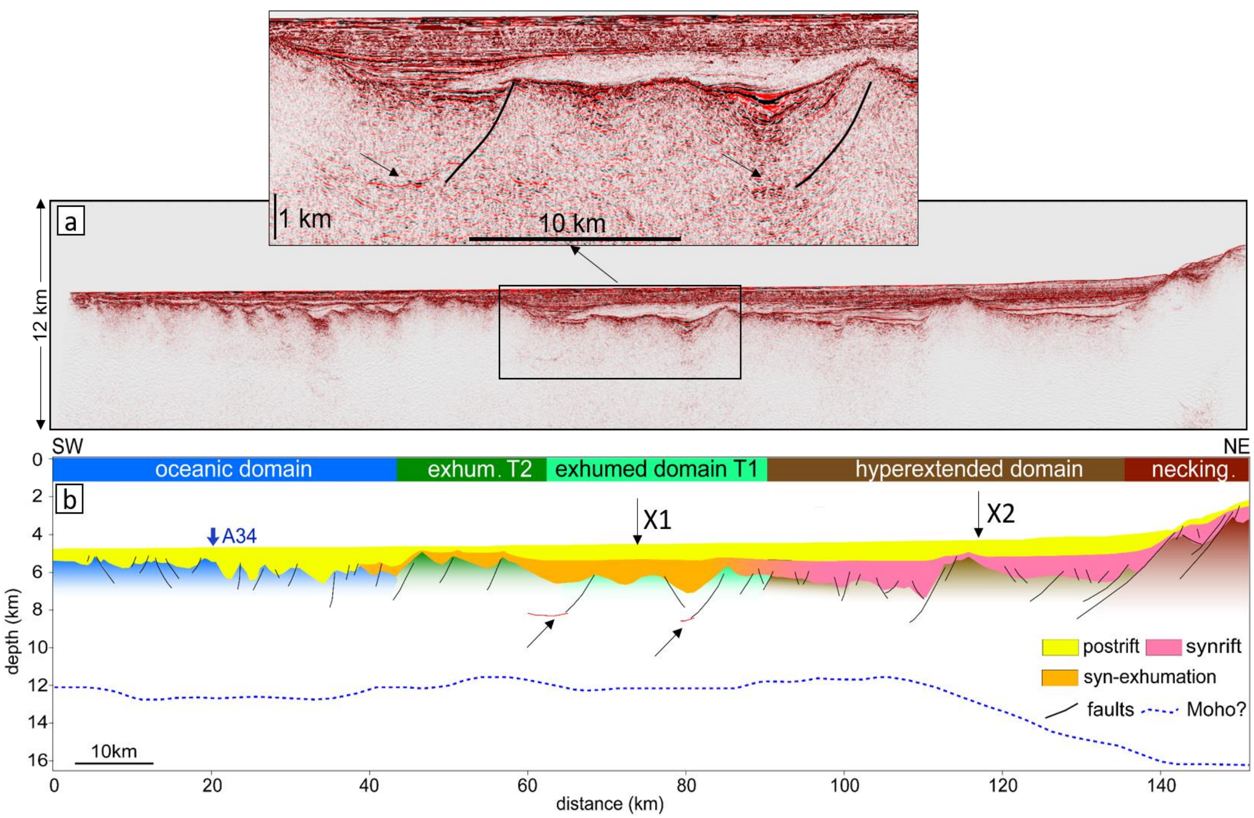

Fig. 9. (a) The uninterpreted depth-converted seismic profile L1. (b) The interpreted seismic profile L1 in the depth domain. The black arrows in the expanded box indicate the red intra-basement reflectors in panel b. Moho in panel b is derived from constrained 3-D gravity inversion (Welford et al., 2010b).

Along X1, the transparent syn-exhumation layer in the exhumed domain appears to be laterally consistent over a distance of 60 km and gradually pinches out towards the hyperextend domain (Fig. 13). Towards the southeast, the basement reflectors become shallower and more chaotic in the transitional domain (~ 65-75 km along line X1) from the exhumed domain to the hyperextended domain (expanded box in Fig. 13). According to the interpretation of sill distribution from PAD (Fig. 4b), magmatic activities occur in the transitional zone (~ 65-75 km, around the light green circle along line X1 in Fig. 4b), which may be responsible for the formation of more chaotic basement reflectors. In addition, the magnetic anomalies in the region show the transition from positive to negative (Fig. 4b).

Compared with seismic profile X1, profile X2 is about 167 km longer and was acquired closer to the continental shelf (Fig. 1b). Along the southeastern portion of the profile X2, both the hyperextended and exhumed mantle zones span approximately 40 km (Fig. 14), interpreted on the basis of a northward extrapolation of the crustal domains from the north Bay of Biscay margin interpreted by Tugend et al. (2015).

In addition to relying on seismic characteristics, gravity inversion results from Welford et al. (2010b) are also used to define the boundary between the hyperextended and necking zones. Along L2, in addition to the shallowing Moho depth in the necking zone, the sag structure (black oval circle in Fig. 10a) and wedge-shaped blocks (dashed black box in Fig. 10a) help to roughly define the border between the two zones at ~ 140 km. However, profiles L1 and L3 do not extend landward enough to adequately capture the necking zone, impeding the interpretation of the boundary between the two domains. Conveniently, profile X2 intersects seismic profiles L1, L2, L3, L4, and the WAM line (Fig. 1b). The necking zone is interpreted based on the decreasing Moho depth, spanning a distance of ~130-250 km along X2 (Fig. 14b). To the northwest of the necking zone along X2, the reflection patterns at the top basement are laterally consistent and the Moho depth is relatively smooth. Furthermore, the intersection point of L2 and X2 falls into the hyperextended domain from the interpretation of L2 above. Thus, the northwestern portion of X2 is interpreted as the hyperextended domain (Fig. 14). Then, the landward edges of the hyperextend zones along L1 and L3 are located inboard of X2 since the intersections of L1 and X2, L3 and X2 fall into the hyperextended zone of X2 (Figs. 9, 11, and 14). It is found that the Moho depth of the interpreted hyperextended zone of L1 to L3 ranges from ~ 16 km to ~10 km, with crustal thickness less than 10 km (Figs. 3b and 9-11). For regional consistency, the border between the hyperextended and necking zones along L4 is placed at ~90 km, where the Moho depth and crustal thickness are approximately 16 km and 10 km, respectively (Fig. 3b and 12). In addition, the prominent continuous high-amplitude reflectors at the top basement within the continental crust along profiles X2 and X1 display similar features (Fig. 15), and are both interpreted as the hyperextended crust (Figs. 13 and 14).

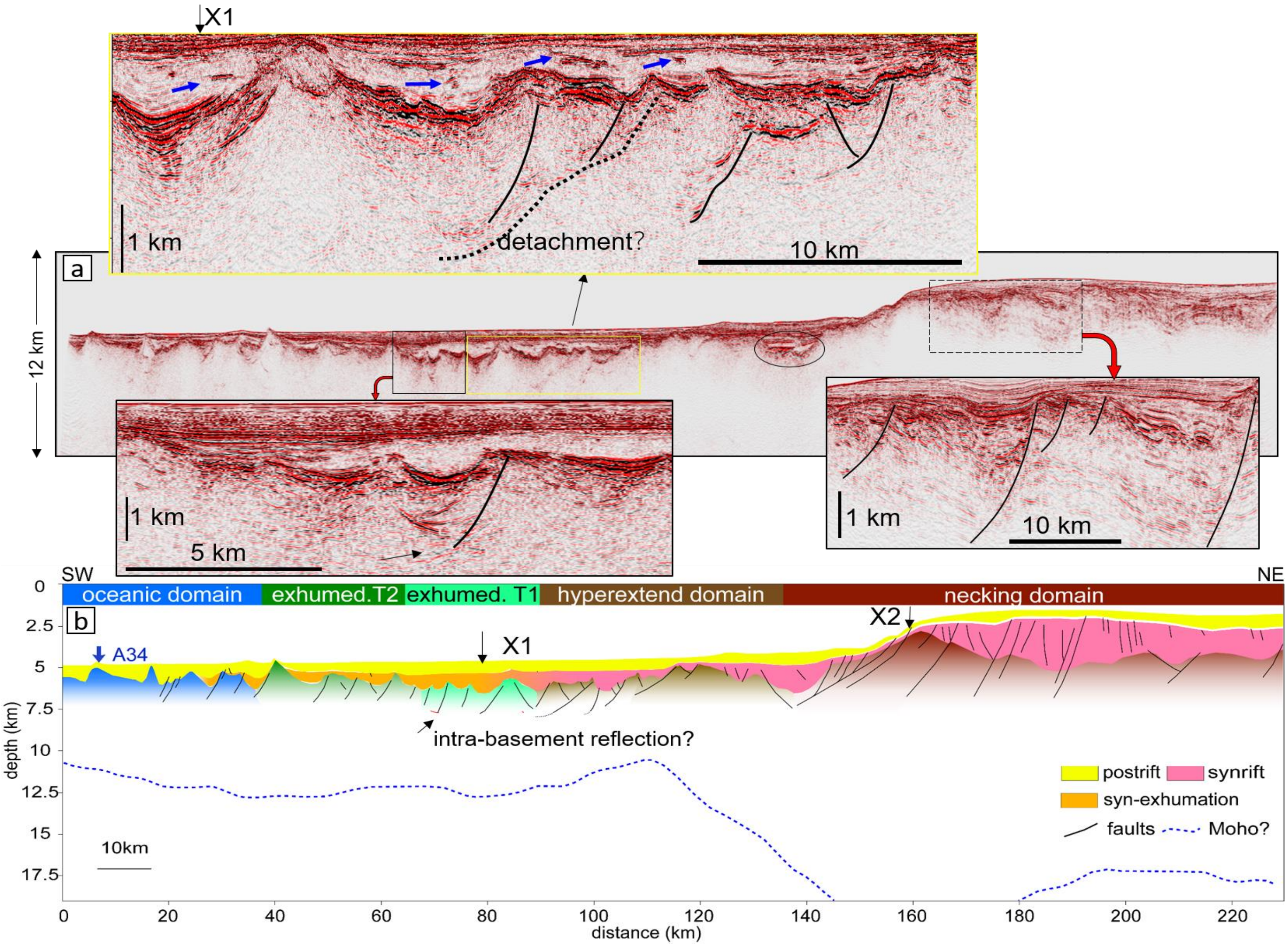

Fig. 10. (a) The uninterpreted depth-converted profile L2. (b) The interpreted profile L2 in the depth domain. The blue arrows indicate sills (?) in the yellow expanded box. The intra-basement reflection (?) is indicated by the arrow in the expanded solid black box.

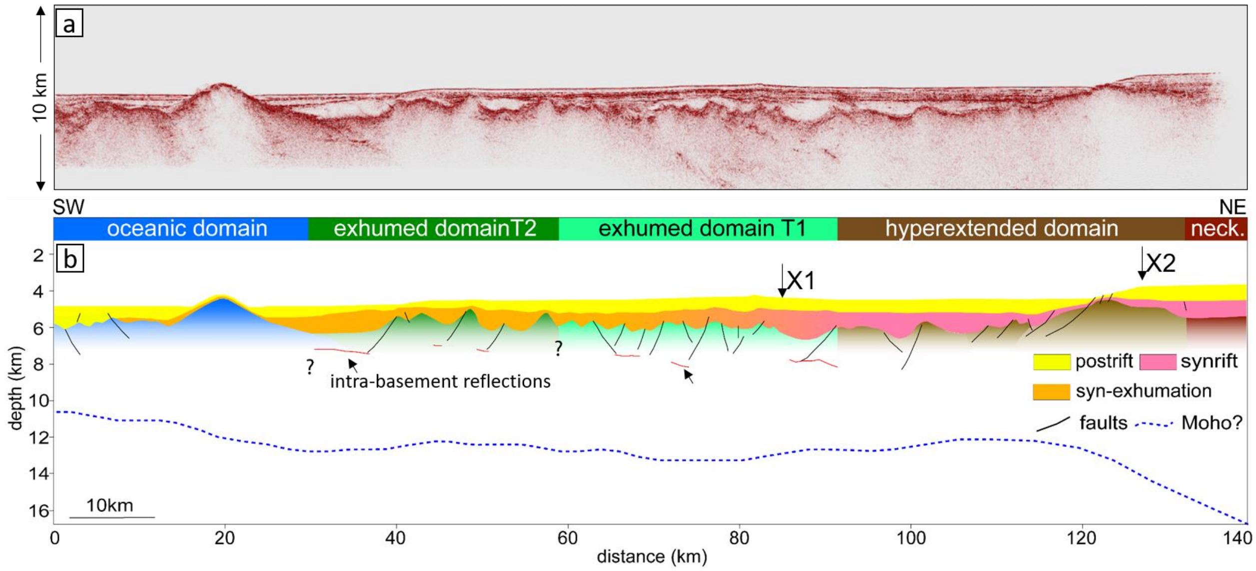

Fig. 11. (a) The uninterpreted depth-converted seismic profile L3. (b) The interpreted seismic profile L3 in the depth domain.

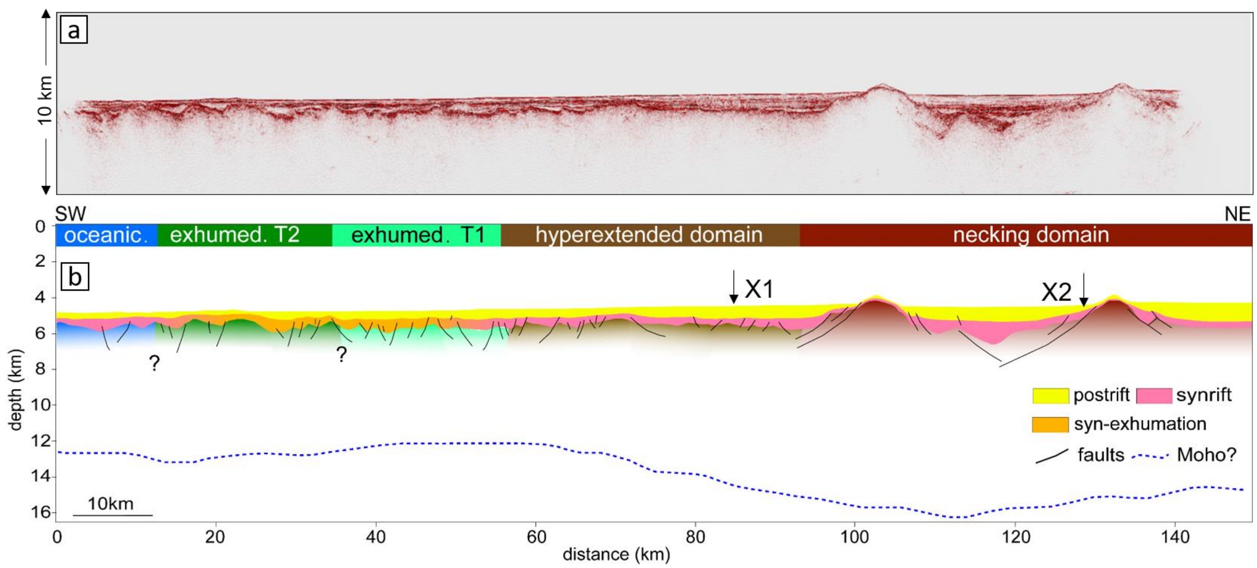

Fig. 12. (a) The uninterpreted depth-converted seismic profile L4. (b) The interpreted seismic profile L4 in the depth domain.

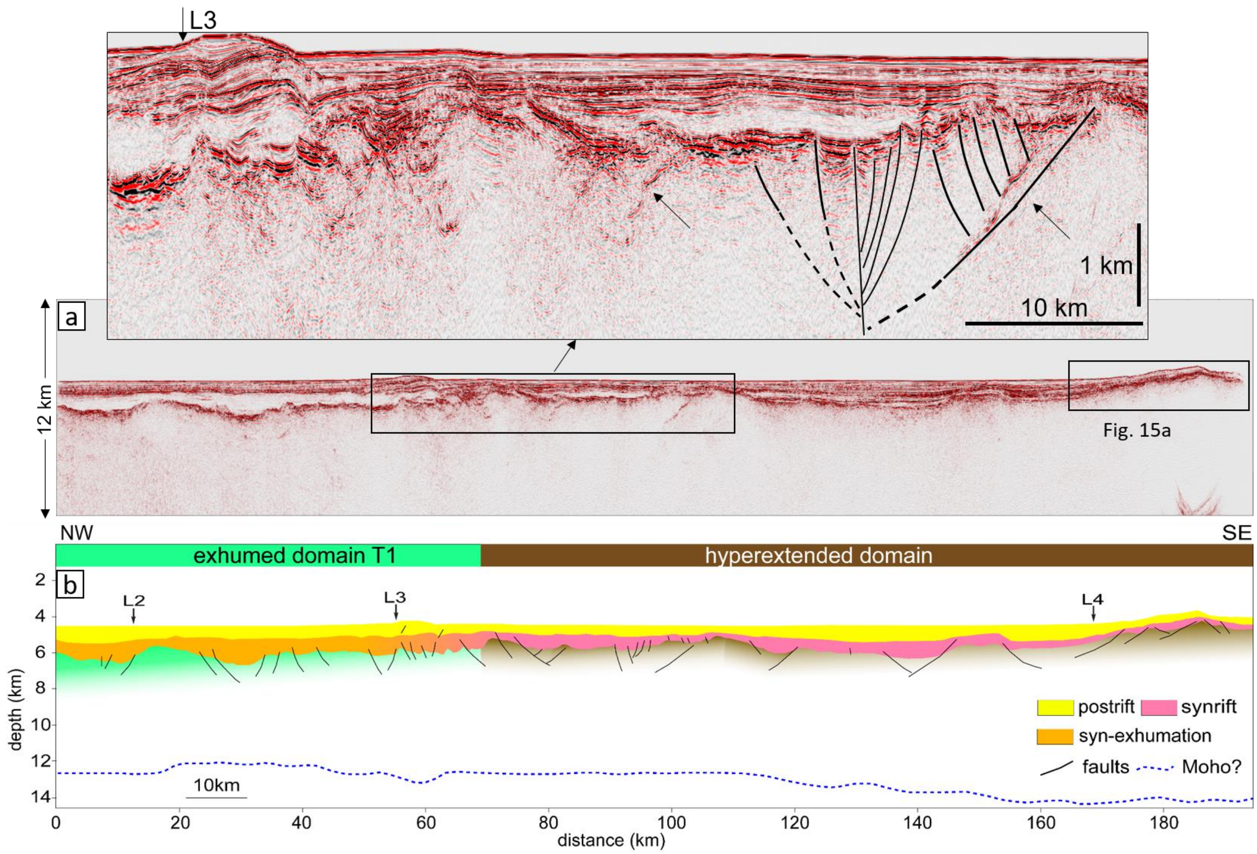

Fig. 13. (a) The uninterpreted depth-converted seismic profile X1. Expanded box above panel a shows an interpreted flower structure. The arrow indicates the detachment fault (?), similar to that in the expanded yellow box in Fig. 10. (b) The interpreted seismic profile X1 in the depth domain.

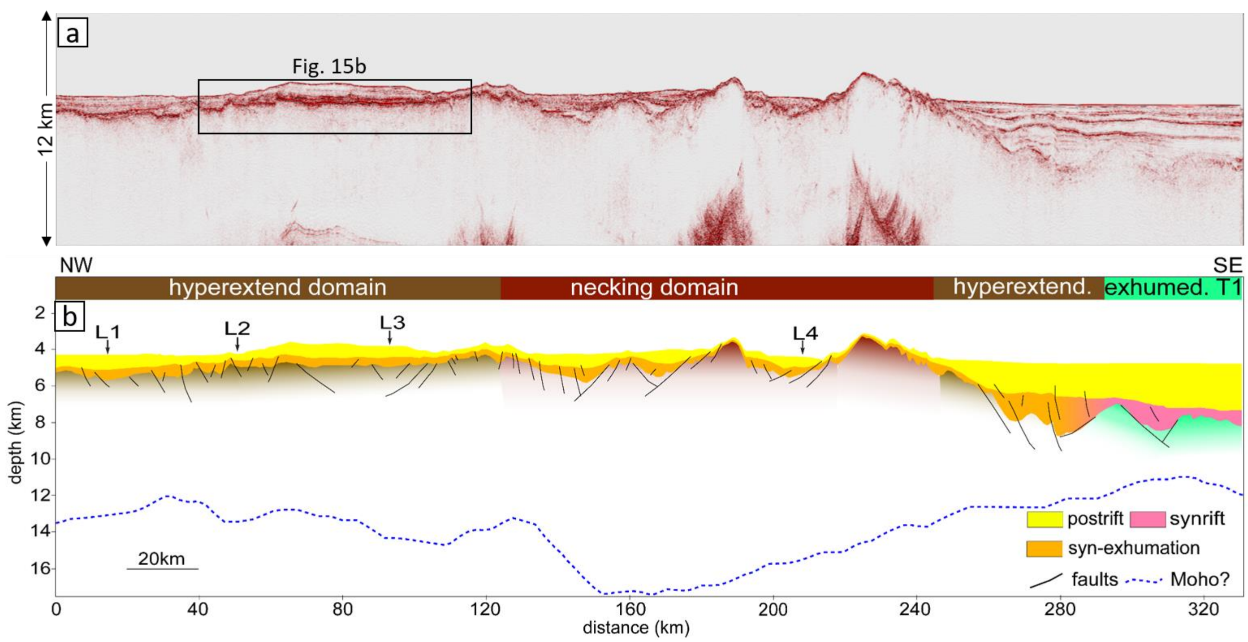

Fig. 14. (a) The uninterpreted depth-converted seismic profile X2. (b) The interpreted seismic profile X2 in the depth domain.

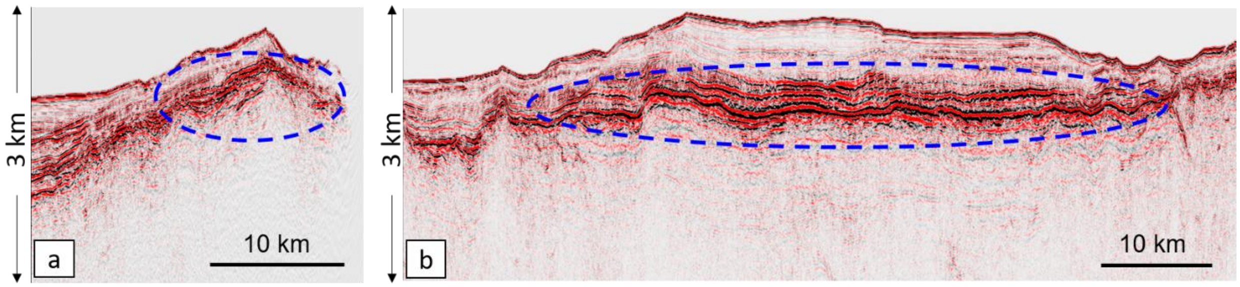

Fig. 15. (a) The expanded seismic section of the black box shown in Fig. 13 and (b) the expanded seismic section of the black box shown in Fig. 14. The blue circles show anomalously strong-amplitude reflectors at the top basement.

6. Discussion

6.1 Crustal architecture

The interpretations presented for the new seismic profiles (Figs. 7 to 14) have allowed us to map the crustal architecture across the Goban Spur margin (Fig. 16). The newly constrained crustal domains are complemented by interpreted domains from the surrounding regions derived from gravity inversion (Welford et al., 2010b; Tugend et al., 2015; Sandoval et al., 2019). The landward extent of the new seismic lines into the stretched continental crust is limited, so the rift-related structures (thrusts, normal faults, and transfer faults) from PAD are used to depict structures in the continental domain (Fig. 16). CM multichannel seismic profiles (white lines shown in Fig. 1b) are also used to help validate our interpretation (Masson et al., 1985), although the data quality is much poorer. Constraints in the south are fewer than to the north, so many uncertainties remain for understanding the southern part of the margin. It is also noted that the boundaries between the crustal domains are much more diffuse than depicted, as reactivation of structures during subsequent rifting stages has likely happened over the tectonic evolution of the margin (Peron-Pinvidic and Manatschal, 2009). Nonetheless, the crustal architecture map in Figure 16 still significantly increases our regional knowledge of the Goban Spur margin structure.

6.1.1 Proximal domain

The proximal domain across the Goban Spur margin experienced limited extension, characterized by normal faults (Fig. 16) (Naylor et al., 2002), which is similar to many other rifted continental margins, such as Iberia-Newfoundland, and the mid-Norway-East Greenland rifted margins (Peron-Pinvidic et al., 2013).

The seaward limit of the proximal zone is in agreement with the WAM line interpretation (Peddy et al., 1989), the only seismic line extending into the proximal domain in this study (Fig. 6). The formation of the proximal zone corresponds to the initial lithosphere stretching during the late Paleozoic and early Mesozoic, accompanied by regional faulting, forming half-grabens and horsts (de Graciansky and Poag, 1985).

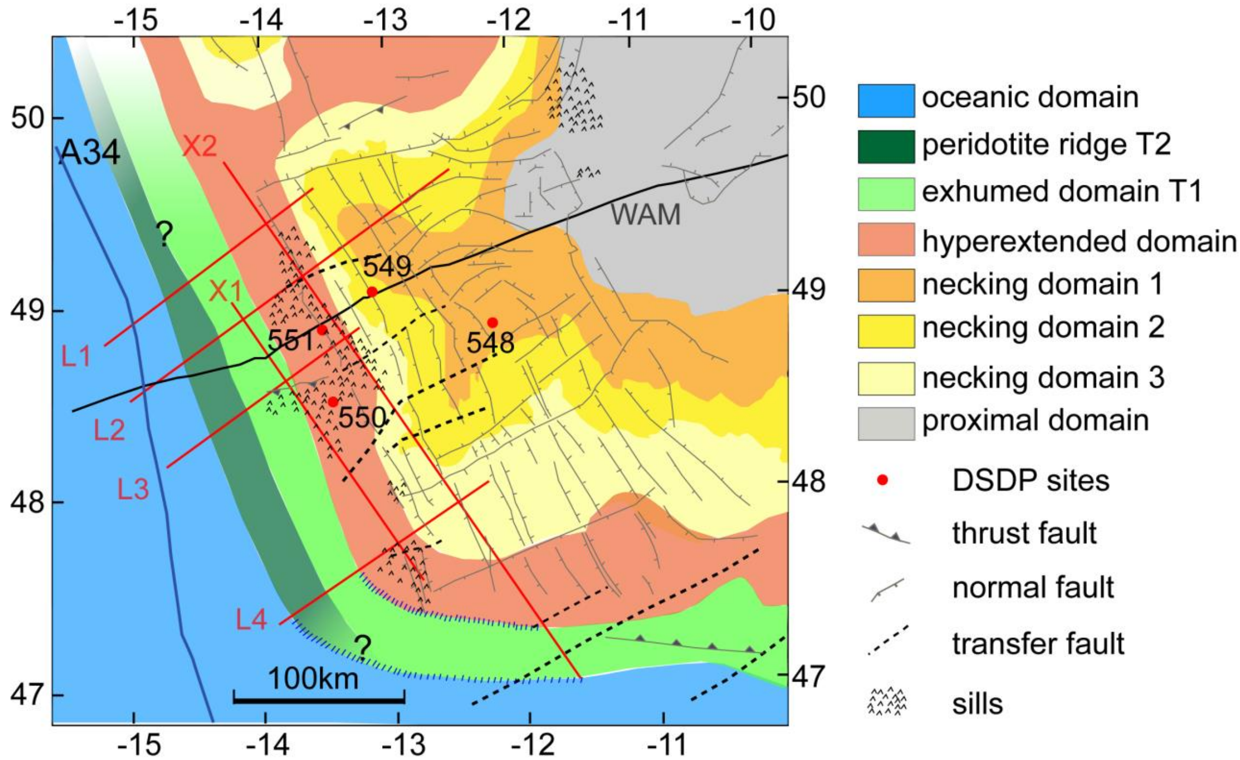

Fig. 16. Crustal architecture of the Goban Spur margin. The dark blue line indicates magnetic Chron 34 (Müller et al., 2016). Seismic profiles are plotted in red (L1, L2, L3, L4, X1, and X2), and in black (WAM line). Crustal domains interpreted beyond the new seismic coverage are constrained from gravity inversion results (Welford et al., 2010b; Tugend et al., 2015; Sandoval, 2019). The hash pattern indicates ill-constrained boundaries between the crustal domains.

6.1.2 Necking domain

The necking zone is divided into three subdomains according to their crustal thicknesses (Welford et al., 2010b; Fig. 3b), as defined and color-coded by Sandoval et al. (2019). The crustal thicknesses for necking domains 1, 2, and 3 range from ~21 km to ~16 km, from ~16 km to ~12 km, and from ~12 km to ~ 9 km, respectively. The oceanward boundary of the subdomain necking zone 3 is also constrained by the interpreted hyperextended region. Along strike of the Goban Spur margin, the width of each necking subdomain is highly variable from northwest to southeast. Since the extension rate has an impact on the final structure of passive rifted margins (Tetreault and Buiter, 2018), the highly variable geometry of each subdomain of the necking zone at the Goban Spur may be associated with differential extension rates, the original crustal compositions, and rheology. It has been postulated that the limit of the seaward-thinning continental crust corresponds to a coupling point, separating decoupled deformation (continentward) from coupled deformation (oceanward) from a lithospheric rheology perspective, according to Perez-Gussinye et al. (2003). The differential stretching in the necking zone may result from rheologically-governed detachment structures overlying the lower crust facilitating greater extension of the upper and middle crust, as has been proposed for the Porcupine Seabight Basin (Naylor et al., 2002). Two major orientations of faulting control the structural patterns within the necking zone: NW-SE trending normal faults and NE-SW faults. The former are approximately parallel to the strike of Goban Spur, as shown in the fault interpretation in the necking zone of X2 (expanded box in Fig. 14). The latter are approximately perpendicular to the margin strike (Dingle and Scrutton, 1979), aligned with the interpretation of line L2 (Fig. 10).

6.1.3 Hyperextended domain

The parallel-margin hyperextended region is deduced by both seismic data interpretation and gravity inversion results, consisting of a belt of slightly variable width along the strike of the Pendragon Escarpment (Fig. 1b). Crustal thickness in the hyperextended zone is less than ~ 10 km (Fig. 3b). From north to south, the magnetic anomaly transitions from negative to positive in this region (Fig. 4b). Margin-parallel variations in the width of the hyperextended continental crustal domain may have been influenced by an interpreted transfer fault close to Sites 548 and 550, across which the deformation changes from ENE-WSW to NE-SW. The pre-existing Variscan orogenic fabrics may also have contributed to shaping the present-day configuration of the proximal to hyperextended crustal domains (Dingle and Scrutton, 1979). Possible transtensional tectonic movement may also have occurred between the northern and southern portions of the margin based on the presence of the interpreted flower structure along X1 (Fig. 13).

6.1.4 Exhumed mantle domain

The identification of the exhumed mantle domain across the Goban Spur margin is primarily based on on seismic velocity constraints and the reflectivity characteristics on the seismic profiles, and how they compare with seismic reflection data on the southern Flemish Cap margin, as shown in Figure 5. This domain is primarily composed of serpentinized mantle peridotite and shows a velocity structure that smoothly increases with depth (Fig. 6d), suggestive of a decreasing degree of serpentinization with depth (Bullock and Minshull, 2005). Nonetheless, the basement rocks in the exhumed domain may have diverse compositions and are generally hypothesized to include: oceanic crust, continental crust, serpentinized mantle peridotite, or hybrid crust composed of any of these (Welford et al., 2010a; Peron-Pinvidic et al., 2013). In addition, some discontinuous intra-basement reflectors are observed in the region (Figs. 9-11), likely acting as a rheological interface that plays a critical role in localized deformation during exhumation and serpentinization (Gillard et al., 2019). The magnetic anomaly is relatively weak and discontinuous in this domain (Fig. 4b). Magmatic additions may also occur in this domain, indicated by the observation of sills along L2 and L3 (enlarged sections in Fig. 10). As introduced previously, we divide the exhumed domain into two subdomains to better characterize the margin (Fig. 16).

1) Subdomain T1

The transition of top-basement seismic facies from concave downward to convex upward reflections (Fig. 7), and extensional detachments (expanded boxes in Figs. 10 and 13) helps to define the landward limit of the subdomain T1. This region, juxtaposed landward against the hyperextended domain, shows deep and smooth basement relief (Fig. 7). The low relief reflective surface at the exhumed basement is interpreted as either a detachment surface allowing for continental crust exhumation (Whitmarsh et al., 2001), or the exhumed serpentinized mantle itself (Sutra et al., 2013). Along strike of the margin, the width of the interpreted subdomain T1 slightly decreases to ~ 22 km to the southeast. At the southeastern limit of the margin, the width of the transitional subdomain T1 averages ~ 40 km, narrower than the equivalent domain along the north Bay of Biscay margin (Tugend et al., 2015).

2) Subdomain T2

Subdomain T2 is characterized by a series of margin-parallel peridotite ridges with shallow and rough basement relief (Fig. 7). This subdomain lies between the oceanic crust and the transitional subdomain T1. The relief and elevation of the basement, respectively, become rougher and higher from the subdomain T1 to the subdomain T2 (Fig. 7). The change in basement morphology may suggest a time-dependent rheological change during the exhumation stage (Sibuet and Tucholke, 2012). In addition, from Figure 7, it can be seen that the basement topography in the T2 subdomain contains three clear serpentinized ridges and shows consistent ridge geometries on the WAM line, L1, and L2. However, the shape of the peridotite ridges becomes more irregular on L3 and L4, with a rougher basement. The diversity of ridge morphologies is probably due to increased igneous addition towards the south portion of the margin due to its proximity to the BTJ. Due to the limitations of 2D seismic data and the absence of borehole data, the geometry, composition, internal structure, and the formation of the basement ridges has been unclear until now.

It is difficult to map the along-strike continuation of the exhumed domain due to the absence of seismic constraints. Since the segments of the subdomain T1 and T2 along L1 are ~ 5 km wider and ~ 9 km narrower than they are along L2, respectively (Fig. 7), the subdomains T1 and T2 are inferred be become slightly wider and narrower to the north, respectively. The basement ridges of the subdomain T2 are not observed in the exhumed domain to the southeast along X2, thus, we assume that the subdomain T2 gradually diminishes (or disappears?) to the southeast of line L4 (Fig. 16). Despite the uncertainties in the interpreted geometres of the two exhumation subdomains along the margin, their consistent presence along strike of the margin implies a regionally significant non-uniform exhumation stage.

6.1.5 Oceanic domain

Seaward of the interpreted peridotite ridges lies the oceanic crust domain, formed through seafloor spreading. Because of relatively dense constraints (L1, L2, L3, and the WAM line), the interpreted oceanic domain geometry along the northern part of the margin is more robust than it is for the southern part. The border between the exhumed mantle domain and the oceanic domain diverges from magnetic Chron 34 towards the south of the margin. By calculating basement roughness of the initial oceanic zone along both the Flemish Cap and Goban Spur conjugate margins, Sauter et al. (2018) argue that this conjugate pair represents typical slow asymmetric seafloor spreading, consistent with the results from Bullock and Minshull (2005).

6.2 Syn-exhumation stratigraphic sequences

In the literature, three main stratigraphic sequences are identified on the Goban Spur: post-rift, syn-rift, and pre-rift sequences (Scrutton, 1979; Masson et al., 1985; de Graciansky and Poag, 1985). Based on the results from drilling site 549 (Fig. 2), the post-rift sequence spans from present-day to Albian, and the syn-rift ranges from Barremian (Hauterivian?) to Aptian. As for the pre-rift basement, it experienced multiple tectonic events, resulting in not only rough basement relief with rotated and tilted horsts and grabens, but also complex compositionally diverse basement rocks (de Graciansky and Poag, 1985). However, based on the new seismic lines in this study, it is observed that the reflections within the syn-rift formations are relatively continuous and clear for hyperextended domains, while syn-rift sedimentary successions typically appear very weak and often transparent above the top basement of the exhumed domain (Figs. 6f and 7). These sedimentary layers in the exhumed domain are associated with mantle exhumation, so they are termed syn-exhumation sediments as introduced in section 5.2. The syn-exhumation sequences are deposited during the transition from the termination of the hyperextended stage to the initiation of seafloor spreading (Peron-Pinvidic et al., 2013). They are still considered syn-rift sequences as mantle exhumation is one of the rifting stages prior to final lithospheric breakup.

Considering the distinctive reflectivity characteristics of sedimentary formations during the evolution of the margin, we have subdivided the sedimentary layers into three parts in this study: syn-rift, syn-exhumation, and post-rift sequences. Due to the lack of drilling data towards the oceanic crust, the three sequences are mainly defined based on reflection characteristics. The post-rift sedimentary layers are parallel or sub-parallel, and have undergone little or no major tectonic movement (Figs. 7-15). The syn-rift sediments deposited in the grabens and the wedge-shaped half-grabens in the continental crust (Figs. 7 and 10), created from the rotation of faulted blocks in the underlying basement (Scrutton, 1979). The thicknesses of syn- and post-rift sequences are highly variable both along and across the strike of the margin (Figs. 7-15). Likewise, the thicknesses of the transparent syn-exhumation layers show striking variations both parallel and perpendicular to the margin. The syn-exhumation sequences reach about 0.8 s in thickness in the subdomain T1 along L1 and L2 (Figs. 7b and 7c). Along L3, the transparent layer disappears above the transition from subdomain T1 to T2, and reappears above the peridotite ridges (Fig. 7e). It gradually disappears to the southeast along the X1 profile (Fig. 13). On lines L1, L2, L3, and the WAM line, "sag" type syn-exhumation sequences are observed above the top exhumed basement (Fig. 7). The formation of this sag architecture may result from a higher sedimentation rate than the exhumation rate, similar to the case for Australian-Antarctic magma-poor rifted margins where the "sag" geometries of sedimentary layers of above the exhumed basement are also observed (Gillard et al., 2015). The difference is that reflectivity is transparent/weak at the former margin, while it is continuous and clear at the latter margin (Gillard et al., 2015).

Interestingly, the low reflectivity characteristics within the syn-exhumation layers are not readily observed at other magma-poor margins. There is a possibility that automatic gain control (AGC) has been used on the seismic data at some margins to balance amplitudes, whereas the new seismic lines in this study are displayed using true amplitudes as the processing procedures are amplitude-preserving. Magmatic additions are one potential component of syn-exhumation sedimentary packages at the Goban Spur (expanded box in Fig. 10). However, the compositions and origin of syn-exhumation sediments are still unclear due to the lack of similar observations on other margins and the lack of drilling data.

6.3 Magmatism on the non-volcanic/magma-poor Goban Spur margin

Based on an interpreted depth-uniform extension of the lithosphere across the Goban Spur margin (Peddy et al., 1989), Bullock and Minshull (2005) propose that the basaltic material observed along the WAM line in the necking zone was extruded prior to mantle exhumation due to decompression melting. At Site 550, located in the exhumed mantle domain, basaltic pillow lavas were also recovered. According to previous interpretations from PAD, the areal extent of sills along the northern Goban Spur margin appears much larger than that along the southern margin, and intrusive and extrusive basaltic bodies appear to be distributed across the necking, hyperextended, and mantle exhumation zones (Fig. 16). This suggests that magmatic events were occurring during rifting, thinning, mantle exhumation, and final continental breakup along the Goban Spur margin. Furthermore, magmatic layers in the exhumed and hyperextended domains along L2 (expanded yellow box in Fig. 10a) illustrate that the region of sills across the Goban Spur may be larger than that previously interpreted by PAD. The distribution of sills across the margin does not appear to correspond to regions with localized high magnetic anomalies (Fig. 4b), noting that some magnetic anomalies may be associated with serpentinization at the Goban Spur margin (Minshull, 2009). In addition, the igneous bodies appear to be distributed close to the transfer faults that represent tectonic weaknesses in the continental crust (Scrutton et al., 1979) and these faults may provide channels for lava flow migration during margin evolution.

6.4 Reconstruction of the Goban Spur and its conjugates

In Figure 17, the crustal architecture across the Goban Spur margin from this study and the crustal architecture across the "conjugate" northeastern margin of Flemish Cap from Welford et al. (2010c) are mapped using a rigid plate reconstruction, back to the onset of seafloor spreading using GPlates 2.1 at 83 Ma (Müller et al., 2016). In order to compare the two margins consistently, the stretched crust interpreted along the Flemish Cap margin is assumed to correspond to the necking and hyperextended zones along the Goban Spur margin.

At the Goban Spur, the necking zone is of variable width ranging from ~ 114 km to ~200 km, indicating along-strike variability in lithosphere thinning. In contrast, although the boundary between the necking and hyperextended domains is not clearly defined along the Flemish Cap margin, the width of the necking domain is much narrower (< ~20 km; Welford et al., 2010c), indicating a more abrupt necking of the crust. In addition, the along-strike exhumed serpentinized mantle domain of the Goban Spur margin spans a much wider (~ 42 - 60 km) area while it is much narrower (~25 km) at the northeastern Flemish Cap margin (Welford et al., 2010c). In the exhumed domain, only peridotite ridges are observed at the Flemish Cap

(Welford et al., 2010c), while both peridotite ridges (subdomain T2) and a wide region of exhumed mantle with deeper basement (subdomain T1) are observed at the Goban Spur.

Overall, the highly variable geometry of each crustal type across the “conjugate” pair is consistent with asymmetric evolutionary mechanisms as hypothesized by Gerlings et al. (2012). However, based on seismic interpretation, Welford et al. (2010c) identified both extensional and strike-slip deformation along the northeastern Flemish Cap margin, consistent with the interpreted rotation and displacement of Flemish Cap with respect to the Orphan Basin during the early Cretaceous period through seismic and potential field data analysis (Sibuet et al., 2007) and more recently deformable plate tectonic reconstructions (Peace et al., 2019). In contrast, the Goban Spur margin experienced mostly margin-perpendicular extension. In addition to the geometric differences in crustal architecture, velocities (> 7 km s^{-1} at depth) in subdomain T2 at the Goban Spur differ from those (7.4-7.9 km s^{-1}) at depth in the serpentinized mantle domain at the northeastern Flemish Cap margin, which may also reflect different degrees of serpentinization (Bullock and Minshull, 2005; Gerlings et al., 2012).

To date, there have been many strikingly different geological and geophysical characteristics (e.g., P-wave velocities, crustal architecture, tectonic deformation mechanism, crustal thickness, etc.) observed across the northeastern Flemish Cap margin and the Goban Spur margin (de Graciansky and Poag, 1985; Keen et al., 1989; Welford et al., 2010a; Gerlings et al., 2012). The mechanism for generaing asymmetric features across the two margins is still unclear, suggestive of a more complex model than previously thought for the Goban Spur margin and its possible conjugates. These differences between the two margins also calls into question the widely-accepted “conjugate” relationship since the conjugate margins generally share some common features (Reston, 2009).

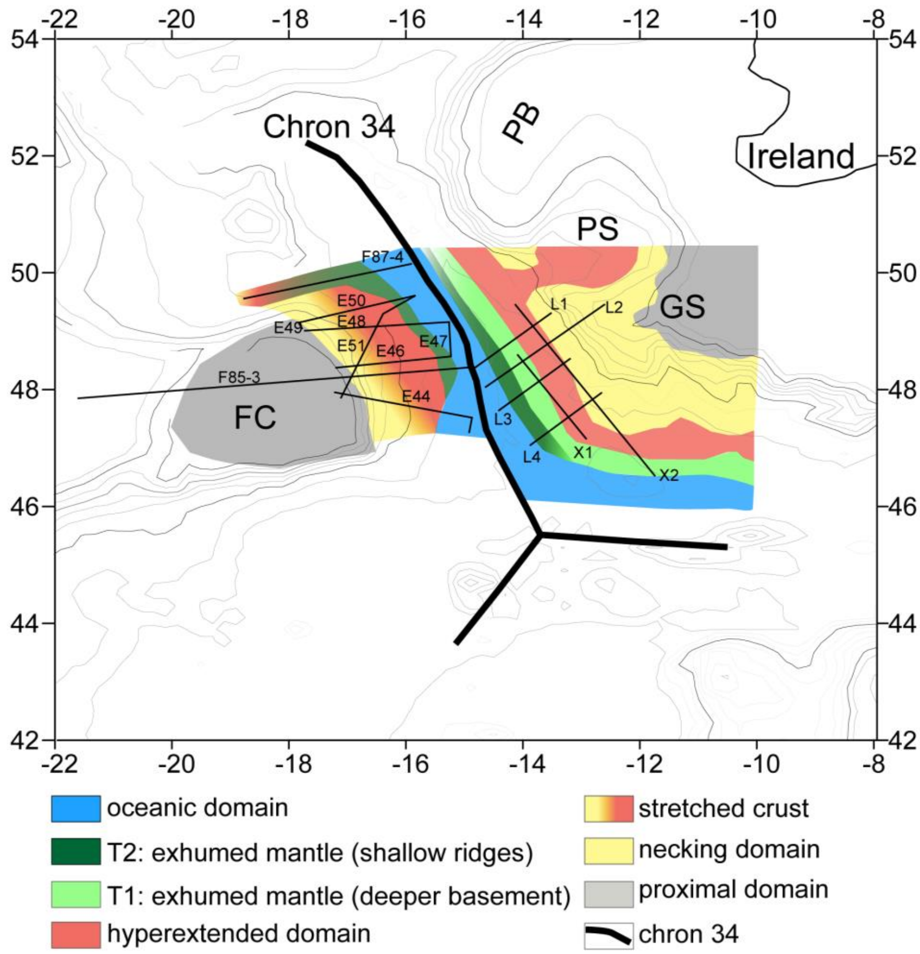

Fig. 17. Crustal architecture across the northeastern Flemish Cap-Goban Spur margins, reconstructed to magnetic Chron 34 at 83 Ma (thick black line from Müller et al., 2016) using a rigid plate reconstruction in GPlates 2.1 (Müller et al., 2016), overlain by the corresponding bathymetric contours (thin grey lines) at 83 Ma. The crustal domains across Flemish Cap are adapted from Welford et al. (2010c). Labelled thin black straight lines show seismic profiles constraining the crustal architecture interpretations. Abbreviations: FC, Flemish Cap; GS, Goban Spur; PS, Porcupine Seabight; PB, Porcupine Bank.

As introduced before, the geometries of the peridotite ridges in the serpentinized exhumed domain at the Goban Spur margin are similar to those observed at the west Iberia margin (Dean et al., 2000). The Goban Spur was adjacent to the Iberia margin (specifically, the Galicia Bank) at 200 Ma prior to rifting according to new kinematic evolution models (Nirrengarten et al., 2018; Peace et al., 2019; Sandoval et al., 2019). If so, the prominent asymmetries recorded along both the Goban Spur and Flemish Cap would have resulted from the motion and southward migration of the Flemish Cap (Sibuet et al., 2007; Welford et al., 2010c; Welford et al., 2012; Peace et al., 2019), or, at the least, oblique rifting (Brune et al., 2018). Superimposed on these plate motions, the variable widths of each of the crustal domains across the two margins may also reflect highly variable rifting rates. At the Goban Spur, lower mantle temperatures are supported by geochemical models, suggestive of relatively slower rifting than along other northern Atlantic margins (Dean et al., 2009). Meanwhile, inferred complexities in the tectonic processes along the northeastern Flemish Cap margin also make it difficult to determine the rifting rate. In spite of these discrepancies and uncertainties, the crustal architecture comparison between the two margins provides insightful constraints for unraveling the margin evolution.

7. Summary

Six new multichannel seismic reflection profiles, integrated with previous seismic reflection and refraction data, magnetic and gravity data, and DSDP drilling sites, for the Goban Spur magma-poor rifted margin have revealed the following:

(1) Five distinct crustal domains related to different rifting stages are identified and their regional extents are evaluated, significantly increasing knowledge of the crustal architecture of the Goban Spur rifted continental margin.

(2) Along strike, the width of the necking domain on the Goban Spur margin gradually increases from northwest to southeast, suggesting along-strike variations in extension, likely related to the variable pre-existing rheological architecture across the Goban Spur margin.

(3) In the northwest, the exhumed domain consists of shallower peridotite ridges (transitional subdomain T2) and deeper exhumed serpentinized mantle (transitional subdomain T1). The different styles of mantle exhumation are inferred to reflect different exhumation rates. Toward the southeast along the Goban Spur margin, the zone of serpentinized peridotite ridges is tentatively interpreted to diminish or disappear.

(4) During the evolution of the Goban Spur continental margin, localized syn-rift magmatism occurred during lithosphere stretching, thinning, subsequent hyperextension and serpentinized mantle exhumation, and final lithosphere rupture, all prior to seafloor spreading initiation.

(5) The striking asymmetries between the Goban Spur margin and its "conjugate" margin, the northeastern Flemish Cap margin, call into question the conjugate relationship between the two margins.

Future work involving the restoration of the margins using deformable plate reconstructions will help resolve this debate. Such research will help unravel the geological significance of the Goban Spur during opening of the southern North Atlantic Ocean, which led to the separation of the Irish, Newfoundland, and Iberian margins.

Acknowledgement

We are grateful to the Department of Communications, Climate Action & Environment of Ireland for providing the multichannel seismic reflection data. WAM data were acquired by the UK NERC BIRPS programme in 1985. Great thanks are also given to Schlumberger for donating Petrel software to Memorial University. AP's postdoctoral fellowship at Memorial was funded by the Hibernia Project Geophysics Support Fund and Innovate NL. We would like to thank the members of the Memorial Applied Geophysics for Rift Tectonics (MAGRiT) group for providing suggestions for this research.

References

Albertz, M., Beaumont, C., Shimeld, J., Ings, S., Gradmann, S., 2010. An investigation of salt tectonic structural styles in the Scotia Basin, offshore Atlantic Canada: 1. Comparison of observations with geometrically simple numerical models. Tectonics 29, TC4017.

Brune, S., Williams, S. E., Müller, R. D., 2018. Oblique rifting: the rule, not the exception. Solid Earth 9, 1187-1206.

Boillot, G., Recq, M., Winterer, E.L., Meyer, A.W., Applegate, J., Baltuck, M., Bergen, J.A., Comas, M.C., et al., 1987. Tectonic denudation of the upper mantle alongpassive margins: a model based on drilling results (ODP leg 103, western Galicia margin, Spain). Tectonophysics 132, 335-342.

Bonvalot, S., Balmino, G., Briais, A., Kuhn, M., Peyrefitte, A., Vales, N., Biancale, R., Gabalda, G., Reinquin, F., Sarrailh, M., 2012. World Gravity Map. Commission for the Geological Map of the World. Eds. BGI-CGMW-CNES-IRD, Paris.

Bullock, A.D., Minshull, T.A., 2005. From continental extension to seafloor spreading: crustal structure of the Goban Spur rifted margin, southwest of the UK. Geophysics Journal International 163, 527-546.

Cande, S.C., Kristoffersen, Y., 1977. Late Cretaceous magnetic anomalies in the North Atlantic. Earth and Planetary Science Letters 35, 215-224.

Davy, R. G., Minshull, T. A., Bayrakci, G., Bull, J. M., Klaeschen, D., Papenberg, C., Reston, T. J., Sawyer, D. S., and Zelt, C. A., 2016. Continental hyperextension, mantle exhumation, and thin oceanic crust at the continent-ocean transition, West Iberia: New insights from wide-angle seismic, Journal of Geophysical Research: Solid Earth 121, 3177-3199.

de Graciansky, P. C., Poag, C. W., Cunningham, R., Loubere, P., Masson, G.D., et al., 1985. The Goban Spur transect: Geologic evolution of a sediment-starved passive continental margin. Geological Society of America Bulletin 96, 58-76.

de Graciansky, P. C., Poag, C. W., 1985. Geologic history of Goban Spur, northwest Europe continental margin. Deep Sea Drilling Project Initial Reports 80, 1187-1216.

Dean, S.M., Murton, B.J., Minshull, T.A., Henstock, T.J., White, R.S., 2009. An integrated kinematic and geochemical model to determine lithospheric extension and mantle temperature from syn-rift volcanic compositions. Earth and Planetary Science Letters 278, 26-39.

Dean, S.M., Minshull, T.A., Whitmarsh, R.B., Louden, K.E., 2000. Deep structure of the ocean-continent transition in the southern Iberia Abyssal Plain frosm seismic refraction profiles: the IAM-9 transect at 40 20'N. Journal Geophysical Research 105, 5859-5886.

Dean, S.L., Sawyer, D.S., Morgan, J.K., 2015. Galicia Bank ocean-continent transition zone: New seismic reflection constraints. Earth and Planetary Science Letters 413, 197-207.

Dingle, R. V., Scrutton, R. A., 1977. Continental margin fault pattern mapped south-west of Ireland. Nature 268, 720-722.

Dingle, R. V., Scrutton, R. A., 1979. Sedimentary succession and tectonic history of a marginal plateau (Goban Spur, southwest of Ireland). Marine Geology 33, 45-69.

Franke, D., 2013. Rifting, lithosphere breakup and volcanism: Comparison of magma-poor and volcanic rifted margins. Marine and Petroleum Geology 43, 63-87.

Gerlings, J., Louden, K.E., Jackson, H.R., 2011. Crustal structure of the Flemish Cap Continental Margin (eastern Canada): an analysis of a seismic refraction profile. Geophysics Journal International 185, 30-48.

Gerlings, J., Louden, K. E., Minshull, T. A., Nedimovi´c, R.M., 2012. Flemish Cap-Goban Spur conjugate margins: New evidence of asymmetry. Geology 40, 1107-1110.

Gillard, M., Autin, J., Manatschal, G., Sauter, D., Munschy, M., Schaming, M., 2015. Tectono-magmatic evolution of the final stages of rifting along the deep conjugate Australian-Antarctic magma-poor rifted margins: constraints from seismic observations. Tectonics 34,753-783.

Gillard, M., Tugend, J., Muntener, O., Manatschal, G., Karner, G.D., Autin, J., Sauter, D., Figueredo, P.H., Ulrich, M., 2019. The role of serpentinization and magmatism in the formation of decoupling interfaces at magma-poor rifted margins. Earth-Science Reviews 196, 102882.

Gillard, M., Autin, J., Manatschal, G., 2016. Fault systems at hyper-extended rifted margins and embryonic oceanic crust: Structural style, evolution and relation to magma. Marine and Petroleum Geology 76, 51-67.

Grevemeyer, I., Hayman, N.W., Peirce, C., Schwardt, M., Van Avendonk, H.J., Dannowski, A. and Papenberg, C., 2018. Episodic magmatism and serpentinized mantle exhumation at an ultraslow-spreading centre. Nature Geoscience 11, 444.

Healy, D., Kusznir, N.J., 2007. Early kinematic history of the Goban Spur rifted margin derived from a new model of continental breakup and sea-floor spreading initiation. Geological Society, London, Special Publications 282, 199-215.

Horsefield, S.J., Whitmarsh, R.B., White, R.S., and Sibuet, J. C., 1994. Crustal structure of the Goban Spur rifted continental margin, NE Atlantic. Geophysics Journal International 119, 1-19.

Huismans, R., Beaumont, C., 2011. Depth-dependent extension, two-stage breakup, and cratonic underplating at rifted margins. Nature 473, 74-78.

Jackson, M.P.,Talbot, C.J., 1986. External shapes, strain rates, and dynamics of salt structures. Geological Society of America Bulletin 97, 305-323.

Keen, C.E., de Voogd, B., 1988. The continent-ocean boundary at the rifted margin off eastern Canada: New results from deep seismic reflection studies. Tectonics 7, 107-124.

Keen, C.E., Peddy, C., deVoogd, B., Mathews, D., 1989. Conjugate margins of Canada and Europe: Results from deep reflection profiling. Geology 17, 173-176.

Li,Y., Oldenburg, D.W., 1996. 3-D inversion of magnetic data. Geophysics, 61, 394-408.

Li, Y., Oldenburg, D.W., 1998. 3-D inversion of gravity data. Geophysics, 63, 109-119.

Louvel, V., Dyment, J., Sibuet, J., 1997. Thinning of the Goban Spur continental margin and formation of early oceanic crust: constraints from forward modelling and inversion of marine magnetic anomalies. Geophysics Journal International 128,188-196.

Masson, D., Montadert, L., Scruiton, R., 1985. Regional geology of the Goban Spur continental margin. Initial Reports of the Deep Sea Drilling Project 80, 1115-1139.

Minshull, T.A., 2009. Geophysical characterisation of the ocean-continenttransition at magma-poor rifted margins. Comptes Rendus Geoscience 341, 382-393.

Mohn, G., Manatschal, G., Beltrando, M., Masini, E., Kusznir, N., 2012. Necking of continental crust in magma-poor rifted margins: evidence from the fossil Alpine Tethys margins. Tectonics 31, 1-28.

Montadert, L., Roberts, D. G., de Charpal, O., Guennoc, P., 1979, Rifting and subsidence of the Northern Continental Margin of the Bay of Biscay. Initial Reports of the Deep Sea Drilling Project 48, 1025-1060.

Müller, R.D., Seton, M., Zahirovic, S., Williams, S.E., Matthews, K.J., Wright, N.M., Shephard, G.E., Maloney, K.T., Barnett-Moore, N., Hosseinpour, M., Bower, D.J., Cannon, J., 2016. Ocean Basin

Evolution and Global-Scale Plate Reorganization Events Since Pangea Breakup. Annual Review of Earth and Planetary Sciences 44, 107.

Naylor, D., Shannon, Murphy, N., 2002. Porcupine-Goban region – a standard structural nomenclature system. Dublin, Ireland: Petroleum Affairs Division.

Nirrengarten, M., Manatschal, G., Tugend, J., Kusznir, N., Sauter, D., 2018. Kinematic evolution of the southern North Atlantic: Implications for the formation of hyperextended rift systems. Tectonics 37, 1-30.

Osmundsen, P.T., Ebbing, J., 2008. Styles of extension offshore mid-Norway and implications for mechanisms of crustal thinning at passive margins. Tectonics 27, TC6016.

Peace, A.L., Welford, J. K., Ball, P.J., Nirrengarten, M., 2019. Deformable plate tectonic models of the southern North Atlantic. Journal of Geodynamics 128, 11-37.

Peddy C., Pinet, B., Masson, D., Scrutton, R., Sibuet, J.C., Warner, M.R., Lefort, J.P., Shroeder, I.J., 1989. Crustal structure of the Goban Spur continental margin Northeast Atlantic, from deep seismic reflection profiling. Journal of the Geological Society 146, 427-437.

Perez-Gussinye, M., Ranero, C.R., Reston, T.J., Sawyer, D., 2003. Mechanisms of extension at nonvolcanic margins: evidence from the Galicia interior basin, west of Iberia. Journal of Geophysical Research:Solid Earth, 108(B5).

Peron-Pinvidic, G., Manatschal, G., 2009. The final rifting evolution at deep magma poor passive margins from Iberia-Newfoundland: a new point of view. International Journal of Earth Sciences 98, 1581-1597.

Peron-Pinvidic, G., Manatschal, G., Osmundsen, P.T., 2013. Structural comparison of archetypal Atlantic rifted margins: A review of observations and concepts. Marine and Petroleum Geology 43, 21-47.

Pickup, S. L. B., Whitmarsh, R. B., Fowler, C.M.R., Reston, T. J., 1996. Insight into the nature of the ocean-continent transition off West Iberia from a deep multichannel seismic reflection profile. Geology 24, 1079-1082.

Reston, T.J., Krawczyk, C.M., Klaeschen, D., 1996. The S reflector west of Galicia (Spain): Evidence from prestack depth migration for detachment faulting during continental breakup. Journal of Geophysical Research: Solid Earth 101, 8075-8091.

Reston, T.J., 2007. The formation of non-volcanic rifted margins by the progressive extension of the lithosphere: the example of the West Iberian margin. Geological Society, London, Special Publications 282, 77-110.

Reston, T.J., 2009. The structure, evolution and symmetry of the magma-poor rifted margins of the North and Central Atlantic: a synthesis. Tectonophysics 468, 6-27.

Sandoval, L., Welford, J.K., MacMahon, H., Peace, A.L., 2019. Determining continuous basins across conjugate margins: The East Orphan, Porcupine, and Galicia Interior basins of the southern North Atlantic Ocean. Marine and Petroleum Geology 110, 138-161.

Sauter, D., Tugend, J., Gillard, M., Nirrengarten, M., Autin, J., Manatschal, G., Cannat, M., Leroy, S., Schaming, M., 2018. Oceanic basement roughness alongside magma-poor rifted margins: insight into initial seafloor spreading. Geophysical Journal International 212, 900-915.

Sawyer, D. S., Whitmarsh, R. B., Klaus, A., et al., 1994. Proceedings of the Ocean Drilling Program, Initial Reports 149, College Station, TX (Ocean Drilling Program).

Sclater, J.G., Christie, P.A., 1980. Continental stretching: An explanation of the post-Mid-Cretaceous subsidence of the central North Sea Basin. Journal of Geophysical Research: Solid Earth 85, 3711-3739.

Scrutton, R.A., 1979. Structure of the crust and upper mantle at Goban Spur, southwest of the British Isles-some implications for margin studies. Tectonophysics 59, 201-215.

Shillington, D. J., Holbrook, W. S., Van Avendonk, H. J. A., Tucholke, B. E., Hopper, J. R., Larsen, H. C., Nunes, G. T., 2006. Evidence for asymmetric nonvolcanic rifting and slow incipient oceanic accretion from seismic reflection data on the Newfoundland margin. Journal of Geophysical Research 111, B09403.

Sibuet, J. C., Collette, B.J. 1991. Triple junctions of Bay of Biscay and North Atlantic: New constraints on the kinematic evolution. Geology 19, 522-525.

Sibuet, J.C., Mathis, B., Pastouret, L., Auzende, J.M., Foucher, J.P., Hunter, P.M., Guennoc, P., de Graciansky, P.C., Montadert, L., Masson, D.G., 1985. Morphology and basement structure of the Goban Spur continental margin (northeastern Atlantic) and the role of the Pyrenean orogeny. Initial Reports of the Deep Sea Drilling Project 80, 1153-1165.

Sibuet, J.C., Srivastava, S.P., Enachescu, M., Karner, G.D., 2007. Early Cretaceous motion of Flemish Cap with respect to North America: implications on the formation of Orphan Basin and SE Flemish Cap - Galicia Bank conjugate margins. Geological Society, London, Special Publications 282, 63-76.

Sibuet, J.C., Tucholke, B.E., 2012. The geodynamic province of transitional lithosphere adjacent to magma-poor continental margins. Geological Society, London, Special Publications 369, 429-452.

Srivastava, S., Verhoef, J., Macnab, R., 1988. Results from a detailed aeromagnetic survey across the northeast Newfoundland margin, part ii: Early opening of the North Atlantic between the British Isles and Newfoundland. Marine and Petroleum Geology 5, 324-337.

Sutra, E., Manatschal, G., Mohn, G., Unternehr, P., 2013. Quantification and restoration of extensional deformation along the Western Iberia and Newfoundland rifted margins. Geochemisty, Geophysics, Geosystems 14, 2575-2597.

Tetreault, J.L., Buiter, S.J.H., 2018. The influence of extension rate and crustal rheology on the evolution of passive margins from rifting to break-up. Tectonophysics 746,155-172.

Tucholke, B. E., Sibuet, J.C., Klaus, A., et al., 2004. Proceedings of the Ocean Drilling Program, Initial Reports 210, College Station, TX (Ocean Drilling Program).

Tugend, J., Manatschal, G., Kusznir, N. J., Masini, E., Mohn, G., Thinon, I., 2014. Formation and deformation of hyperextended rift systems: Insights from rift domain mapping in the Bay of Biscay-Pyrenees. Tectonics 33, 1239-1276.

Tugend, J., Manatschal, G., Kusznir, N.J., Masini, E., 2015. Characterizing and identifying structural domains at rifted continental margins: application to the Bay of Biscay margins and its Western Pyrenean fossil remnants. Geological Society, London, Special Publications 413, 171-203.

Van Avendonk, H. J. A., Holbrook, W. S. Nunes, G.T., Shillington, D.J., Tucholke, B.E., et al., 2006. Seismic velocity structure of the rifted margin of the eastern Grand Banks of Newfoundland, Canada. Journal of Geophysical Research 111, B11404.

Van Avendonk, H.J., Davis, J.K., Harding, J.L., Lawver, L.A., 2017. Decrease in oceanic crustal thickness since the breakup of Pangaea. Nature Geoscience 10, 58.

Welford, J.K., Smith, J.A., Hall, J., Deemer, S., Srivastava, S.P., Sibuet, J.C., 2010a. Structure and rifting evolution of the northern Newfoundland Basin from Erable multichannel seismic reflection profiles across the southeastern margin of Flemsih Cap. Geophysical Journal International 180, 976-998.

Welford, J.K., Shannon, P.M., O'Relly, B.M., Hall, J., 2010b. Lithospheric density variations and Moho structure of the Irish Atlantic continental margin from constrained 3-D gravity inversion. Geophysical Journal International 183, 79-95.

Welford, J.K., Hall, J., Sibuet, J.C., Srivastava, S.P., 2010c. Structure across the northeastern margin of Flemish Cap, offshore Newfoundland from Erable multichannel seismic reflection profiles: evidence for a transtensional rifting environment. Geophysical Journal International 183, 572-586.

Welford, J.K., Shannon, P.M., O'Relly, B.M., Hall, J., 2012. Comparison of lithosphere structure across the Orphan Basin–Flemish Cap and Irish Atlantic conjugate continental margins from constrained 3D gravity inversions. Journal of the Geological Society, 169, 205-420.

White, R.S., Minshull, T.A., Bickle, M.J., Robinson, C.J., 2001. Melt generation at very slow-spreading oceanic ridges: Constraints from geochemical and geophysical data. Journal of Petrology 42, 1171-1196.

Whitmarsh, R. B., Beslier, M.O., Wallace, P. J., et al., 1998. Proceedings of the Ocean Drilling Program, Initial Reports 173, College Station, TX (Ocean Drilling Program).

Whitmarsh, R.B., Manatschal, G., Minshull, T.A., 2001. Evolution of magma-poor continental margins from rifting to seafloor spreading. Nature 413, 150-154.